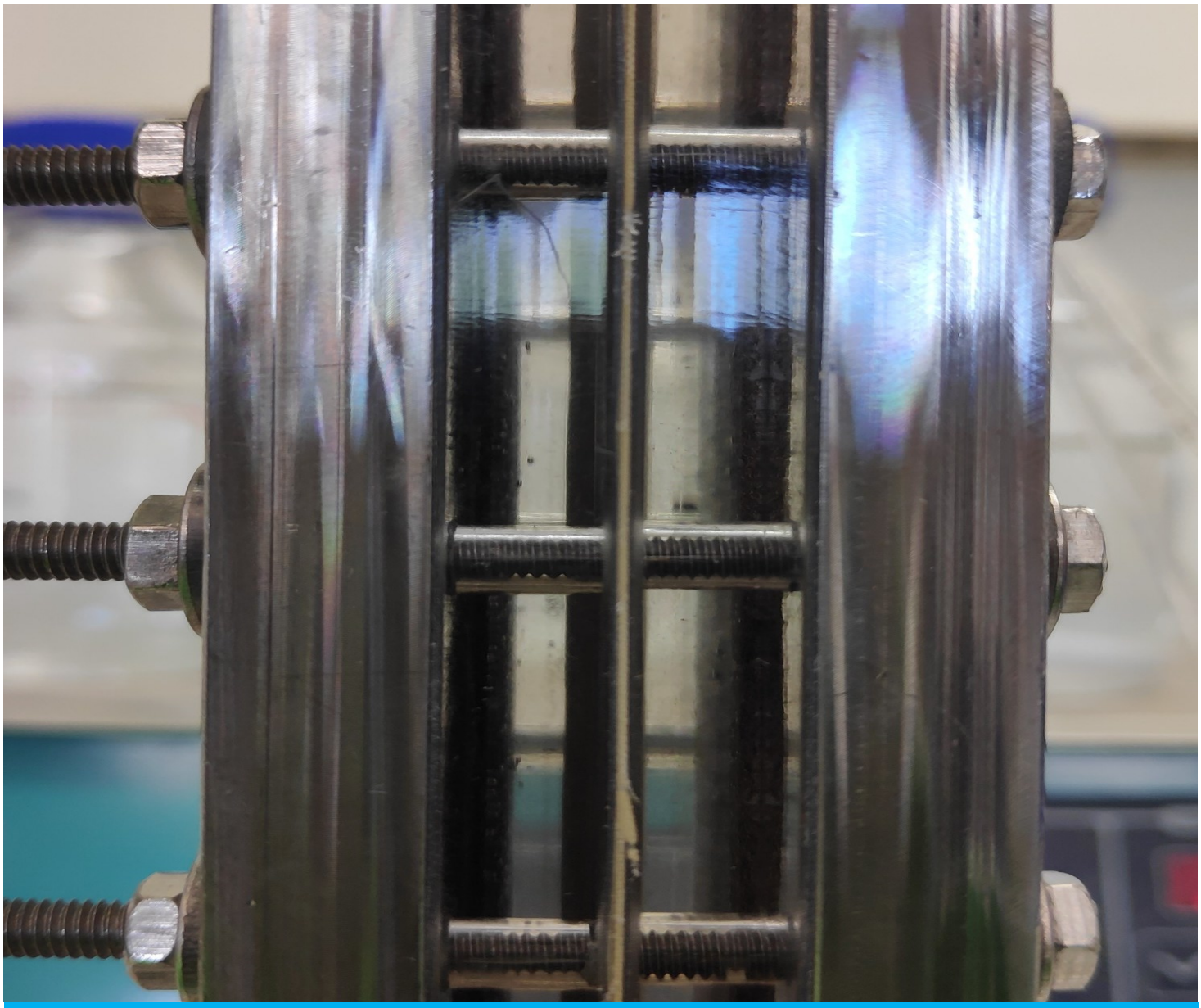

Hydrogen Production via the Electrolysis of Municipal Effluent Using Carbon Fibre and Nickel-Foam Anode

Ranjeev Kumar Bhatia
5264561

Hydrogen Production via the Electrolysis of Municipal Effluent Using Carbon Fibre and Nickel-Foam Anode

By

Ranjeev Kumar Bhatia
5264561

in partial fulfilment of the requirements for the degree of

Master of Science
in Civil Engineering, Environmental Engineering

at the Delft University of Technology,
to be defended publicly on TBD.

Supervisor:	Prof. Dr. Ir. Henri. Spanjers
Thesis committee:	Prof. Dr. Ir. Jules van. Lier, TU Delft
	Prof. Dr. Ir. David. Vermaas, TU Delft

Contents

List of Figures

List of Tables

Nomenclature

HER- Hydrogen Evolution Reaction

OER- Oxygen Evolution Reaction

CLER – Chlorine evolution Reaction

CLRR-Chlorate Reduction Reaction

COD-Chemical Oxygen Demand (mg O_2/L)

DSA- Dimensionally Stable Anode

TOC- Total Organic Carbon (mg-C/L)

SHE – Standard Hydrogen Electrode (V)

HHV – Higher Heating Value (Wh /mol)

WEC- Wastewater electrolysis Cell

PV- Photovoltaic cell

PTFE- Poly Tetra Fluoroethylene

VFA-Volatile Fatty Acids

F – Faradays Number (Coulomb/mole e^-)

k_m= Mass transport coefficient(m/s)

P – Pressure(bar)

R – Universal Gas constant ($L \cdot bar \cdot K^{-1} \cdot mol^{-1}$)

T - Temperature (K)

E^o- Theoretical Decomposition Voltage (V)

E_{cell}- Cell Potential (V)

J_{lim}- Limiting Current Density (A/m^2)

i – Current (A)

η_a -anodic overpotential (V)

η_c -cathodic overpotential (V)

Q_r- Molar production rate of Gas species (mol/s)

Q_H- Hydrogen production rate (mol H_2/s)

Abstract

This study aims to explore hydrogen production via alkaline water electrolysis using municipal effluent. The experiments were conducted in a flow cell electrolyzer using carbon fibre and Ni-foam as the anode, with another Ni-foam electrode employed as the cathode for all experiments. Synthetically prepared effluent and real municipal effluent obtained from the Harnaschpolder water treatment plant effluent was used with potassium hydroxide (KOH) as the supporting electrolyte. The composition of the synthetic effluent was prepared with 23.0 ± 2.1 mg O_2/L humic acid (Sigma Aldrich) as the primary organic pollutant. Experiments were conducted to investigate the effect of electrolyte concentration ranging from 0.01M -1M KOH and the effect of applied current density ranging from 25 A/m^2, 50 A/m^2, 100 A/m^2 and 150 A/m^2. Further experiments were conducted to assess the effect of humic acid concentration ranging from 23.0 ± 2.1 mg O_2/L to 90.0 ± 0.7 mg O_2/L. This was subsequently investigated under potentiostatic conditions at an applied cell voltage of 1.5V using the carbon fibre anode and under galvanostatic conditions for the Ni-foam anode. Regarding the Ni-foam anode, the current density was calculated based on the concentration using the relationship for limiting current density of humic acid oxidation. The investigation focused on assessing the performance of the electrolyzer in terms of volumetric hydrogen production rate and energy efficiency of hydrogen production. The performance data was also compared with conventional alkaline water electrolysis using Ni-foam as the anode and cathode in 1M KOH solution. In addition, the extent of humic acid oxidation was also assessed in terms of COD removal efficiency, TOC removal efficiency and changes in the spectral scans obtained via UV-Vis spectrophotometry.

The performance data revealed that the energy efficiency of hydrogen production was lower for both synthetic and municipal effluent compared to alkaline water electrolysis; this was evident for both carbon fibre and Ni-foam anode. Further, the energy efficiency was also higher when the Ni-foam anode was used compared to the carbon fibre anode. For the electrolysis of municipal effluent, a maximum energy efficiency of 75 ± 2.7% was obtained for the carbon fibre electrode, whereas for the Ni-foam anode, the maximum energy efficiency obtained was 83 ± 3.0% at an applied current density of 12.55 A/m^2 with 1M KOH as the electrolyte. Despite this observation, the volumetric hydrogen production rates were not significantly affected because the rates converged closely to their theoretical values; this was also evidenced by the coulombic efficiency of hydrogen evolution reaction (HER), which exceeded 90% in all the experiments.

Concerning the extent of humic acid degradation, the Ni-foam anode was able to oxidize some of the humic acid molecules during electrolysis, and a maximum COD removal of 24.6 ± 8 % was observed after electrolysis of synthetic effluent at an applied current density of 100 A/m^2 with 1M KOH as the supporting electrolyte. In contrast, the carbon fibre anode was not able to do so. Instead, the humic acid molecules tended to adsorb on the surface of the carbon fibre anode, evidenced by the increase in COD and TOC after electrolysis. Similar behaviour was also observed for the carbon fibre anode when the effect of humic acid was investigated under potentiostatic conditions, whereas under galvanostatic conditions for the Ni-foam anode, oxidation of humic acid was evident. The extent of oxidation was dependent on the duration of electrolysis, i.e., humic acid concentrations of 49.8 ± 0.98 mg O_2/L and 90.0 ± 0.7 mg O_2/L required a duration of 6 hrs and 8 hrs to achieve a COD removal efficiency of 43.5 ± 5.0 % and 60.4 ± 4.2 %, respectively. Additionally, the possibility to integrate an electrolyzer with an aerobic treatment plant to supply high purity oxygen was investigated. The comparison was done using BioWin simulations with a standard aerobic bioreactor for a flow of 10,000 m^3/day under two conditions: 1) with atmospheric O_2(baseline) 2) with high purity O_2(95% purity). The investigation revealed that combining a 1 MW electrolyser with the aerobic wastewater treatment plant would provide sufficient amount of oxygen for the proper functioning of the high purity O_2 plant. In addition, the flow requirement to produce the required amount of oxygen was only 0.03% of the discharged effluent(i.e., only 3.1 m^3/day of the discharged 9708 m^3/day).

Further, the use of high purity oxygen in the aerobic wastewater treatment plant was accompanied by energy savings of 1.2 kWh(4320 kJ) due to reduced load on the air pumps.

Background: Fundamentals of water electrolysis

Water electrolysis is a process in which the water molecule is split into its constituent gases via the application of electrical energy. In general, a water electrolyzer is an electrochemical cell consisting of an anode and a cathode; during the water-splitting process, oxygen is evolved at the anode, which releases protons known as the Oxygen Evolution Reaction (OER). The protons are then reduced at the cathode resulting in the evolution of hydrogen gas, also known as the Hydrogen Evolution Reaction (HER)(Godula-Jopek, 2015). The corresponding half-cell reactions are described in the following equations:-

Anode Half Reaction : $2H_2O_{(l)} \rightarrow O_{2(g)} + 4H^+ + 4e^-$ $E^0(SHE) = 1.229V$ *Eq 1*

Cathode Half Reaction : $2H^+ + 2e^- \rightarrow H_{2(g)}$ $E^0(SHE) = 0\ V$ *Eq 2*

Full reaction: $H_2O_{(l)} \rightarrow H_{2(g)} + ½\ O_{2(g)}$ $E^0_{cell}(SHE) = -1.229V$ *Eq 3*

Thermodynamically, water splitting is a non-spontaneous process, i.e., the reaction given by Eq 3 has a positive Gibbs free energy (237.19kJ / mol H_2O). As a consequence, the forward reaction requires an external driving force which is provided via an external power supply. Based on the free energy, approximately 1.229 V is required for the electrolysis of water; however, on applying this potential, the reactions will not be able to maintain isothermicity, and the electrochemical cell will begin to cool. This occurs because the formation of gas molecules O_2 and H_2 have a higher entropy and extract heat from the H_2O molecule. To compensate for this energy loss, heat has to be supplied to the reaction; this is done via the application of a thermoneutral voltage which is estimated based on the enthalpy of the reaction (285.8 kJ/mol) and is approximately 1.48 V (Godula-Jopek, 2015). In practice, for industrial water electrolysis, a voltage range between 1.8-2.0V is usually applied(Godula-Jopek, 2015). The practical cell voltage is expressed as follows:-

$$E_{cell} = E_a - E_c + i.\sum R = E^o + |\eta_a| + |\eta_c| + i.\sum R \qquad Eq\ 4$$

Where E_a is the anode potential for the oxygen evolution reaction (V), E_c is the cathode potential for the hydrogen evolution reaction (V), i is the applied current (A), ΣR is the total ohmic resistance of the cell, E^o is the theoretical decomposition voltage (1.23 V), η_a is the anodic overpotential, and η_c is the cathodic overpotential.

In general, energy efficiency is related to the amount of hydrogen produced via electrolysis and the voltage applied, i.e., it gives the ratio of the energy that can be potentially extracted to the amount of energy applied. The expression for energy efficiency (EE) is as follows:-

$$EE = \frac{HHV \cdot Q_H}{E_{cell} \cdot i} \qquad Eq\ 5$$

Where EE is the energy efficiency, HHV is the higher heating value of H_2(78 Wh/mol H_2), E_{cell} is the applied cell potential (V), i is the current (A), and Q_H is the molar production rate of H_2. Similarly, coulombic efficiency describes the efficiency with which charge is transferred with the system facilitating the electrochemical reaction. This is expressed as shown below: -

$$CE = \frac{n_r \cdot F \cdot Q_r}{i} \qquad Eq\ 6$$

In the above equation, CE is the coulombic/current efficiency of the electrochemical reaction of interest, n_r is the number of electrons required for the reaction, F is Faraday's constant (96485 C/mol), and Q_r is the observed molar production rate of the gaseous species. In both Eq 4 and Eq 5, the molar production rate of a species can be calculated using the volume of a gas produced (V) by applying the ideal gas equation Eq 7 by

$$Q_r = \frac{MW_r \cdot V_r \cdot P}{R \cdot T} \qquad Eq\ 7$$

Where MW_r is the molecular weight of the gas(g)(hydrogen or oxygen), V_r is the volume of gas generated(H_2 or O_2) via electrolysis (L), P is the pressure (1 atm or 0.99 bar), T is the temperature (K), and R is the universal gas constant (0.0831 $L \cdot bar \cdot K^{-1} \cdot mol^{-1}$).

Theoretically, to produce 1 m^3 of hydrogen via water electrolysis at a potential of 2 V, the energy efficiency is about 61.5% assuming the complete transfer of electrons (100 % coulombic efficiency) (El-Emam & Özcan, 2019; Wang et al., 2014). The loss in energy efficiency is attributed to the additional energy needed to overcome the ohmic voltage loss and electrode overpotential. In addition, during water electrolysis, bubbles formed on the electrode surface can disperse in the electrolyte leading to high overpotentials and larger ohmic voltage drop within the cell. (El-Emam & Özcan, 2019; Wang et al., 2014). Moreover, in an undivided

cell crossover of gases can occur between the electrodes leading to the recombination of the hydrogen and oxygen, which can result in a parasitic current within the cell and disrupt the gas production rates, thereby reducing the energy efficiency of hydrogen production(Godula-Jopek, 2015; Wang et al., 2014). To mitigate this, diaphragms or separators are usually employed; the diaphragm must be porous and should have good chemical stability. Generally, for an alkaline water electrolyzer, an anion exchange membrane is usually employed to facilitate the transport of hydroxide ions, and in the case of a polymer electrolyte membrane electrolyzer, a proton conducting membrane is used, that acts as a solid electrolyte and a separator (Godula-Jopek, 2015; Holladay et al., 2009).

Moreover, the thermodynamic decomposition voltage is a function of the temperature and, thus, the efficiency, i.e., at higher electrolyte temperatures, the decomposition voltage decreases as the free energy decreases. Hence lower electrical energy is required to sustain the process (Godula-Jopek, 2015). This is also illustrated in Figure 1.

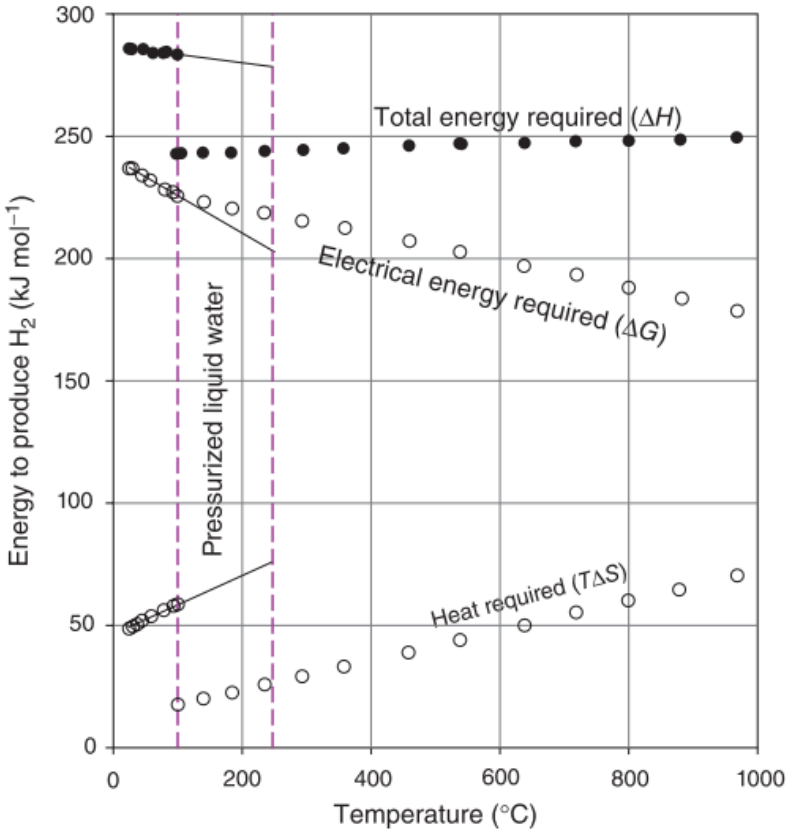

Figure 1: ΔG(T), ΔH(T) and TΔS(T) of the water splitting reaction at P = 1 bar (Godula-Jopek, 2015)

The type of electrode is an important factor as the overpotential required to drive the OER depends on the inherent properties of the anode; these include conductivity, chemical stability in extreme conditions, and high activity(Marco Panizza & Cerisola, 2009; Wang et al., 2014). Further, studies have been conducted to improve the efficiency of electrolytic hydrogen production by employing electrode materials with lower overpotentials and also by increasing the cell operating temperatures(Godula-Jopek, 2015; Grigoriev et al., 2006). For instance, alkaline water electrolysis makes use of Ni-based alloys for both cathode and anode materials as they are cost-effective, have relatively high stability in alkaline conditions, and they provide active sites for the cathodic evolution of hydrogen(Khan et al., 2018; Zhou et al., 2020). At present, the most dominant type of electrolysis technology is alkaline water(AWE) electrolysis, with research and development being conducted on Polymer Electrolyte Membrane (PEM) electrolyzers and Solid Oxide Electrolyzers (SOE) (Dincer & Acar, 2014; Ji & Wang, 2021).
In addition to the electrode material properties, the composition of the water source used for electrolysis also affects the efficiency of hydrogen production. Generally, for PEM and AWE electrolysis, deionized water is usually employed to ensure that there is no loss in the coulombic efficiency of the HER as a result of side reactions that can occur due to the various anions and cations present in potable water(Amikam et al., 2018; Cho & Hoffmann, 2017). Previously conducted research on electrolysis of brine and seawater, which usually contain high chloride ion concentrations, showed that the chloride ions lead to the formation of Cl_2 chlorine gas at the anode(CLER); this competes for electrons with the OER as the CLER has faster kinetics compared to the OER since a transfer of only $2e^-$ are required(Bennett, 1980; Cho, Qu, et al., 2014; Dresp et al., 2019).

Moreover, the free chlorine can get hydrolysed at pH < 7.42 resulting in the formation of hypochlorous acid that dissociates to give chlorate ions at pH > 7.42(Cho, Qu, et al., 2014; Dresp et al., 2019). The chlorate ions formed are then reduced to chloride ions via the chlorate reduction reaction (CLRR) at the cathode; this is summarized in Eq 8 – Eq 11. Due to the reaction pathways of the CLER and CLRR, both the anodic and cathodic reactions result in the inhibition of the HER(Cho & Hoffmann, 2017). Because seawater is a potentially abundant source of water electrolysis, studies have been conducted to inhibit the CLER by using OER selective anode such as TiO_2 doped with MnO_2 that acts as a diffusive barrier for chloride ions on the electrode surface (Bennet, 1979). Amikam et al. 2018 investigated chlorine-free seawater electrolysis by simply dosing NaOH as OH^- ions inhibit the CLER, which prevents

the formation of hypochlorite ions; possibly due to the OH^- ions adsorbed on the surface of the electrode, which limits the mass transfer of Cl^- ions on the anode surface. In addition, the presence of divalent ions such as calcium (Ca^{2+}) and magnesium (Mg^{2+}) can also lead to a decrease in the production of hydrogen. Considering the cathodic reactions, the consumption of protons to form hydrogen results in a localized increase in pH. The increase in pH can cause the precipitation of $Mg(OH)_2$ and $Ca(OH)_2$ on the cathode surface; the surface precipitates form an insulating layer which inhibits the transfer of electrons to the H^+ ions for H_2 generation(Dresp et al., 2019).

Chlorine oxidation and chlorate reduction reaction

Anodic Reaction

$2Cl^- \rightarrow Cl_2 + 2e^-$ $E^0 = -1.36$ *Eq 8*

Cathodic Reaction

$ClO^- + H_2O + 2e^- \rightarrow Cl^- + 2OH^-$ $E^0 = 0.81$ *Eq 9*

Hydrolysis of Chlorine

$Cl_2 + H_2O \rightarrow HOCL + Cl^- + H^+$ *Eq 10*

$HOCl \rightarrow OCl^- + H^+$ $pH > 7.42$ *Eq 11*

1. Literature Review

1.1 Existing research on hydrogen production wastewater/seawater as electrolyte

Concerning hydrogen production via wastewater electrolysis, research has been conducted using industrial and municipal effluent as a water source. Treated wastewater effluents, in general, have a low electrical conductivity of about 0.98-1 mS/cm(Rietveld et al., 2011) and a high COD. To minimize the ohmic voltage drop within the electrochemical cell, a conductivity of at least 20-30 mS/cm would be required. Thus, a supporting electrolyte is generally employed to make wastewater suitable for electrolysis. These include NaCl, $NaClO_4$, Na_2SO_4, and H_2SO_4. NaCl is preferred because the free chlorine and corresponding chlorine radicals generated can oxidize the organic pollutants and disinfect the water but can also generate chlorinated organics, which are carcinogenic and toxic to human health (Huang et al., 2016). In general, the electrochemical oxidation of organic pollutants at the anode can be explained via direct and indirect pathways(Cho, Qu, et al., 2014; Marco Panizza & Cerisola, 2009). In direct electrolysis, the pollutants are oxidized after adsorption on the surface of the anode, i.e., oxygen is transferred from water to the organic pollutant using electrical energy. In this reaction, water is the source of oxygen atoms for oxidation, and the protons generated from the pollutant oxidation are discharged at the cathode to produce hydrogen. This is better described in (Eq 12-15), with a simple aromatic compound such as phenol as an example. This would also apply to other organic molecules as well.

Direct pathway for oxidation of phenol

Anodic Reaction

$C_6H_5OH + 11H_2O \rightarrow 6CO_2 + 28H^+ + 28e^-$ *(on surface of anode)* *Eq 12*

$2H_2O_{(l)} + 2e^- \; -> \; O_{2(g)} + 4H^+ + 4e^-$ *(source of oxygen for pollutant oxidation)* *Eq 13*

Cathodic Reaction

$28H^+ + 28e^- \rightarrow 14H_2$ *Eq 14*

$2H^+ + 2e^- \rightarrow H_2$ *Eq 15*

Now via the indirect pathway, surface-bound reactive oxygen species (ROS) such as *OH radicals are formed on the anode as intermediates in the oxygen evolution reaction during water splitting, these intermediates can themselves oxidize organic pollutants via direct oxidation of pollutants(Eq 21-22), or the ROS can react with chloride in wastewater(if present naturally or

added as electrolyte). This results in the formation of reactive chlorine species(RCS), such as free chlorine(FC) and chlorine radicals, similar to that of brine electrolysis. The mechanism is summarized in the following equations:-

Indirect Pathway for oxidation of pollutant 'R' on electrode surface S[](Marco Panizza & Cerisola, 2009)

Discharge of water molecule at the anode; generation of surface-bound radical

$S[] + H_2O \rightarrow S[^*OH] + H + e^-$ *Eq 16*

Oxidation of pollutant R by surface-bound hydroxyl radical

$S[^*OH] + R \rightarrow S[] + RO + H^+ + e^-$ *Eq 17*

OER on the anode surface

$S[^*OH] + H_2O \rightarrow S[] + O_2 + 3H^+ + 3e^-$ *Eq 18*

Cathodic reaction

$nH^+ + ne^- \rightarrow n/2\ H_2$ *Eq 19*

Indirect Pathway for oxidation of pollutant 'R' on electrode surface S[] via chlorine intermediates(Hyunwoong Park et al., 2009)

Anodic Reactions:

Discharge of water molecule at the anode; generation of surface-bound radical

$S[] + H2O \rightarrow S[^*OH] + H + e^-$ *Eq 20*

Reaction of surface-bound hydroxyl radical with chloride ions

$S[^*OH] + Cl^- \rightarrow S[OH\ ]Cl^{*-}$ *Eq 21*

Generation of chlorine radical

$S[OH\ ]Cl^{*-} + H_2O + H^+ \rightarrow S[] + 2H_2O + Cl^*$ *Eq 22*

Cathodic reaction

$nH^+ + ne- \rightarrow n/2\ H_2$ *Eq 23*

The electrode material also influences the reaction mechanism of pollutant oxidation, i.e., some favour partial oxidation of pollutants while others favour complete mineralization to CO_2. The electrode selectivity depends on the oxygen evolution reaction (OER) overpotential. Electrodes are active if they have a low OER potential, that is, they have high catalytic activity towards the OER and allow for only partial oxidation of organics, whereas non-active anodes have a high OER potential and low catalytic activity towards the OER; thus, these types of electrodes can facilitate complete oxidation of organics under the water stability region (without water splitting). Theoretically, it is possible to directly oxidize organics at low potentials before the oxygen evolution reaction. However, the reaction usually proceeds at a lower rate and is also usually accompanied by a reduction in the catalytic activity of the electrode due to the formation of a polymer layer on the electrode surface; for instance, the oxidation of 4-chlorophenol with BDD, the polymeric layer is believed to have hydroquinone and quinone monomeric units mimicking the structure of synthetic humic acids(Cañizares et al., 1999; Li et al., 2005; Rodrigo et al., 2001).

To this end, electrochemical oxidation of organics in wastewater has been conducted using various types of electrode materials. For instance, DSA(dimensionally stable anodes), comprised of a titanium base covered with a thin metal oxide layer, includes TiO_2/RuO_2 and TiO_2/IrO_2 anodes as they have good conductivity and good catalytic activity towards the OER and CLER, respectively. The general mechanism associated with this electrode is the indirect oxidative pathway. Due to the low OER overpotential, these anodes are relatively active; hence they favour the OER. As a consequence, the electro-combustion of organics usually has low coulombic efficiency, and complete organics combustion is not observed(Cavaliere et al., 2021). However, studies have reported that DSA anodes have the potential to be used for organics oxidation via the generation of chlorine radicals, i.e., in chloride-rich wastewater or chloride-containing electrolytes (Cho & Hoffmann, 2017).

Boron Doped Diamond (BDD) is also extensively used as an anode for organics oxidation mainly because it has a wide potential window because the OER begins at 2.3V; it is a non-active anode hence it allows for indirect organics oxidation via hydroxyl radical generation, which can non-selectively oxidize organics to CO_2. Studies have reported that BDD can be used efficiently to mineralize a range of organic pollutants such as carboxylic acids, herbicides,

phenolic compounds, pharmaceuticals, textile dyes, and wastewater organics with close to 100% coulombic efficiency (Panizza et al., 2001). Moreover, a study conducted by Jiang et al., 2008 showed that it is possible to have simultaneous hydrogen production and organics oxidation in a wastewater electrolysis cell with BDD as the anode and stainless steel cathode. However, due to the high cost of BDD and the requirement of expensive metals such as tantalum, niobium, and tungsten as a substrate for the deposition of the diamond layer, scale-up operations become largely limited.

Carbon and graphite electrodes have also been studied for the anodic oxidation of organics majorly because carbon-based electrodes are readily available, relatively cheap, and possess a large surface area that can combine both adsorption of organic pollutants and degradation on the electrode surface. Studies conducted by Fan et al., 2008 on the use of activated carbon fibres for the degradation of amaranth showed that the electrode was able to cleave the azo bond but was not able to completely mineralize the intermediates formed, i.e. COD and TOC removal efficiencies were approximately 20% and 35%, respectively. Furthermore, a similar study using activated carbon fibre anodes for the electrochemical degradation of alizarin red also reported that the electrode was able to efficiently remove colour (98% removal) with only 76.5 % COD removal(Yi & Chen, 2008).

A drawback concerning carbon anodes is that they usually undergo surface corrosion at higher potentials, thereby reducing the durability and increasing the electrode resistance. However, studies conducted on the impact of corrosion conditions on carbon paper electrodes reported that though surface corrosion occurs, the electrocatalytic activity of the electrode remains largely unchanged or, in some conditions, increased the electrocatalytic activity of the anode due to an increase in surface area of the anode as a result of corrosion(Nourani et al., 2019). With respect to water electrolysis, the application of carbon fibre anodes could increase the energy efficiency of hydrogen production as the electrodes exhibit an OER overpotential of 1.7 V similar to that of platinum(Fan et al., 2008; Panizza & Cerisola, 2009). Hence, lower input energy is required for electrolytic hydrogen production, provided the hydrogen gas generated is of sufficient purity.

Another inexpensive electrode that is employed for the oxidation of organics is lead dioxide (PbO_2). It is easy to prepare, has good conductivity, a large surface area, and good chemical

stability. They have been extensively used to oxidize several kinds of organic compounds, such as synthetic dyes, landfill leachates, anionic surfactants, tannery wastewater, phenolic compounds, and organic acids. Similar to BDD, this electrode also favours the formation of hydroxyl radicals due to its high OER potential of 1.8 -1.9V (Yeo et al., 2010). As a result, PbO_2 can also non-selectively oxidize organics with relatively good TOC removal efficiencies in the range of 75% - 83%(Panizza & Cerisola, 2009). Though very promising for organics oxidation, studies have reported that PbO_2 is not very stable in alkaline conditions and can lead to the release of toxic lead ions(Bock & MacDougall, 1999). This limits the applicability of the electrode for simultaneous organics oxidation and hydrogen production under conditions of alkaline water electrolysis.

Studies conducted on wastewater electrolysis showed that the presence of organic acids, such as volatile fatty acids generated in fermented wastewater, can potentially enhance hydrogen production and energy efficiency(Eker & Kargi, 2010; Kargi & Catalkaya, 2011b).In a study conducted by using vinegar fermentation wastewater and olive mill wastewater, it was observed that the VFA's generated via fermentation dissociated to give H^+ ions while electrons were provided by the anodic oxidation of the metal electrodes(Fe or Al) upon application of DC voltage(Kargi & Catalkaya, 2011b). The protons and electrons then combine at the cathode to produce hydrogen. The reaction is summarized below:-

Anodic Reaction

$$Fe \rightarrow Fe^{+2} + 2e^- \qquad \text{Eq 24}$$

Dissociation of VFA

$$CH_3COOH \rightarrow CH_3COO^- + H^+ \qquad pH > 3 \qquad \text{Eq 25}$$

Cathodic Reaction

$$nH^+ + ne^- \rightarrow n/2\ H_2 \qquad \text{Eq 26}$$

1.2 Overview of existing research

An overview of literature pertaining to hydrogen production from various water sources is shown in Table 1.

Table 1: Overview of literature concerning water and wastewater electrolysis cell(WEC) for H_2 production

Author	Water Type	Electrochemical cell specifications	Electrolyte	Figures of Merit
(Amikam et al., 2018)	Seawater	Anode: Ti/TiO_2-IrO_2-RuO_2(DSA) Cathode: Ni200 Plate	NaOH/NaCl electrolyte	[a]Energy Efficiency = 53 [b]Coulombic Efficiency= 76% Applied Current = 470 A/m^2
(Cho & Hoffmann, 2017)	Municipal wastewater	Anode: BiO_x/TiO_2 Cathode: AISI 304 stainless steel	NaCl	Energy Efficiency = 23% Coulombic Efficiency= 80% Applied Current = 200 A/m^2
(Cho, Kwon, et al., 2014)	Untreated Human Waste	Anode: BiO_x/TiO_2 Cathode: AISI 304 stainless steel	NaCl	Energy Efficiency = 15% Coulombic Efficiency= 50% [c]H2 molar production rate = 15 µmol/min Applied Current = 96 A/m^2
(Cho, Qu, et al., 2014)	Municipal wastewater	WEC coupled PV cell Anode: BiO_x/TiO_2 Cathode: AISI 304 stainless steel	NaCl	Energy Efficiency = 18% Coulombic Efficiency= 44.8% H2 molar production rate = 5.02 µmol/min Applied Current =66.7 A/m^2
(Eker & Kargi, 2010)	Untreated Industrial Wastewater	WEC coupled PV cell Anode: Stainless Steel Cathode: stainless steel	NaCl	Energy Efficiency = 92% H2 molar production rate = 0.5 mmol/min.
(Grigoriev et al., 2006)	Ultrapure Water	PEM Electrolysis Anode: Ir, RuO_2, Cathode: Pt/C or Pd/C	Solid Polymer electrolyte	Energy Efficiency = 95.1% H2 productivity = 1-2 m^3/h (lab Scale) up to 100 m^3/h (R&D scale) Applied Current = 1 A/m^2
(Hyunwoong et al., 2008)	Synthetic Wastewater (Phenol as a pollutant)	WEC coupled PV cell Anode: BiO_x/TiO_2 Cathode: AISI 304 stainless steel	NaCl	Energy Efficiency = 50 .5% Coulombic Efficiency= 86% H2 molar production rate = 86 µmol/min. Applied Current = 3.1 A
(Jiang et al., 2008)	Synthetic wastewater (Phenolic pollutants)	WEC-based cell Anode: BDD (Boron Doped Diamond) Cathode: stainless steel	Na_2SO_4	COD removal = 90% Coulombic Efficiency= 90% H2 molar production rate (in Na2SO4) = 0.91 mmol/min Applied Current = 2.49 A
(Kargi & Arikan, 2013)	Vinegar Fermentation Wastewater	WEC-based cell Anode: Aluminium Cathode: Aluminium	NaCl+ Al scrap	COD removal = 10.5% Energy Efficiency = 74% H2 molar production rate = 27.8 µmol/min

				Applied Current =0.1 A
(Kargi & Catalkaya, 2011b)	Olive Mill Wastewater	WEC-based cell Anode: Aluminium Cathode: Aluminium	Olive Mill WW	COD removal = 44% Energy Efficiency = 65% H2 molar production rate = 17.3 µmol/min Applied Current = 0.06 A
(Kargi et al., 2011)	Anaerobic Waste Sludge	WEC-based cell Anode: Aluminium Cathode: Aluminium	waste sludge (VFA)	COD removal = 84% Energy Efficiency = 75% H2 molar production rate = 19.4 µmol/min
(Kim et al., 2013)	Synthetic Wastewater (Urea) Human Urine	WEC coupled PV cell Anode: BiO_x/TiO_2 Cathode: AISI 304 stainless steel	NaCl	Urea Degradation =80% Energy Efficiency = 8% Hydrogen Production rate = 1.75 µmol/min Applied Current = 0.03 A
(Hana Park et al., 2013)	Municipal Wastewater	WEC coupled PV cell Anode: BiO_x/TiO_2 Cathode: AISI 304 stainless steel	NaCl	COD Removal = >90% Energy Efficiency= 64% Coulombic Efficiency=87% Hydrogen production rate= 83.3 µmol/min Applied Current = 5 A/m^2
(Hyunwoong Park et al., 2009)	Synthetic Organic Aqueous Pollutants (Phenolic Compounds and Acids)	WEC (three Electrode Setup) Anode: BiO_x/TiO_2 Cathode: AISI 304 stainless steel X 2	NaCl/Na_2SO_4	Energy Efficiency = 45-50% (in NaCl); 55-75%(Na2SO4) only for Phenol Hydrogen Production Rate = 100 µmol/min (Na2SO4) Organics removal: Phenol >95% Benzoic Acid 10% Salicylic acid 40% Applied Current = 147 A/m^2
(Hyunwoong Park et al., 2012)	Synthetic Wastewater (Phenol as a pollutant)	WEC coupled PV cell Anode: BiO_x/TiO_2 Cathode: AISI 304 stainless steel	NaCl	Phenol Degradation: 40% Hydrogen Production rate: 0.25 mmol/min
(Lu et al., 2020)	Synthetic Industrial Wastewater (Aniline as a pollutant)	WEC based Cell Anode: Carbon paper Cathode: Platinum (Pt foil)	H_2SO_4	Coulombic efficiency: > 95% Hydrogen production: 6.7 µmol/min Applied Current = 300 A/m^2
(Ma et al., 2014)	Synthetic Wastewater (Phenol as a pollutant)	WEC based Cell Anode: Ti/IrO_2– RuO_2 Cathode: Platinum (Pt foil)	Na_2SO_4	COD removal = 90% Phenol Degradation = >95% Energy Efficiency = 50% H2 molar production rate (in Na2SO4) = 84 mmol/min Applied Current = 0.5 A
(Pathak et al., 2020)	Textile Industry Wastewater	WEC based Cell Anode: Carbon/SS/Pt Cathode: Carbon	Wastewater (Dye polluted)	COD Removal: Carbon (55%); SS (80%); Pt (80%) Energy Efficiency : Carbon anode (49.6%) ; SS(67.8%) ;Pt(57.1 %) Hydrogen Production rate:36

				µmol/min (Carbon) ; 23 µmol/min(SS); 30µmol/min(Pt) Applied Current = 7.6 A
(Ojaomo et al., 2020)	Brine	WEC-based cell Anode: Aluminium Cathode: Aluminium	NaCl present in Brine	Hydrogen Production rate: 3.75 mmol/h Energy Efficiency= 12.7% Applied Current = 12 A
(Marzo et al., 2012)	UF, UV disinfection, and Membrane Distillation Treated Wastewater	PEM Electrolysis Anode: Ir (Iridium) Cathode: Pt (Platinum)	Solid Polymer electrolyte	Hydrogen production rate: 0. 52 mol/min
(Tufa et al., 2018)	Reverse Electrodialysis Treated (SO^{2-}_4 rich Industrial Wastewaters)	AWE-based cell Anode: Ni foam Cathode: Ni foam	Na_2SO_4	Hydrogen Production Rate: 0.75 mol/min Applied Current = 0.11 A/m^2
(Dubey et al., 2010)	Distilled Water	AWE Based Cell Anode: Carbon Nanotube Cathode: Pt	NaOH	Hydrogen Production: 0.27 mol/min/m2 Applied Curent = 101 A/m^2
[a]Energy Efficiency is defined as per Eq 5 **[b]Coulombic Efficiency is defined as per Eq 6** **[c]Hydrogen production rate calculated as per Eq 7**				

1.3 Discussion

From Table 1, it is evident that significant research has been conducted on the electrolytic production of hydrogen using wastewater of different compositions. Hydrogen production using wastewater electrolysis was focused more on pollutant oxidation rather than water splitting for the generation of pure hydrogen. In addition, the energy efficiencies obtained for wastewater electrolysis were lower than conventional alkaline water electrolysis(Cho & Hoffmann, 2017). Considering the information provided in the literature, the requirements for wastewater for hydrogen production are as follows:-

- Sufficient conductivity
- Easily available
- Organic matter (only if the COD is high, at least 200 mg /L of COD should be present if the hydrogen production is to be significantly affected)

With this criterion in mind, municipal effluent/sewerage (treated wastewater)is selected in this study. The general composition of municipal effluent/sewerage obtained is summarized in Table 2. Though the COD is much lower than previously discussed (range of 20 – 40 mg O_2/L),

the focus would be more on hydrogen production via water splitting rather than organics oxidation. Moreover, it is hypothesized that hydroxyl radicals (OH^*) generated as a precursor to the OER during water splitting could result in partial oxidation of the COD. Hence, high COD though an advantage (if the oxidation of organics was the focus), may not be a major requirement for the current investigation.

Table 2 Average Water Composition of Municipal Effluent in The Netherlands(Terneuzen DECO Plant, Gkoutzamani, Ioanna, 2019)

Parameter	**Unit**	**Value**
Temperature	°C	16
TOC(Total Organic Carbon)	mg/L C	10
COD(Chemical Oxygen Demand)	mg/L O_2	28
BOD 5 (Biochemical oxygen Demand after 5 days)	mg/L O_2	1.1
DOC - Dissolved	µg/L C	8972
DOC - HOC, hydrophobic	µg/L C	1154
DOC - CDOC, hydrophilic	µg/L C	7817
CDOC - Humic substances (HS)	µg/L C	4256
Chloride	mg/L Cl	300
Sulfate	mg/L SO4	82
Calcium	mg/L Ca	67
Magnesium	mg/L Mg	21
Iron	mg/L Fe	0.05

Municipal effluent/sewerage is a promising water type because, after treatment, this water meets the above criteria (Table 2); it satisfies the requirements of freshwater and would otherwise be discharged. Secondly, because it is discharged from wastewater treatment plants, the water is easily accessible and sufficiently abundant. According to CBS, in the year 2019, approximately 1700 million cubic meters of treated effluent was discharged into surface water bodies from wastewater treatment plants(CBS, 2022). Moreover, from the literature survey, it was observed that the majority of the studies on electrolytic hydrogen production employ either synthetically produced wastewater or untreated wastewater directly(Table 1), i.e. the water sources have a high COD in order of (100 – 800 mg/L), and a high biodegradability (BOD/COD ≈ 0.3 – 0.8) as the H_2 production is dependent on the oxidation of organics(Marco

Panizza & Cerisola, 2009). In contrast, municipal effluent has a low COD (20-40 mg/L), and the composition of organics in municipal effluent is likely to contain recalcitrant organics such as trinitrobenzene, chlorophenol, sodium benzyl sulfonate, humics, pharmaceuticals, and azo dye molecules (Jiang et al., 2008; Yacouba et al., 2021).

Since an electrochemical technique is employed, biodegradability may not be an important parameter as the reactive oxygen species, such as hydroxyl radicals or reactive chlorine species generated during the electrolytic water splitting, can mineralize the recalcitrant organics(Jiang et al., 2008; Ma et al., 2014). However, the mechanism and the oxidation of these organics are dependent on the electrolyte and the type of anode used. *Furthermore, based on the literature survey, studies using municipal effluent for electrolytic hydrogen production are not extensively available*. The studies that do utilize municipal wastewater(influent) usually treat the water using membrane filtration, electrodialysis, or membrane distillation before electrolysis, and the treated water is then electrolyzed using PEM electrolysis or Alkaline electrolysis(Marzo et al., 2012; Hana Park et al., 2013). The utilization of municipal effluent could serve as a novel approach for electrolytic hydrogen production as both water reusability, and energy storage needs can be addressed. The utilization of municipal effluent also contributes to the circular economy, i.e., a resource of negative economic value (municipal effluent) is being converted to a resource with a higher economic value i.e.an an energy carrier (H_2) is produced from wastewater.

It is also apparent from Table 1 that NaCl is used as an electrolyte for wastewater electrolysis for the majority of studies because chlorine radical species can be generated at the anode due to the presence of Cl^- ions(Eq 21 and Eq 22), the generated chlorine radical species oxidize organic substrates which in turn provide protons for HER(Kargi & Catalkaya, 2011b; Kim et al., 2013; Hana Park et al., 2013). According to (Cho & Hoffmann, 2017), the coulombic efficiency of HER is dependent on the current density applied in the cell and the conductivity of the solution determined by the electrolyte concentration, in this case, NaCl. Though organics degradation and hydrogen production are observed, the efficiency is much lower than conventional alkaline water electrolysis. Also, there is a possibility of the formation of chlor-organics in the WEC system, which is a drawback concerning water reusability(Huang et al., 2016; Hana Park et al., 2013).

In an effort to improve the efficiency of hydrogen production and also the conductivity of wastewater KOH or NaOH could potentially be used as an electrolyte. Both KOH and NaOH are used as an electrolyte that can inhibit the generation of free chlorine; however, the conductivity of KOH solution is higher than NaOH as K^+ ions are less likely to form hydration spheres compared to Na^+ ions, i.e. K^+ has higher activity in the solution hence higher conductivity; thus KOH is preferred over NaOH(Ho et al., 2001). *Moreover, wastewater electrolysis for hydrogen production using KOH as an electrolyte is not extensively studied in terms of organics removal, hydrogen production, and the composition of the spent water-electrolyte solution after electrolysis*. As mentioned previously, the type of electrode also influences hydrogen production on the basis of electrode durability, conductivity, and, most importantly, energy consumption in terms of the OER overpotential required. A variety of electrodes have been studied for the purpose of pollutant oxidation, such as IrO_2, RuO_2, PbO_2, Pt, and Pd. Though these electrodes can easily oxidize pollutants at low OER overpotentials, they major issue arises with respect to scalability for commercial application(Cho, Kwon, et al., 2014; Cho & Hoffmann, 2017), the fact that platinum group metals(Ru, Ir, Pd) are required further limits commercial application as these materials have a low abundance and high costs.

Now concerning wastewater electrolysis, it is observed from Table 1 that TiO_2/BiO_x is widely used as the anode and SS as the cathode coupled with NaCl as the electrolyte. The active surface sites on the anode allow for CLER, which allows for mediated organics oxidation via RCS. The corresponding protons are then reduced at the cathode for HER. Further, electrodes such as boron-doped diamond (BDD) and carbon fibre have also been studied for the direct oxidation of organics, i.e. on the surface of the electrode(Eq16 – Eq19), and have been shown to completely mineralize recalcitrant organics at low overpotentials and provide high current densities(Fan et al., 2008; Jiang et al., 2008; Marco Panizza & Cerisola, 2009). In addition, a study by (Dubey et al., 2010)showed that carbon-based multiwalled nano tube anodes have the potential to produce hydrogen at the cathode at a low overpotential comparable to Pt electrodes. Moreover, for this study, hydrogen production using carbon fibre anodes electrodes seems to be more promising as the OER overpotential of carbon fibre anode is 1.7V, and for BDD, it is 2.3V, also considering the composition of municipal effluent, the contribution of organics oxidation to hydrogen production may not be significant due to low COD, thus the focus would be more on hydrogen production via water splitting rather than only pollutant oxidation. The low biodegradability indicates the presence of recalcitrant organics such as humics, phenols,

pharmaceuticals (acetaminophen , diclofenac, or ibuprofen)(Yacouba et al., 2021). Carbon fibre electrodes would satisfy the requirement of both pollutant oxidation(recalcitrant organics) and hydrogen production due to low OER overpotential, good conductivity, and high surface area. Furthermore, for Conventional alkaline water electrolysis, Ni-based alloys are generally employed due to their good chemical stability in alkaline conditions, low cost, and high activity towards the oxygen evolution reaction(Godula-Jopek, 2015; Khan et al., 2018; Zeng & Zhang, 2010). *However, studies on the application of carbon fibre anodes or Ni-foam anodes for wastewater electrolysis for H_2 production are very scarce.*

1.4 Focus of this Study

In consideration of the knowledge gaps discussed previously, the aim of this study is to investigate hydrogen production in a flow cell electrolyzer using municipal effluent as the water source. Subsequently, based on the water quality data obtained for municipal effluent, humic substances represent a significant amount of the chemical oxygen demand and the dissolved organic carbon in the water. Hence, in this study, humic acid has been selected as the model organic pollutant for anodic oxidation/degradation. Further, the electrolysis experiments will be conducted using carbon fibre and Ni-foam as the anode. The following research questions will be focused on during this study.

RQ1: How is hydrogen production affected in an STP effluent electrolysis cell if KOH is used as a supporting electrolyte for the electrolysis of synthetic and real municipal effluent?
RQ2: What is the extent of humic acid oxidation at the carbon fibre and Ni-foam anode when used in a wastewater electrolysis cell?
RQ3: What is the fate of the humic acid molecules in the solution after electrolysis?
RQ4:How does the electrolysis performance compare with conventional alkaline water electrolysis with Ni-foam as both the anode and cathode in the electrolysis cell?
RQ5:How is the energy efficiency for hydrogen production affected when carbon fibre or Ni-foam is used as the anode to electrolyze synthetic effluent and real municipal effluent?
RQ6: How can this electrolysis technique be integrated with existing wastewater treatment plants?

2. Introduction

The arrival of the industrial revolution in the 18th century paved the way for the development and dissemination of a fossil fuel-based economy and energy sector. In recent years, the rising human population has led to an unprecedented increase in anthropogenic greenhouse gas (GHG) emissions (IPCC, 2022). Increased GHG emissions, mainly the increased CO_2 levels, have driven world governments to shift from the current fossil-fuels-based economy to a more sustainable and carbon-neutral economy. The subsequent mitigation strategies employed are focused on reducing the current CO_2 emissions such that the global temperature increase is limited to 2^o Celsius relative to preindustrial levels (IPCC, 2022). One of these mitigation strategies involves shifting the current fossil fuel-based energy sector to a more hydrogen-oriented sector (IEA, 2021; Marzo et al., 2012; Muradov & Veziroğlu, 2005).

Hydrogen is considered to be a versatile energy carrier and can potentially lead to the decarbonization of various industrial sectors such as transport, chemical production, and steel production (Bourne, 2012; Sharmila et al., 2020). Implementation of a hydrogen-based economy can contribute to a resilient and sustainable future, provided the hydrogen is produced via cleaner alternative renewable production methods; these include biohydrogen production using MEC(Microbial electrolysis cell), electrolysis coupled with solar photovoltaics, and also using dark fermentation and photo fermentation (Bourne, 2012; El-Emam & Özcan, 2019). The hydrogen produced via renewable energy sources is collectively termed green hydrogen (Dincer & Acar, 2014). Furthermore, the produced green hydrogen can also be used as a feedstock for the production of methane, ammonia, synthetic liquid fuels, and methanol(Bourne, 2012; Dresp et al., 2019). According to the net zero emissions strategy provided by the international energy association, it is estimated that by 2030 the number of plug-in hybrids and Fuel Cell Electric Vehicles(FCEV) will reach 320 million, and this number is expected to reach almost 2 billion by 2050 (IEA, 2021). In addition, this shift is also expected to reduce the emissions in the transportation sector from 8.5 Gt CO_2 in 2019 (pre-Covid 19) to 5.5 Gt CO_2 in 2030 and 0.7 Gt CO_2 by 2050(IEA, 2021).

At present, it is estimated that 96% of the world's hydrogen demand is satisfied via fossil fuel reforming, i.e., 48% of the hydrogen is produced from steam reforming, 30% from oil reforming,18% from coal gasification, and the remaining 4 % is provided by water electrolysis(Ji & Wang, 2021). However, a direct consequence of the fossil fuel-based

production techniques is the emission of CO and CO_2 gases into the atmosphere; stoichiometrically, steam methane reforming releases approximately 10 kg of CO_2 per kg of hydrogen produced. To put in perspective, the combined CO_2 emissions of fossil fuel-based hydrogen production techniques are about 830 Mt CO_2/year; this is equivalent to the combined annual CO_2 emissions of The United Kingdom, The Netherlands, and Australia, (IEA, 2021; Roser & Rosado, 2022). Moreover, due to diminishing fossil fuel reserves, ever-increasing energy demand, and climate change, the current fossil-fuel-based hydrogen production mechanism may not be feasible, taking into account the net zero emission strategy(Holladay et al., 2009; IEA, 2021). This has led to renewed interest in hydrogen production by electrolysis, majorly due to the fact that 99.9% pure hydrogen can be produced with a minimal carbon footprint compared to the current fossil fuel-based techniques. Currently, the most mature type of electrolysis technology is alkaline water electrolysis(AWE) which is used on the commercial scale for hydrogen production(El-Emam & Özcan, 2019; Holladay et al., 2009).

A possible solution to address the issue of CO_2 emissions, water reuse and clean hydrogen production is to employ wastewater electrolysis. Municipal or industrial wastewaters of sufficient conductivity (at least 20 mS/cm) could serve as an abundant electrolyte for the production of hydrogen at reasonable rates and energy efficiencies in a wastewater electrolysis cell(WEC)(Cho, Kwon, et al., 2014; Cho & Hoffmann, 2017). Further reduction in energy requirements can be obtained if the WEC is integrated with renewable energy sources such as solar photovoltaics and wind energy. A wastewater electrolysis cell(WEC), when implemented correctly, has the capability to produce hydrogen via water splitting and also allows for the anodic oxidation of organics in the wastewater via chlorine radicals or hydroxyl radicals (Cho & Hoffmann, 2017; Hana Park et al., 2013). The oxidation of organic carbon innately present in wastewater could also serve to enhance the hydrogen yield (Eker & Kargi, 2010; Kargi & Catalkaya, 2011b), for instance without water splitting, the oxidation of 500 mg/L COD could theoretically produce 31 mol H_2/ m^3 of wastewater electrolyzed. In general, the type of oxidation mechanism is very much dependent on the type of anode and the composition of the electrolyte(Marco Panizza & Cerisola, 2009). The two general mechanisms involved in the oxidation organics are as follows:- 1) direct mechanism, in which the pollutants are oxidized after adsorption on the surface of the anode, without the involvement of any substances other than the electron 2) indirect mechanism, in which the pollutants are oxidized via the generation of physisorbed, or chemisorbed radicals generated on the anode surface. The nature of the

radicals formed is dependent on the anode; that is, anodes which have high catalytic activity(active anodes) towards the oxygen evolution reaction will tend to form chemisorbed radicals, for example, IrO_2, RuO_2 ,$NiFeO_x$(Ni-Foam) and carbon fibre. On the other hand, the anodes with low catalytic activity towards the oxygen evolution reaction (non-active anodes) tend to form physisorbed radicals, for example, Boron Doped Diamond (BDD).
Moreover, the type of radicals generated is dependent on the composition of the electrolyte, i.e., if the dominant species in the electrolyte are chloride ions, the oxidation proceeds via chlorine radicals (Cl^*), and if the hydroxide ions (OH^-) are the dominant species, hydroxyl radicals would be the primary oxidant. It should be emphasized that though chlorine radicals can oxidize and disinfect the wastewater, there is a high possibility of the formation of chlorinated organics, which are carcinogenic. The application of NaOH or KOH can mitigate the formation of chlorinated organics as the supporting electrolyte instead of NaCl which is generally used in WEC's.

In this study, the WEC employed has a similar configuration to an AWE cell, consisting of an anode, cathode, and an anion exchange membrane, the water type employed for this study was municipal effluent. Municipal effluent generally conforms to freshwater quality, with only humic acid as the primary organic pollutant. Depending on the performance of the wastewater treatment plant, the concentration of humic acid can range from 20 mg O_2/L to 40 mgO_2/L. Herein, this research aims to investigate the electrolytic hydrogen production using municipal effluent with KOH as the supporting electrolyte using carbon fibre and Ni-foam as the anode. The volumetric hydrogen production rate, energy efficiency of hydrogen production and the extent of humic acid oxidation in terms of COD removal efficiency and TOC removal efficiency were assessed using synthetically prepared effluent containing 23.0 ± 2.1 mg O_2/L of humic acid and real municipal effluent with humic acid concentration ranging from 25 to 34 mg O_2/L of humic acid. The corresponding performance data pertaining to energy efficiency and volumetric hydrogen production rate was also compared with conventional alkaline water electrolysis.

3. Methodology

3.1 Materials

Synthetic wastewater was produced for the electrolysis experiments. The synthetic wastewater was produced using humic acid powder (Sigma Aldrich). A stock solution of 1 g/L HA was prepared, and the corresponding COD was measured for dilution calculations. To ensure the humic acid remains dissolved in the solution, the pH of the solution was maintained above 9 by dissolving the humic acid powder in 0.01M KOH (Sigma Aldrich) solution. Fresh solutions of 20 mg/L humic acids as COD were prepared for each experiment using the stock HA solution. For the supporting electrolyte, KOH was used, and corresponding dilutions were made for the experiments using a 5M stock solution. For the electrolyzer, one set of experiments was conducted using carbon fibre as the anode and nickel foam as the cathode, and in the second set of experiments, Ni-foam was used as both anode and cathode. The carbon fibre electrode was sourced from the fuel cell store; specifically, the electrode was a carbon fibre gas diffusion layer without a poly tetrafluoro ethylene (PTFE) coating manufactured by Sigracet. The cathode Ni-foam was prepared via thermal deposition of nickel and iron on nickel foam (Recemat BV, Netherlands) and was provided by the Applied Sciences Laboratory at TU Delft.

3.2 Electrochemical Flow Cell Reactor Setup

The experiments were conducted in a laboratory-scale flow cell electrolyzer. The flow cell consists of the following components: -

- Stainless Steel Back Plates
- Carbon Anode
- Ni-Foam Cathode
- Acrylic Spacers
- Selemion Anion Exchange Membrane

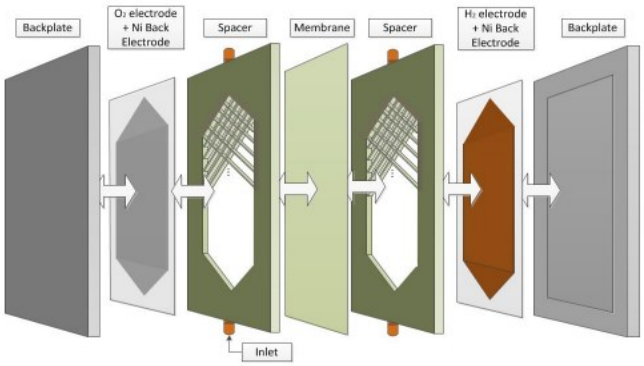

Figure 2: Exploded view flow cell (M M Bakker, 2018)

The flow cell components are illustrated in Figure 2, respectively. The acrylic spacers had a thickness of 8 mm and a geometric are of 87.6 cm^2, as depicted in Figure 2. The flow cell has two acrylic spacers for the anode chamber and the cathode chamber, resulting in a total fluid volume of 140 mL. The cathode and anode chambers of the cell were separated by an anion exchange membrane whose sole function was to prevent gas crossover within the cell. The corresponding stainless-steel plates in both the anode and cathode chambers consist of two protruding connection points, which were connected via alligator cables to a DC power supply

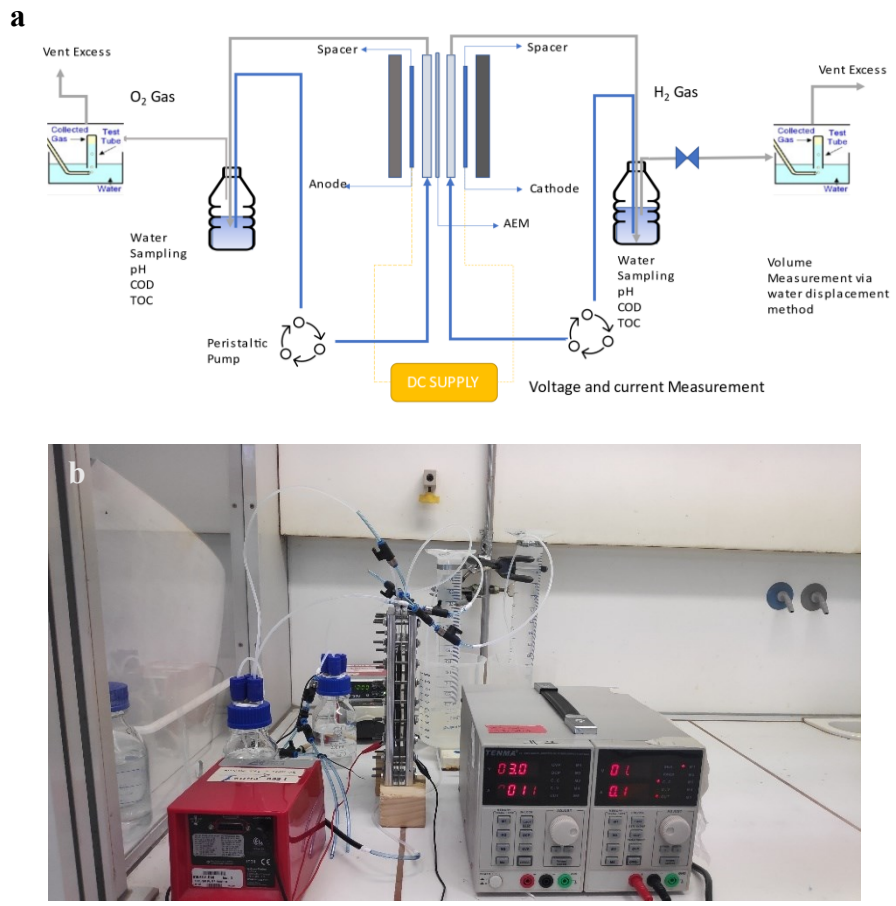

Figure 3: Overview of reactor setup a) Schematic; b) Lab setup

(Tenma Digital Control DC power supply). The inlet ports of both the spacers were connected via 1/8 inch OD tubing to a peristaltic pump (Watson Marlow 120U), whereas the outlets were connected to a reservoir that contains synthetically prepared wastewater. The reservoirs also functioned as gas separators; the collected gas within the reservoirs was then allowed to flow to a water displacement apparatus for volume measurement. The overall configuration of the electrolytic flow cell is shown in Figure 3

3.3 Cyclic Voltammetry

Cyclic voltammetry is an electrochemical technique used to investigate the reduction and oxidation of electrochemical species occurring on the electrodes in an electrochemical cell(Elgrishi et al., 2018). In general, the cyclic voltammogram traces consist of the applied potential on the x-axis and the corresponding current response on the y-axis. According to the IUPAC convention, the potential is scanned from left to right in increasing increments of potential. This is known as the forward scan, and the corresponding peaks in the voltammogram indicate the oxidation of a species at the anode. The potential is also scanned backwards from high potentials to low potentials(right to left) to complete the cycle, and the subsequent peaks observed in the backward scan of the voltammogram indicate a reduction process at the cathode. The rate at which the potential is scanned determines the thickness of the diffusion layer on the electrode surface; generally, at faster scan rates, the smaller the thickness of the diffusion layer, and, as a consequence, higher current responses are observed(Elgrishi et al., 2018). For this study, a scan rate of 400 mV/s was used at 40 mV increments to understand the redox mechanism of the humic acid molecule on the electrodes in the STP effluent electrolysis cell. Further, the electrochemical response of the carbon fibre anode and the Ni-foam anode in the presence of humic acid was investigated using cyclic voltammetry analysis. The analysis was done with 20 mg/L humic acids as COD in the presence of 0.1M KOH as the supporting electrolyte, and cell potential was scanned between 0V to 2V. All measurements were performed using an Ivium potentiostat controlled with the Iviumsoft software for a 2-electrode setup. In one case, carbon fibre was used as the working electrode, and in the second case, Ni-foam was used as the working electrode, whereas for the counter electrode, another Ni-foam electrode was used.

3.4 Electrolysis Experiments

The electrolysis experiments were essentially conducted in batch mode for all experiment sets. The experiments were divided into five sets. The first set of experiments was done for different electrolyte concentrations varying from 0.01M – 1M KOH at a limiting current density of 12.55 A/m^2 for 20 mg O_2 L humic acid. The second set of experiments was done at variable current densities ranging from 25 A/m^2 to 150 A/m^2 in 1M KOH as the supporting electrolyte for 20 mg O_2/L humic acid. The third set of experiments was conducted using real municipal effluent obtained from the Harnaschpolder water treatment plant. The first three sets were done for both carbon fibre as the anode as well as Ni-Foam as the anode; in addition, baseline experiments

were conducted to simulate conventional alkaline water electrolysis with Ni-foam as both anode and cathode.

The fourth set of experiments was conducted under potentiostatic conditions with carbon fibre anode for variable humic acid concentrations ranging from 20 mg O_2/L, 50 mg O_2/L, and 100 mg O_2/L. For this set, the cell potential was selected based on the redox peaks obtained in the cyclic voltammetry analysis. The fifth set was again conducted for humic acid concentrations of 20 mg O_2/L, 50 mg O_2/L, and 100 mg O_2/L using the Ni-foam anode under galvanostatic conditions.

3.5 Analytical Control.

For the aqueous phase analysis, the degradation of humic acid in the system was assessed using Chemical Oxygen Demand (COD) analysis and Total Organic Carbon (TOC) Analysis, respectively. For the sampling, both the anolyte and catholyte chambers were decanted completely, and 100 mL samples were extracted. COD analysis was performed on the samples after filtration through a 0.45 µm disc filter, the analysis was based on the dichromate digestion techniques using the Hach test kits (LCK 314), and the corresponding absorbance was scanned at 448 nm. For the TOC analysis, the samples were first diluted accordingly with demi water, the diluted samples were then filtered using a 0.45 µm disc filter, and the samples were analysed using the Shimadzu TOC-V CPH analyser.

Further, qualitative analysis of the samples was done using size-exclusion high-performance liquid chromatography (SEC-HPLC). The samples for HPLC were prepared by first filtering 5 mL of a sample through a 0.2 µm disc filter, then neutralized with an equal amount of 1M HCL solution; from the neutralized sample, 2 mL was taken for analysis. The SEC was conducted using a Phenomenex column (Yarra™ 3 µm SEC-2000, LC Column 300 × 7.8 mm), paired to a Shimadzu ultra-fast liquid chromatography (UFLC) system. The eluent used was 25% acetonitrile in ultrapure water with 10mM sodium phosphate buffer (pH 7). The flowrate of eluent was 1 mL/min, and an injection volume of 10 µL was used. Polystyrene sulfonate standards of molecular weights 3610Da, 1110Da, and 498Da, were used for calibrating the column. Separation of molecules was obtained for a 20 min duration, and the humic substances were identified using a UV detector at a wavelength of 254 nm. In addition, the samples were also analysed using a UV-vis spectrophotometer to assess the degradation of the humics after electrolysis. The samples were scanned from a wavelength of 190 – 500 nm. The pH and

conductivity of the solutions were recorded before and after electrolysis using WTW pH and conductivity probes.

For the gaseous products obtained, the volumetric production rate of oxygen and hydrogen was measured via the water displacement method using two inverted graduated cylinders. Lastly, the applied cell voltage and current were also recorded form the DC power supply.

4. Results and Discussion

4.1 Electrode Characterization

The electrochemical behaviour of the carbon fibre electrode and the Ni-foam electrode was assessed under two situations. Under the first situation, the response of the electrode was measured independently of the cell; electrode pieces were placed in 0.1M and 1M KOH solutions with 20 mg O_2/L humic acid as COD. The cyclic voltammograms for the same are depicted in Figure 4 and Figure 5. In the second case, the analysis was performed using the electrolyzer cell. The analysis was performed for 1M KOH solution with 20 mg O_2/L humic acid as COD; this is shown in Figure 6. For all cases, the analysis was done via cyclic voltammetry at a scan rate of 400 mV/s at 40 mV increments for a total of 3 scans.

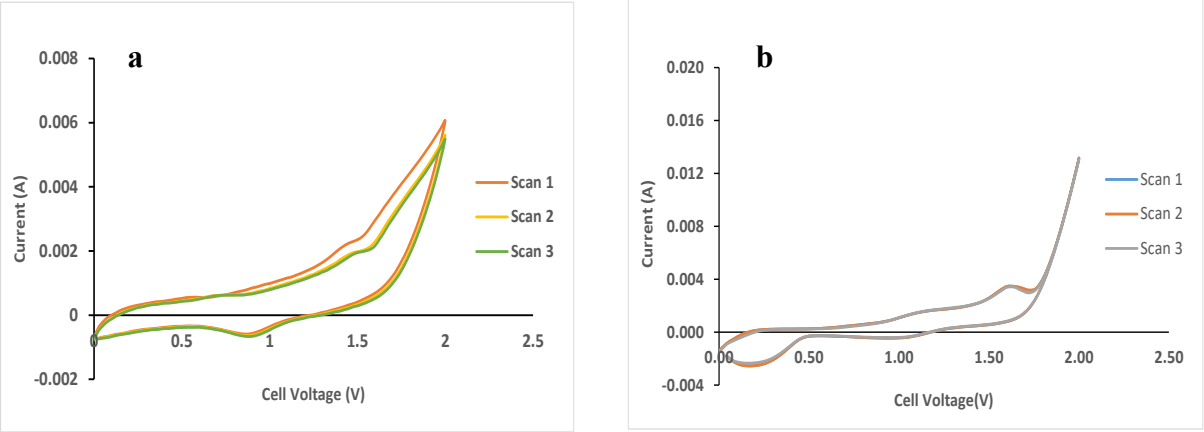

Figure 4 Cyclic Voltammogram 0.1M KOH 20 mg O_2/L humic acid a) Carbon Fibre b) Ni-Foam

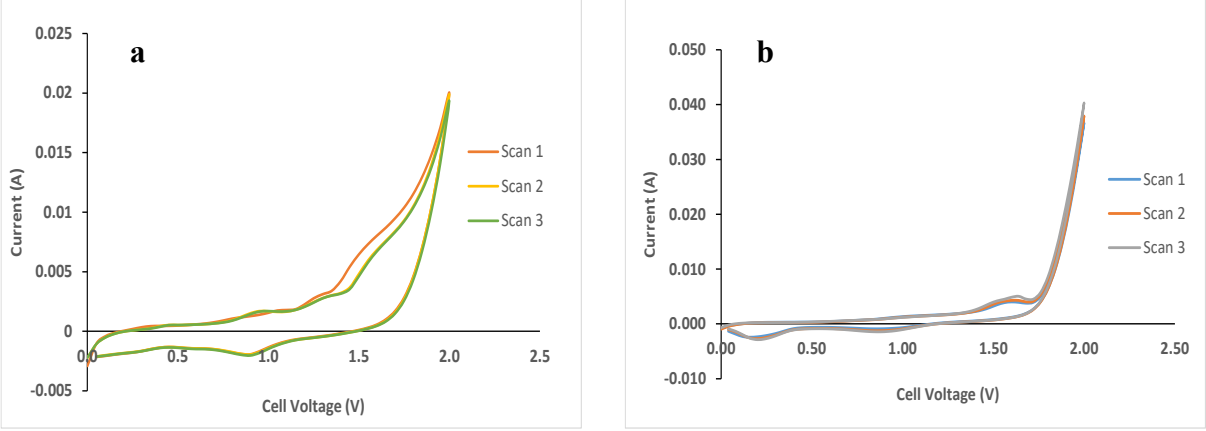

Figure 5 Cyclic Voltammogram 1M KOH 20 mg O_2/L Humic Acid a) Carbon fibre b) Ni-Foam

It is observed from the batch cyclic voltammograms of the carbon fibre electrode (Figure 4a and Figure 5a) that a peak occurs in the cyclic voltammograms between cell potential 1.55V and 1.67V, i.e., for the 0.1M KOH solution, the peak is observed at 1.55V whereas the for the

1M KOH solution the peak was observed at 1.6V. Similarly, when the Ni-foam anode was used, the peaks were obtained at 1.6V for both the 0.1M KOH solution and the 1M KOH solution(Figure 4b and Figure 5b). The sharp increase in the cell current observed after the peaks for both electrodes corresponds to the beginning of the oxygen evolution reaction(OER), i.e., under batch conditions, the OER potential for carbon fibre for 1M KOH was approximately 1.75 V, whereas the same for the Ni-foam electrode in 1M KOH was 1.72V.

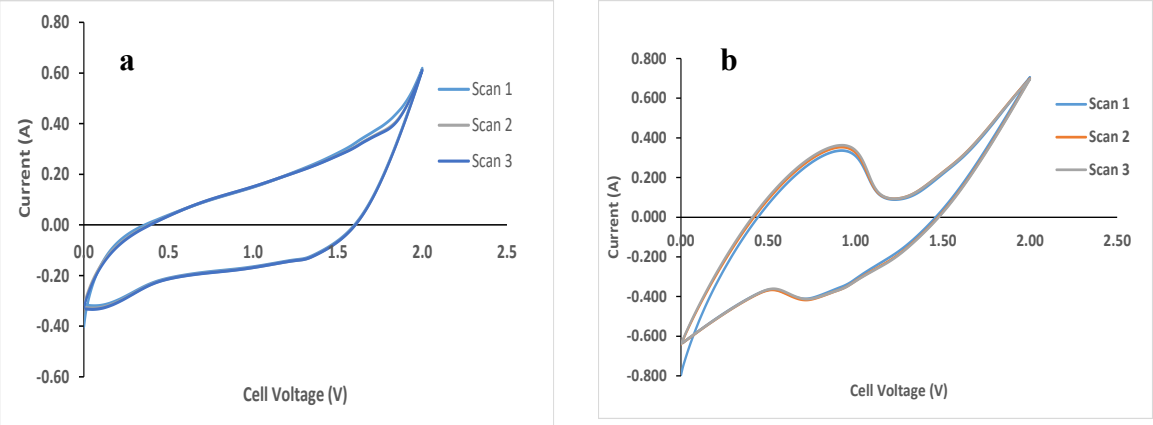

Figure 6 Cyclic Voltammogram 1M KOH 20 mg O_2/L (Flow Cell) a) Carbon Fibre b) Ni-Foam

Figure 6a and Figure 6b represent the cyclic voltammograms of both the carbon fibre anode and the Ni-foam anode when used directly in the flow cell electrolyzer. It is observed from Figure 6a that a peak occurs at approximately 1.72 V though not quite as apparent as the peaks obtained in Figure 4 and Figure 5a. In contrast, the peak obtained for the Ni-foam electrode was quite pronounced and was observed at a cell voltage of 0.93V. In addition, the OER potential recorded for the electrodes in the flow cell was approximately 1.82V for the carbon fibre electrode and 1.4V for the Ni-foam electrode. Subsequent linear sweep analysis conducted with a DC voltage supply in the flow cell with 1M KOH supporting electrolyte containing 20 mg O_2/L of humic acid showed that the corresponding OER potential for the carbon fibre anode was 1.7V and for the Ni-foam anode was 1.6V (Figure 7). The relatively low OER potential for the electrodes indicates that they are both active anodes; that is, they have high catalytic activity toward the oxygen evolution reaction.

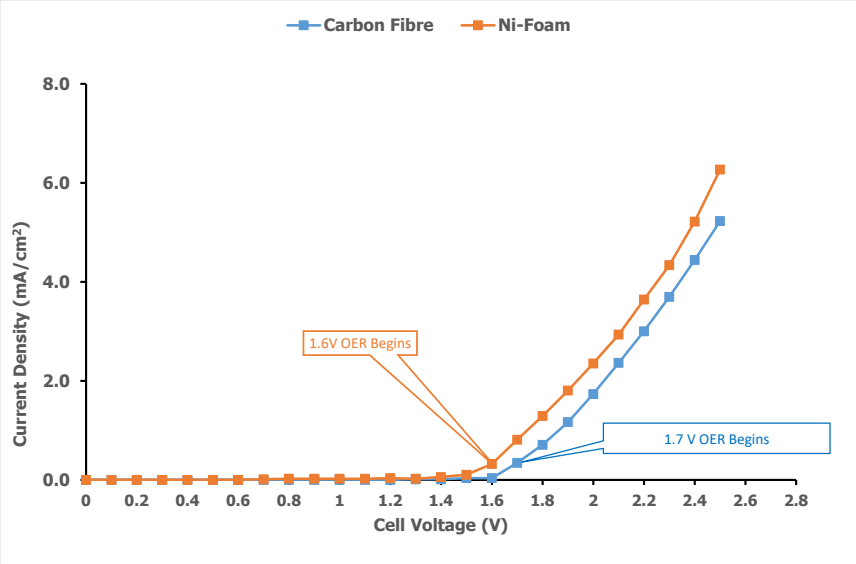

Figure 7 Linear Sweep DC Voltage Supply 1M KOH 20 mg O_2/L for Carbon Fibre and Ni-Foam Anodes

The nature of the cyclic voltammogram can be indicative of the oxidation mechanism of the organic pollutant, in this case, humic acid. Considering the behaviour of the Ni-foam electrode(Figure 6b), the pronounced peak could suggest that the humic acid molecule interacts with the anode surface resulting in a direct electron transfer for the oxidation of the humic acid molecules (Elgrishi et al., 2018; Marco Panizza & Cerisola, 2009). Though it is possible for direct electron transfer to occur, the peak in CV scans for the Ni-foam anode could most probably be attributed to the formation of nickel oxyhydroxide (NiOOH) as a result of anodic oxidation of Ni; this phenomenon is observed under alkaline conditions(pH > 8.5) based on the stability diagram of Ni-H_2O system(Kartikaningsih et al., 2017; Marcel Pourbaix, 1974). Further, because pronounced peaks were not obtained in the CV scans for the carbon fibre anode,

the dominant oxidation mechanism for the oxidation of humic acid molecules on both the anodes would likely be the indirect mechanism. i.e., reactive oxygen species(ROS) such as hydroxyl radicals generated as a precursor to the OER are responsible for mediating the electron transfer for the oxidation of the humic acid molecules(Fan et al., 2008; Vlaicu et al., 2011).

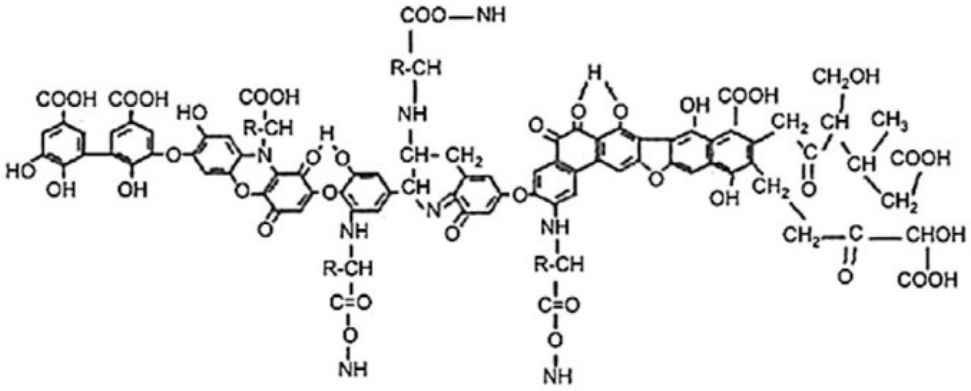

Figure 8 Model Structure of Humic Acid(De Melo et al., 2016)

Moreover, when assessing the anodic peaks in the voltammograms structure of humic acid molecules (Figure 8), it is important to consider the electron-accepting and donating moieties present. These include phenols, hydroquinones (electron-donating groups), and quinones (electron-withdrawing group). It is possible that the applied potential leads to the activation of the hydroquinone compounds in the humic acid molecules, which can lead to the formation of radical intermediates such as semiquinones (De Melo et al., 2016; Struyk & Sposito, 2001); this could also explain the presence of anodic peaks in the voltammograms represented in Figure 4, Figure 5 and Figure 6, respectively.

4.2 Effect of Electrolyte Concentration

4.2.1 Carbon Fibre Anode

The results for electrolysis of synthetic wastewater containing 20 mg O_2/L of humic acid using carbon fibre as the anode and Ni-foam as the cathode are represented in Figure 9 – Figure 14, respectively. The experiments were performed for a duration of 3 hrs under galvanostatic conditions at an applied current density of 12.55 A/m^2. The current density was calculated based on the equation for limiting current density given by Eq 27 and Eq 28.

$$J_{Lim} = n.F.k_m.C_{org} \qquad Eq\ 27$$

$$J_{Lim} = 4.F.k_m.COD \qquad Eq\ 28$$

In the above equations, k_m is the mass transport coefficient taken as 5.2 10^{-5} (m/s)(Liao et al., 2008), n is the number of electrons transferred in the mineralization reaction of the organic compound (mole e^-), C_{org} is the concertation of the organic molecule (mole C/m^3), F is Faraday's constant (96500 C / mole e^-), and COD is the chemical oxygen demand (mole O_2/m^3), respectively. Both Eq 27 and Eq 28 are representative of the limiting current density, the difference being that Eq 28 substitutes the concentration of the organic for the COD, and the corresponding number of electrons is replaced by 4 (mole e^-/mole O_2).

To serve as a baseline for comparison, conventional alkaline water electrolysis was also performed under the same conditions with demi water using Ni-foam as both anode and cathode within the flow cell. It is observed from Figure 9 that the energy efficiency of hydrogen production for wastewater electrolysis using the carbon fibre anode is significantly lower

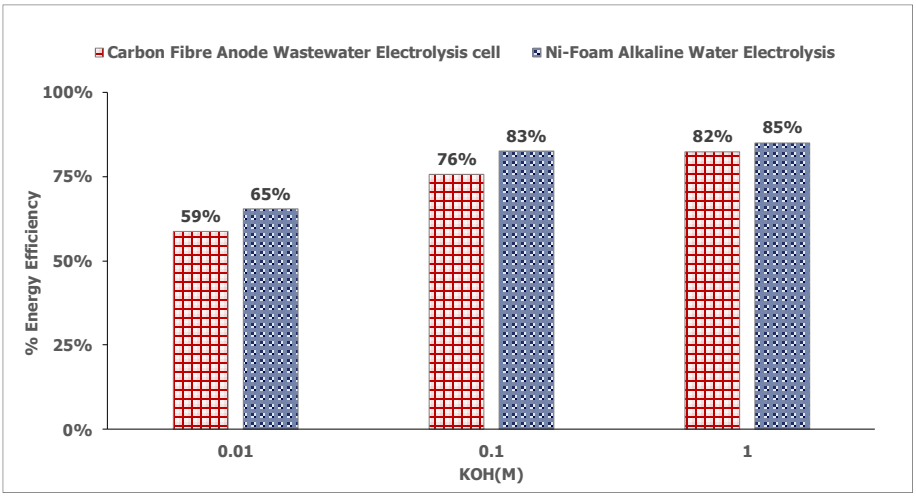

Figure 9 Effect of Electrolyte Concentration: Energy Efficiency

compared to conventional alkaline water electrolysis using Ni-foam electrodes. This can be attributed to the fact that the cell potential required to initiate the oxygen evolution reaction(OER) for the carbon fibre anode is 1.82 V, whereas, for the Ni-foam anode, the OER cell potential required was 1.72 V. Moreover, from Figure 9, it can be seen that the energy efficiency for both electrodes has an increasing trend with respect to the concentration of KOH in the solution. For the carbon fibre anode, the efficiency increased from 58 ± 1.2% for 0.01M KOH to 82 ± 1.2% for 1M KOH. Similarly, for the Ni-foam anode, the efficiency increased from 65 ± 6.5% at 0.01M KOH to 85 ± 7 % at 1M KOH. This trend is likely as the conductivity of the solution is dependent on the KOH concentration; the measured conductivity at 0.01M KOH was approximately 2.64 mS/cm and increased to 211 mS/cm for 1M KOH, i.e., the ohmic losses within the flow cell would be higher for an electrolyte with a lower conductivity lower for an electrolyte with higher conductivity.

The corresponding volumetric hydrogen production is represented in Figure 10. From the data, it is observed that the hydrogen production for the carbon fibre anode was, on average, approximately 0.81 ± 0.02 mL H_2/min for KOH concentrations varying from 0.01M to 1M. Subsequently, the volumetric hydrogen production obtained for conventional alkaline water electrolysis using Ni-Foam as the anode was, on average, 0.81 ± 0.07 mL H_2/min; these rates were compared with the amount of hydrogen that can be theoretically produced based on faradays law and the applied current density (J_{app}=12.55 A/m^2). The calculated volumetric hydrogen production rate was approximately 0.83 mL H_2/min at 25 ºC .

From Figure 10, it is evident that even though synthetic wastewater containing 20 mg/L of humic acid was utilized, the hydrogen production was not significantly affected when compared to conventional alkaline water electrolysis. This was corroborated by the corresponding coulombic efficiencies obtained for the hydrogen evolution reaction (HER) for both the carbon fibre anode under wastewater electrolysis and the Ni-foam electrode under conventional water electrolysis were very close to unity, i.e., 98 ± 0.07% for the carbon fibre anode and 98 ± 1 % for the Ni- foam anode(Appendix A.4). In addition, a literature survey revealed that carbon-based electrodes can be employed to oxidize organic pollutants such as dye pigments and phenolic compounds at the anode of an electrochemical cell (Cañizares et al., 1999; Fan et al., 2008; Polcaro & Palmas, 1997; Yi & Chen, 2008).

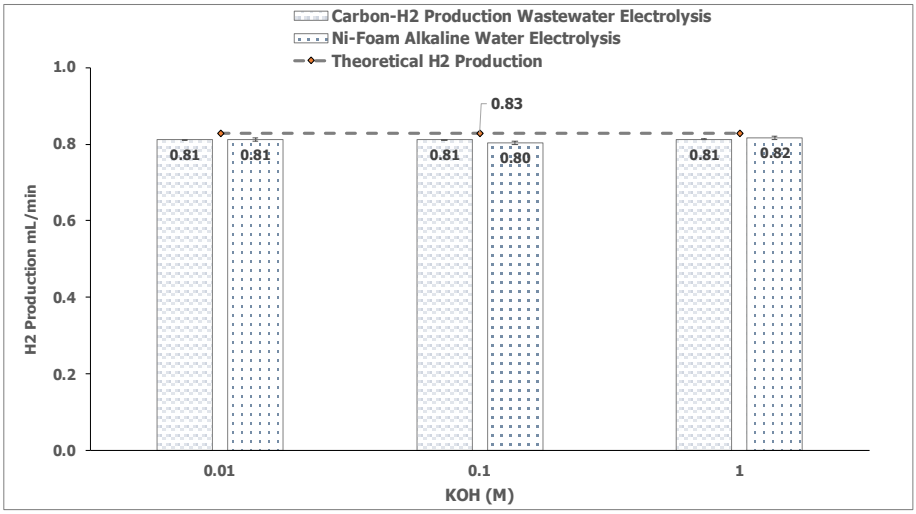

Figure 10 Effect of Electrolyte Concentration: Volumetric Hydrogen Production Rate(ml H_2/min)

In light of this information, the ability of the carbon fibre electrode to oxidize the humic acid molecules present in the synthetically produced wastewater was investigated

To assess the extent of degradation, the COD and TOC before and after electrolysis were measured; the corresponding data is represented in Figure 11 and Figure 12, respectively. It can be seen from Figure 11 that the COD of the electrolyte solution for all concentrations of KOH is considerably higher after electrolysis than the COD prior to electrolysis. The trend was also apparent in the TOC measurements.

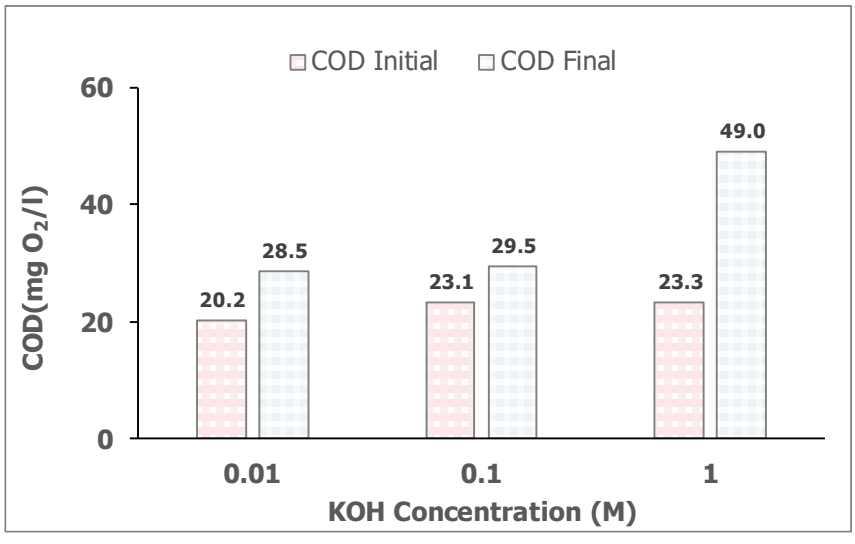

Figure 11 Effect of Electrolyte Concentration: Chemical Oxygen Demand (COD) mg O_2/L

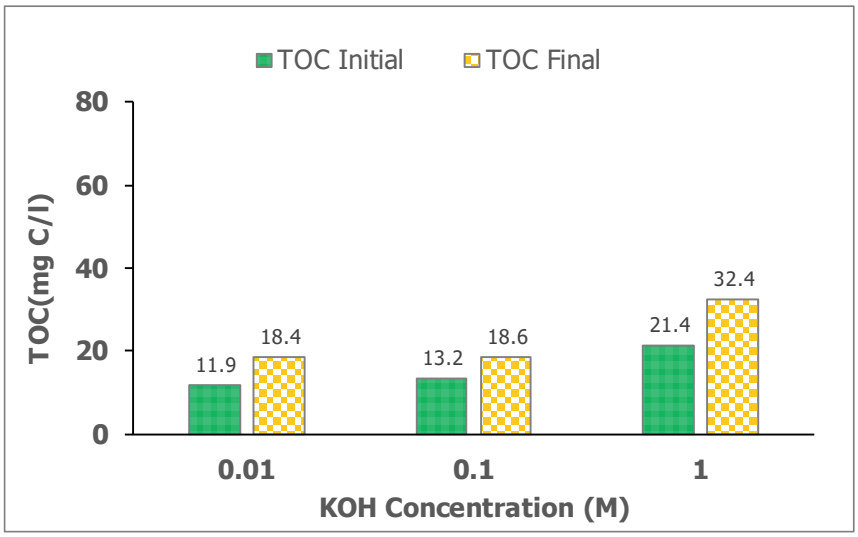

Figure 12 Effect of Electrolyte Concentration: Total Organic Carbon (TOC) mg-C/L

This increase in both the TOC and COD can be attributed to the adsorption of the conjugate base of the humic acid molecules(humate) on the carbon fibre surface (Polcaro & Palmas, 1997). The adsorption may be enhanced further by the applied potential; the resulting electric field generated causes a flow of anions (humate) towards the anode leading to electro-sorption/adsorption on the carbon fibre surface(Ban et al., 1998). Additionally, because humic acid is a weak acid, the activity of the dissociated humic acid (humate) would be enhanced at a more alkaline pH, i.e., for the experiments conducted, the measured pH was greater than 10; hence there would be a higher activity of the humate species in the flow cell. The liberation/desorption of the humic acid was also evidenced by the change in colour of the cleaning solutions (0.1M KOH) prior to changing the electrolyte for the experiment batch. This serves to indicate that when the next batch of the solution is employed for electrolysis, it is likely that humate desorption may occur from the carbon anode resulting in an increase in the concentration of humics in the system and hence resulting in a higher measured COD and TOC.

To confirm this observation, the samples were analysed spectrophotometrically. The samples were scanned from a wavelength of 190 nm to 600 nm, and the data obtained is represented in Figure 13, Figure 14 and Figure 15, for 0.01M KOH, 0.1M KOH, and 1M KOH with 20 mg O_2/L humic acid COD, respectively. It is observed from Figure 13 – Figure 15 that the excitation wavelength for the humic acid molecules is between 288-290 nm based on the observed peak in the graph for the initial and final scans for all concentrations of KOH,

respectively. It can be seen from the graphs that the absorbance of the peak obtained after electrolysis is significantly higher than the initial solution, i.e., for 0.01M KOH solution, the initial peak absorbance was approximately 0.449 and increased to 0.801 for the final solution after electrolysis. The observations were similar for 0.1M KOH and 1M KOH solutions, wherein the absorbance increased from 0.4 to 0.6 for the former and increased from 0.4 to 0.7 for the latter. These observations were also substantiated by images of the solutions taken before and after electrolysis; this is represented in Figure 16; from the image cluster, the increase in the colour saturation of the solutions after electrolysis in contrast to the solutions before electrolysis is apparent.

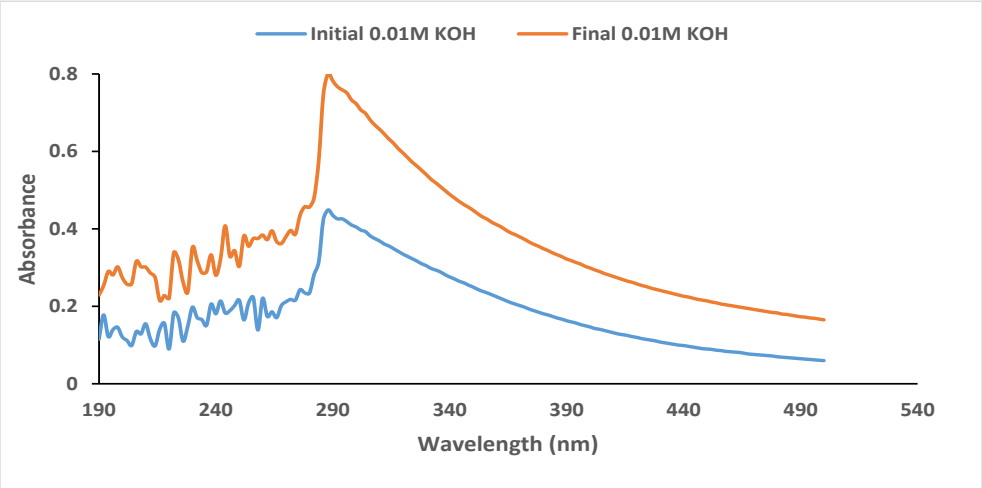

Figure 13 Spectrophotometric analysis before and after electrolysis 0.01M KOH

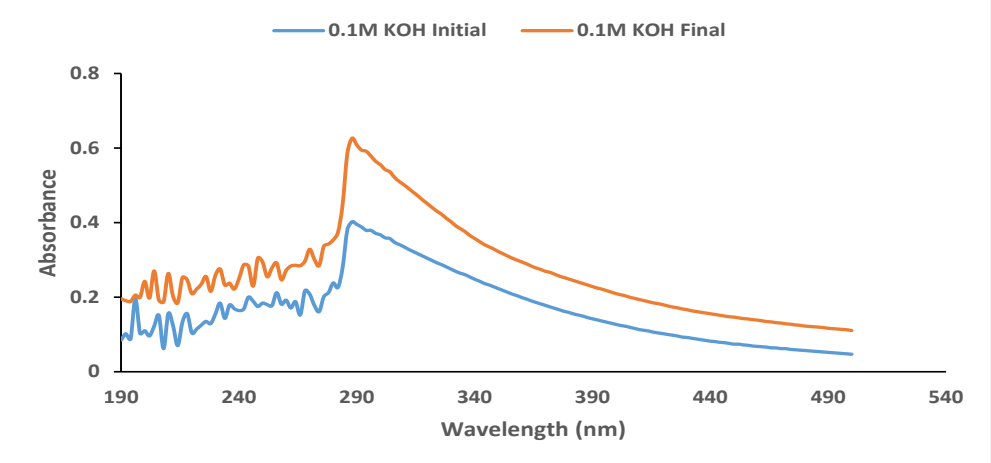

Figure 14 Spectrophotometric analysis before and after electrolysis 0.1M KOH

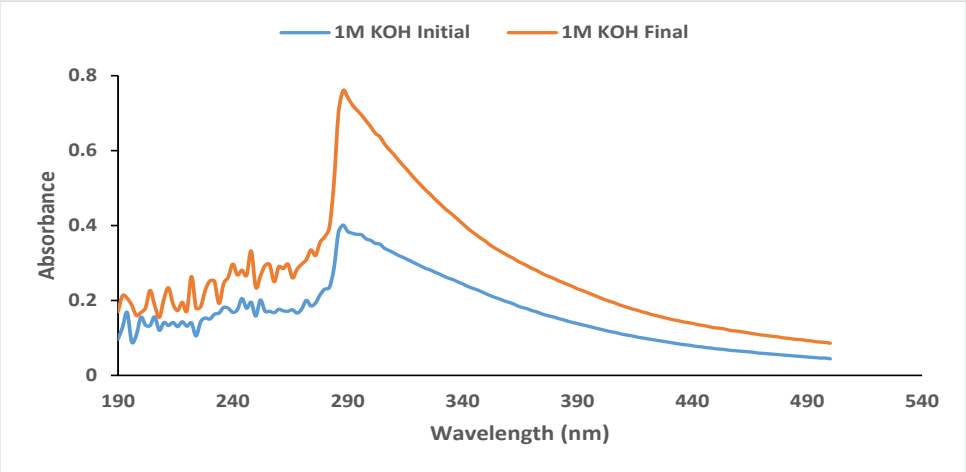

Figure 15 Spectrophotometric analysis before and after electrolysis 1M KOH

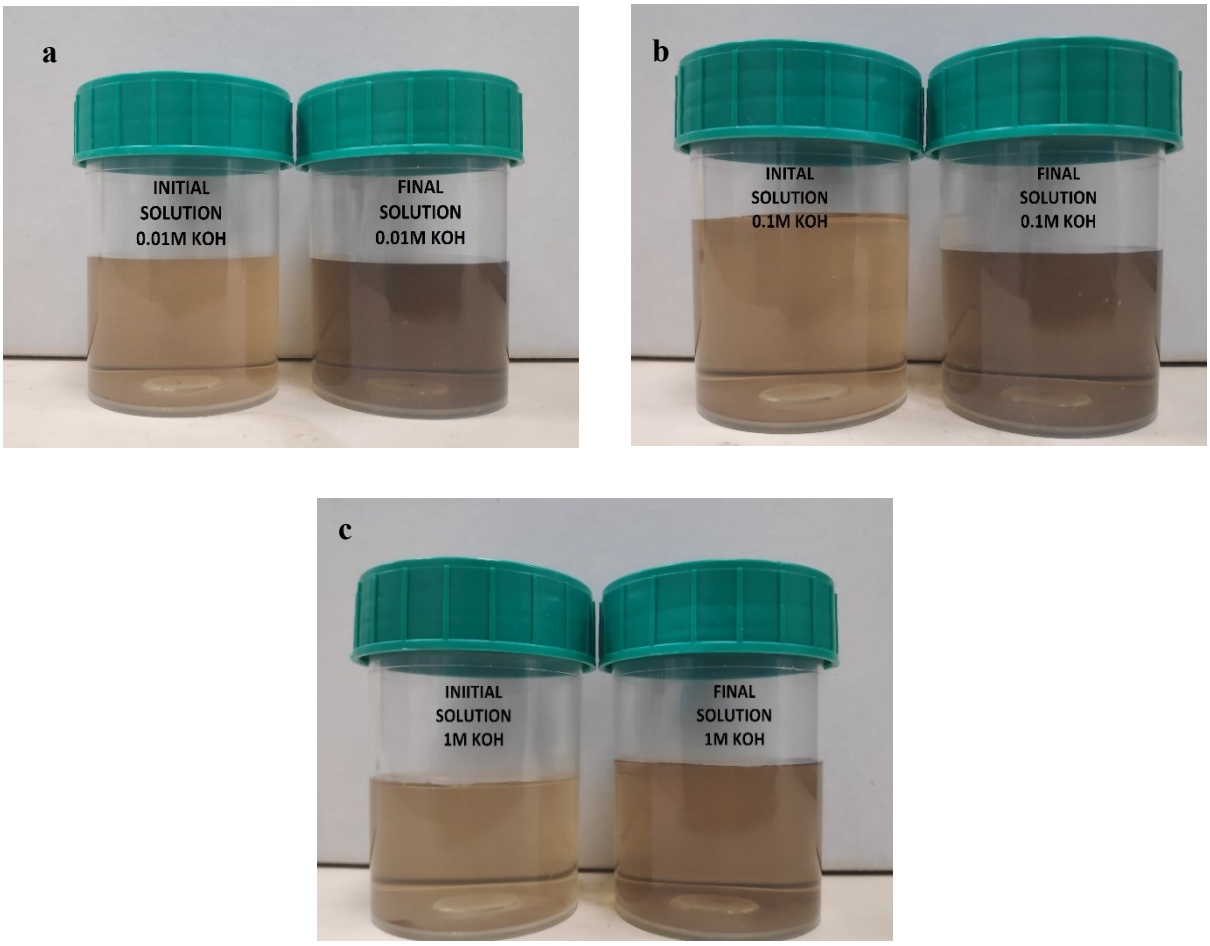

Figure 16 Effect of KOH: Images of the initial and final solutions a- 0.01M KOH; b-0.01M KOH ; C-0.01M KOH

An interesting occurrence was detected during the electrolysis of the synthetic wastewater containing humic acid. It was observed that as electrolysis proceeded, the catholyte solution would turn lighter while the anolyte solution would become darker (Figure 17). This was observed when the duration of electrolysis exceeded 3 hrs. This was subsequently investigated by electrolyzing 25 ± 1.2 mg O_2/L of humic acid in 1M KOH for a duration of 6 hrs. In accordance with the results discussed earlier, the final COD of the combined solution of equal volumes of anolyte and catholyte after electrolysis was significantly higher than the initial solution, i.e., the measured final COD was approximately 66 ± 0.5 mg O_2/L. This, once again, can be ascribed to the adsorption and desorption of the humic acid molecules on the surface of the carbon fibre anode. When the COD of the anolyte and the catholyte were measured separately, the COD of the anolyte was considerably higher than the measured COD of the catholyte, i.e., the measured COD of the anolyte chamber was 91± 0.6 mg O_2/L while the measured COD of the catholyte chamber was 41± 0.4 mg O_2/L.

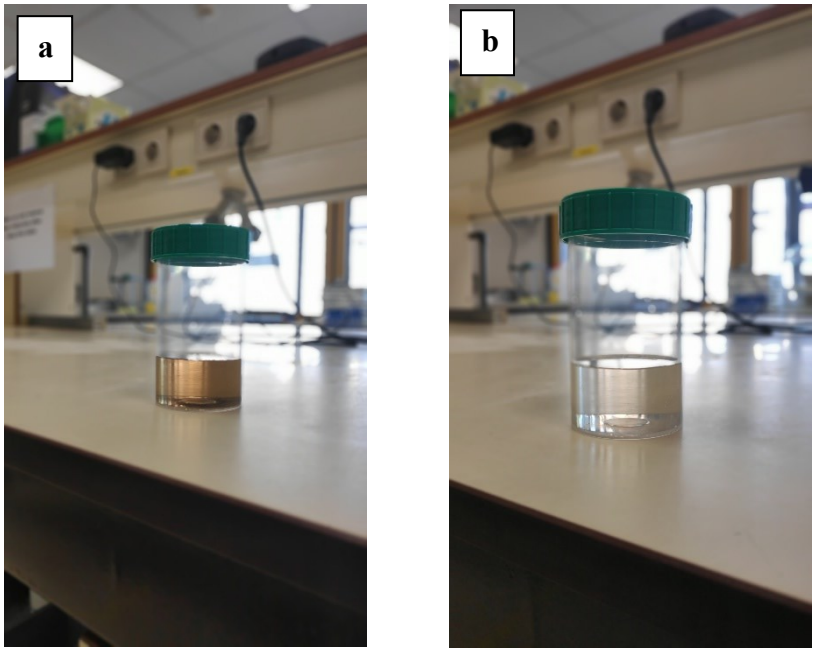

Figure 17 a) Anolyte and b) Catholyte solution after 6hrs of electrolysis.

This phenomenon can be attributed to the presence of an electric field and an anionic exchange membrane, similar to how the electrodialysis process works. Since both the anolyte and catholyte used in this experiment were the synthetic wastewater containing humic acid, it would seem that due to the presence of the anionic membrane, the conjugate base of humic acid (humate) would permeate through the membrane from the catholyte chamber to anolyte chamber. The samples were also scanned spectrophotometrically and are subsequently represented in Figure 18. From Figure 18, the increase in absorbance of the anolyte after 6 hrs of electrolysis with respect to both the initial solution at T= 0 and the catholyte at T= 6 hrs is apparent. It can be seen that the peak absorbance decreases for the catholyte solution from the initial 0.40 to 0.21, indicating a decrease in the humic acid concentration in the catholyte. In contrast, the absorbance increases for the anolyte chamber to 0.91 with respect to the initial solution indicating an increase in the concentration of humic acid.

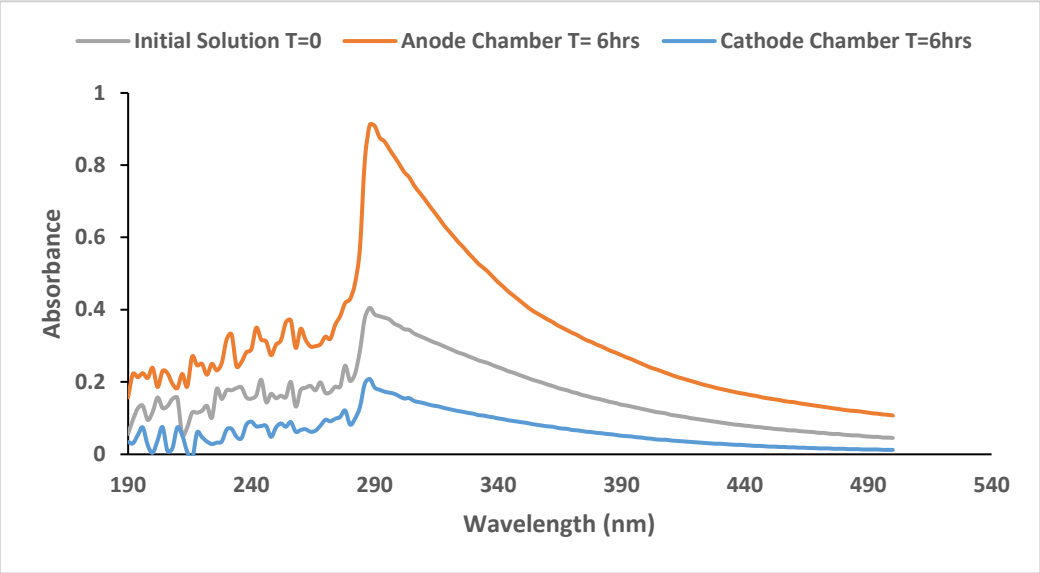

Figure 18 Spectrophotometric Analysis: Initial Solution, Anolyte and Catholyte

To further understand what was happening with the humic acid molecules after electrolysis, the samples were analysed using size exclusion chromatography high-performance liquid chromatograph (SEC-HPLC). When performing SEC-HPLC analysis, the molecules are separated based on the size within the column; that is, the larger molecules have a short retention time compared to smaller size molecules which would consequently have a longer retention time. The size of the molecule can be correlated with the molecular weight, i.e., larger molecules will have a higher molecular weight, while smaller molecules will have a lower weight.

To understand the molecular weight distribution of the sample, standards were prepared for 3610 Da, 1100 Da, and 498 Da, and their retention times were noted. The comparison between the solutions was made based on the area under the chromatogram integrated over the time intervals based on the retention times of the standards, i.e., for a molecular weight of 3610 Da, the corresponding retention time was 6.2 mins, similarly for 1100 Da and 498 Da where the corresponding retention times 8.7 mins and 12 mins. The time intervals were divided into two categories: high molecular weight ranging between 3610 Da – 1100 Da and low molecular weights ranging from 1100 Da – 498 Da. The general chromatogram of the humic acid molecules marked with corresponding standards is illustrated in Figure 19, and the subsequent results for the sample analysis are shown in Figure 20.

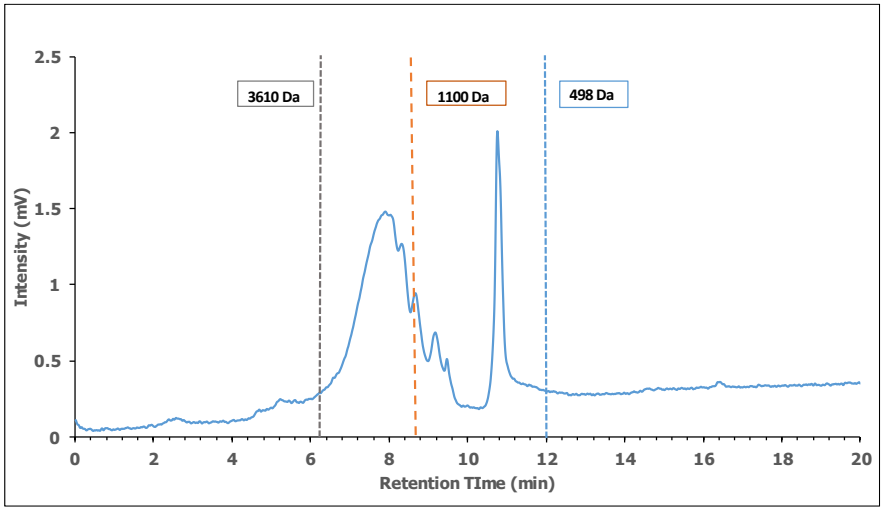

Figure 19 General chromatogram of humic acid molecules obtained from SEC-HPLC

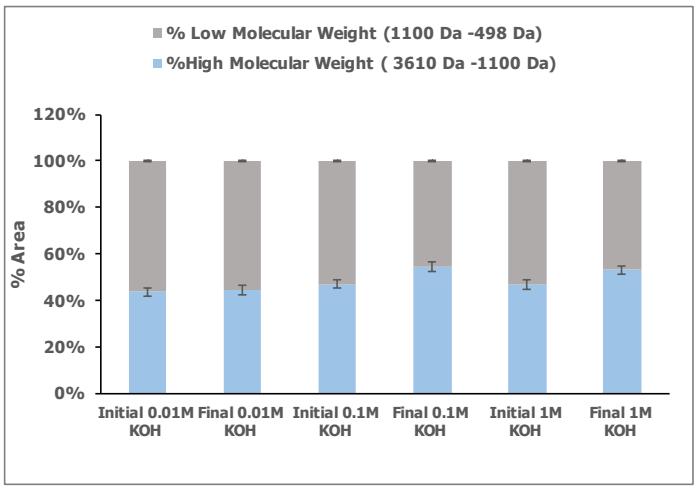

Figure 20 Effect of Electrolyte Concentration: Carbon Fibre: SEC-HPLC(Area Under the Curve)

An intriguing observation was noticed from Figure 20, i.e., the final solution after electrolysis exhibited an increase in the area for higher molecular weights(3610 Da – 1100 Da) and a subsequent decrease in the area for lower molecular weights(1100 Da – 498 Da) when compared with the initial solutions. Though the phenomenon was observed for all concentrations of electrolyte, the change was quite apparent for 0.1M KOH and 1M KOH. For instance, if we consider the 0.1M KOH solution, the contribution of high molecular weights to the total area increased from the initial 47% to 54% after electrolysis, and for the low molecular weights, the area decreased from 52% at the initial to 45% after electrolysis.

The increase in the contribution of higher molecular weights to the total area indicates that there is an increase in the size of the molecules after electrolysis; it could be suggested that there is a polymerization reaction occurring on the surface of the electrode due to the activation of the moieties (phenols and quinones) present in the molecules of the humic acid(Figure 8). Similar observations were reported by Cañizares et al. 1999 when they employed the carbon fibre anode for the electrochemical oxidation phenol and also by Li et al., 2005 while investigating the degradation of phenol using Ti/RuO_2 DSA anode(Figure 21).

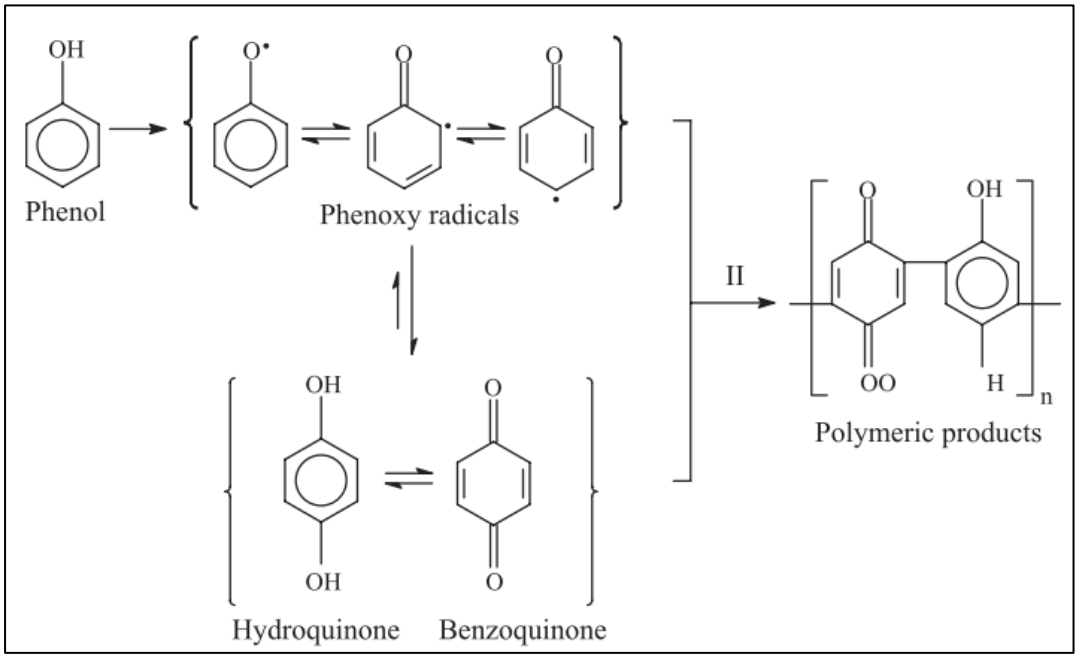

Figure 21 Reaction pathway for polymerization of phenols and quinones(Li et al., 2005)

4.2.2 Nickel Foam Anode

Electrolysis experiments with synthetic wastewater containing 20 mg O_2/L of humic acid with KOH as the supporting electrolyte were also conducted with Ni-foam as both the anode and cathode. The configuration of the electrolysis cell is similar to that of conventional alkaline water electrolysis, with the difference being the composition of the electrolyte solution, which in the case of conventional alkaline water electrolysis is a KOH solution. The following results are illustrated in Figure 22 to Figure 30, respectively. The experiment was conducted for a duration of 3hrs under galvanostatic conditions at a current density of 12.55 A/m^2. The graph depicted in Figure 22 represents the energy efficiency of hydrogen production of the Ni-foam electrode when used for both synthetic wastewater and alkaline water electrolysis. It is evident from Figure 22 that the energy of efficiency of the hydrogen production is slightly lower when using synthetic wastewater compared to conventional alkaline water electrolysis, i.e., for the 1M KOH electrolyte solution prepared with the synthetic wastewater, the energy efficiency was 83 ± 3.40%. In contrast, the same for alkaline water electrolysis was 85 ± 7.0%. This trend was apparent for 0.1M KOH and 1M KOH solutions as well. The decrease in energy efficiency could be associated with the extra energy required to maintain a constant current density while allowing for the simultaneous oxidation of the humics and water splitting at the anode (Eq 17 and Eq 18).

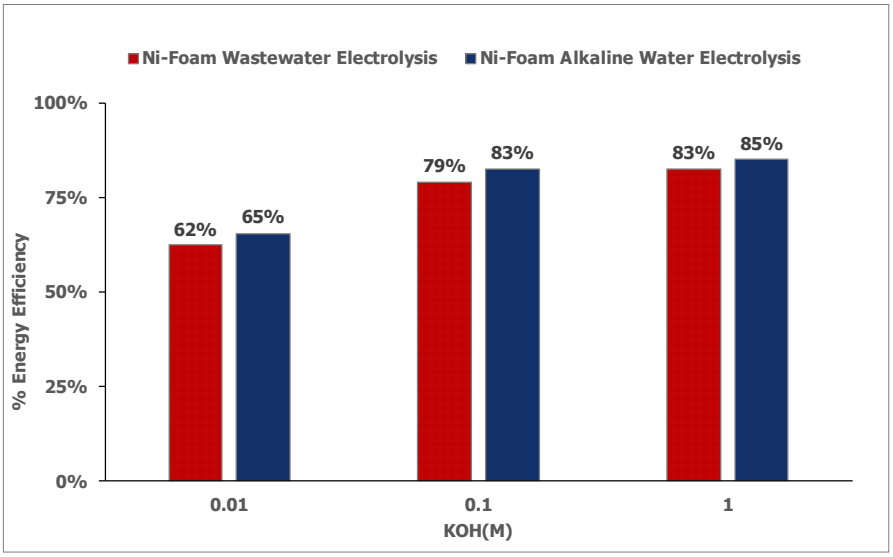

Figure 22 Effect of Electrolyte Concentration- Ni-Foam Anode: Energy Efficiency

Additionally, continuous experiments with humic acid in the flow cell electrolyzer resulted in fouling of the anion exchange membrane. Fouling of the membrane can lead to an increase in

cell resistance, and as a consequence, higher ohmic losses occur in the cell resulting in a higher energy requirement to maintain galvanostatic conditions(Rijnaarts et al., 2019).
An increasing trend in energy efficiency is also observed for both wastewater electrolysis and alkaline water electrolysis, similar to Figure 9. This trend is again to be expected due to an increase in solution conductivity as the concentration of electrolyte (KOH) increases.

The subsequent hydrogen production rate measured using Ni-foam anode for the electrolysis of synthetic effluent and alkaline water is represented in Figure 23; similar to the results obtained with the carbon fibre anode, it is observed that the hydrogen production rate is not substantially affected. The average hydrogen production rate for the Ni-foam anode used for the electrolysis of synthetic wastewater was approximately 0.80 ± 0.05 mL H_2/min for KOH concentrations ranging from 0.1M to 1M, respectively. Further, the hydrogen production rate for synthetic wastewater and for alkaline water the hydrogen production rate was approximately 0.81 ± 0.07 mL H_2/min. When compared to the theoretically calculated rate of 0.83 mL H_2/min for a current density of 12.55 A/m^2, the rates are quite similar. Moreover, because a decrease in COD was observed in the solution after electrolysis(Figure 24), it would be expected to be reflected as an increase in hydrogen production based on a previously

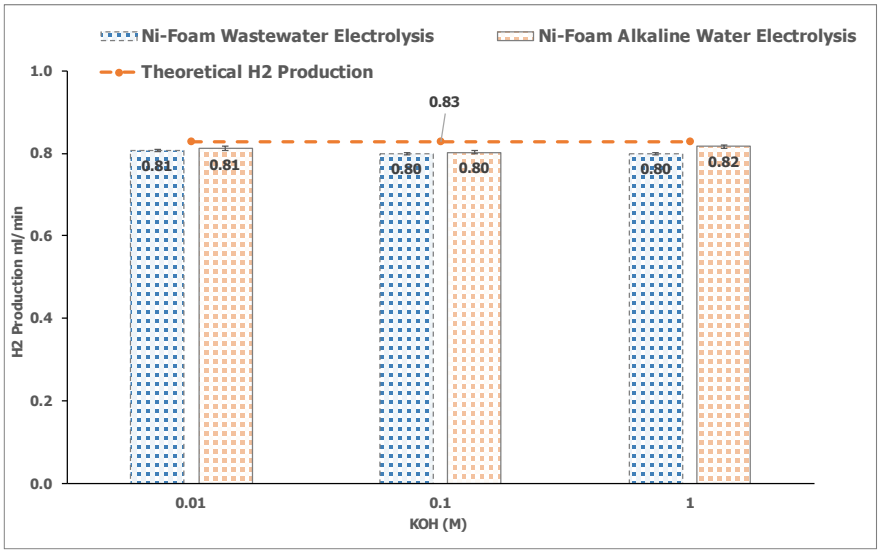

Figure 23 Effect of Electrolyte Concentration- Ni-Foam Anode: Volumetric Hydrogen Production Rate (mL H_2/min)

conducted study by Eker & Kargi, 2010. However, this was not observed in this study mainly because the amount of hydrogen produced would depend on the strength of COD in the wastewater and the extent of COD removal and TOC removal. Since the synthetic effluent used

in this investigation only contained 20 mg O_2/L of COD compared to 10,000 mg O2/L in the study by Eker & Kargi, 2010, the contribution to the hydrogen production rate would not be that significant. Furthermore, experimental observations showed that the COD removal was a maximum of 50.9 ± 9.0 % for 0.01M KOH(Figure 24) solution but was only 21 ± 10% and 24.6 ± 8 % for 0.1M and 1M KOH solutions, respectively. This was also observed in Figure 25, wherein the TOC removal efficiencies calculated were not that substantial; with a maximum removal of 14.1 ± 0.2% for 0.01M KOH, 2.4 ± 0.7 % for 0.1M KOH solution, and 6.2 ± 0.3% for 1M KOH solutions.

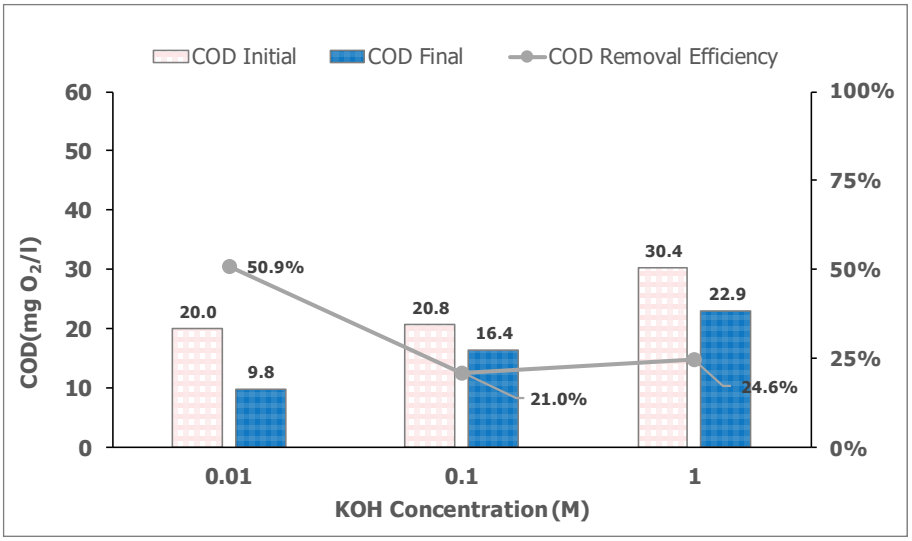

Figure 24 Effect of Electrolyte Concentration- Ni-Foam Anode: COD removal efficiency

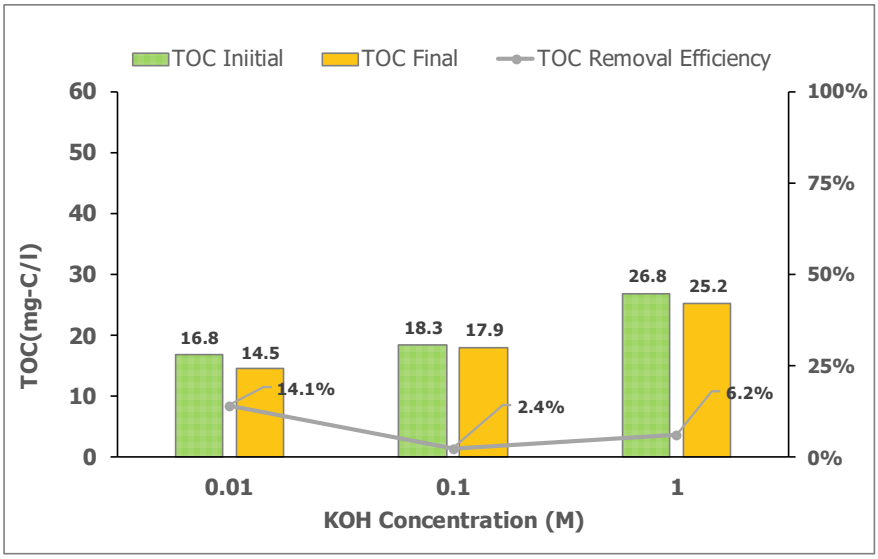

Figure 25 Effect of Electrolyte Concentration- Ni-Foam Anode: TOC removal efficiency

Regarding the COD and TOC removal efficiencies, it was observed that for the 0.01M KOH solution, the efficiency was relatively higher compared to the removal efficiencies for the 0.1M KOH and 1M KOH solutions. It could be suggested that at higher KOH concentrations, the mass transfer of humic acid molecules on the active sites of the Ni-foam anode could be limited, resulting in a lower oxidation efficiency of the humics. It is possible that the higher activity of the OH^- ions in the system could out-compete the humic acid molecules to favour the oxidation evolution reaction rather than the anodic oxidation of humics. The formation of higher oxides via chemisorbed hydroxyl anode surface radicals which can indirectly oxidize the humics is better described in Eq 29, Eq 30, Eq 31 and Eq 32 (Becker et al., 2010; Marco Panizza & Cerisola, 2009). Note in the following equations MO_x represents metal oxide which in case of Ni-foam anode would be $NiFeO_x$ or NiO_x (Mischa M. Bakker & Vermaas, 2019; Diaz-Morales et al., 2016; Kartikaningsih et al., 2017)

Discharge of water molecules to form adsorbed hydroxyl radicals

$$MO_x + OH^- \rightarrow MO_x[^*OH] + e^- \qquad \text{Eq 29}$$

Formation of chemisorbed hydroxyl radicals on the anode surface

$$MO_x[^*OH] \rightarrow MO_{x+1} + H^+ + e^- \qquad \text{Eq 30}$$

Oxidation of organics "R" on the anode surface

$$MO_{x+1} + R \rightarrow MO_x + RO \qquad \text{Eq 31}$$

Oxygen Evolution Reaction

$$MO_{x+1} + OH^- \rightarrow MO_x + O_2 + H^+ + 2e^- \qquad \text{Eq 32}$$

Moreover, because the Ni-foam electrode has a relatively low OER potential(1.6 V), the electrode is more active toward the oxygen evolution reaction as opposed to the oxidation of humics (Panizza et al., 2001). This was also evident from the coulombic efficiencies for the oxygen evolution reaction(Eq 6) and organics oxidation. The coulombic efficiency for the oxidation of humics was calculated based on the following equation(Marco Panizza & Cerisola, 2009):-

$$CE_{oxidation} = \frac{F.V.[COD_{Initial} - COD_{Final}]}{8..I.t.1000} \qquad \text{Eq 33}$$

where COD_{inital} and COD_{final} are the chemical oxygen demands before and after electrolysis(g O_2/L), F is Faraday's constant (96500 C/ mole e^-), V is the volume of the sample treated (L),

I is the applied current (A) and t is the duration(s), and 8 is the equivalent mass of oxygen in (g/eq).

The average coulombic efficiency for the OER for all concentrations of electrolyte was 96 ± 1%, and the coulombic efficiency for organics oxidation was 5 ± 0.3% for 0.01M KOH, 2 ± 0.2 % for 0.1M KOH and 4 ± 0.5% for 1M KOH solutions, considerably lower(Appendix A.4). Furthermore, this also can explain why the coulombic efficiencies for the OER are lower compared to that of conventional alkaline water electrolysis, which had an average efficiency of 98 ± 0.8%(Appendix A.4). Generally, it would be anticipated that if the coulombic efficiency of the organics oxidation increases, there would be a corresponding decrease in the coulombic efficiency of the oxygen evolution reaction since the total current/coulombic efficiency cannot exceed unity(Cho, Kwon, et al., 2014; Cho & Hoffmann, 2017).

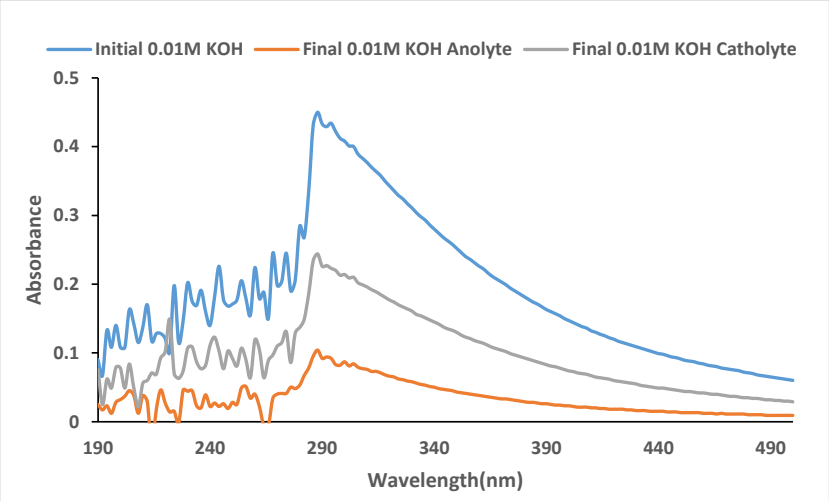

Figure 26 Spectrophotometric Analysis- Ni-Foam anode before and after Electrolysis 0.01M KOH

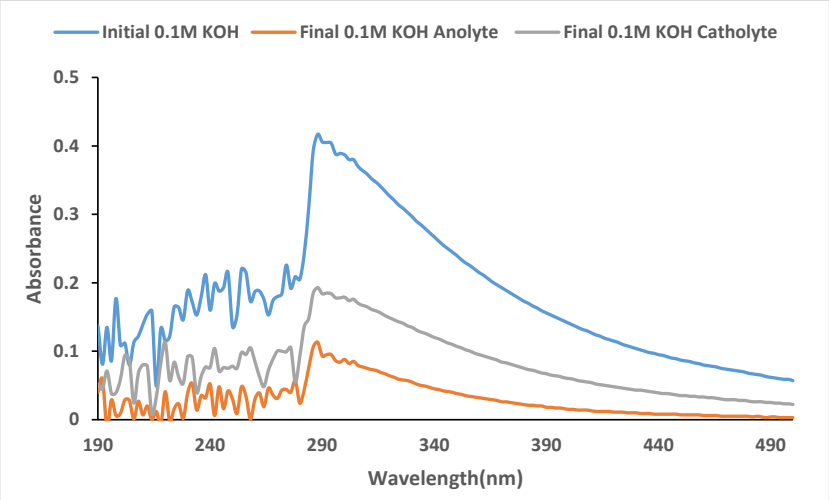

Figure 27 Spectrophotometric Analysis- Ni-Foam anode before and after Electrolysis 0.01M KOH

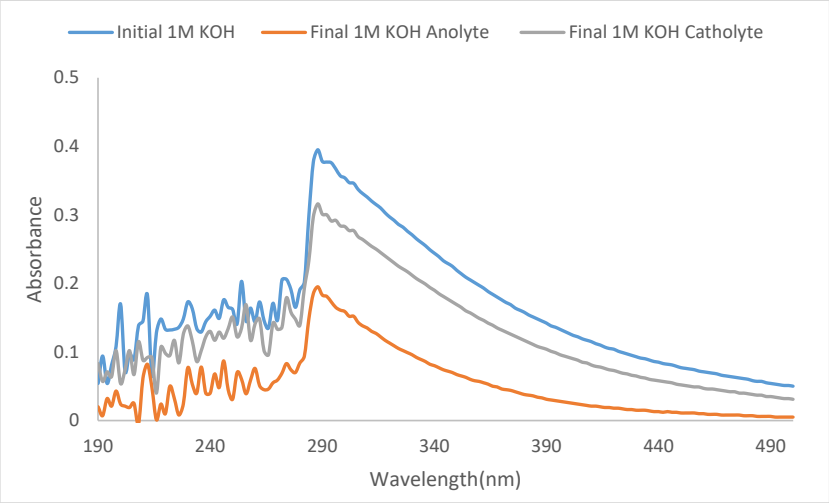

Figure 28 Spectrophotometric Analysis- Ni-Foam anode Before and After Electrolysis 1M KOH

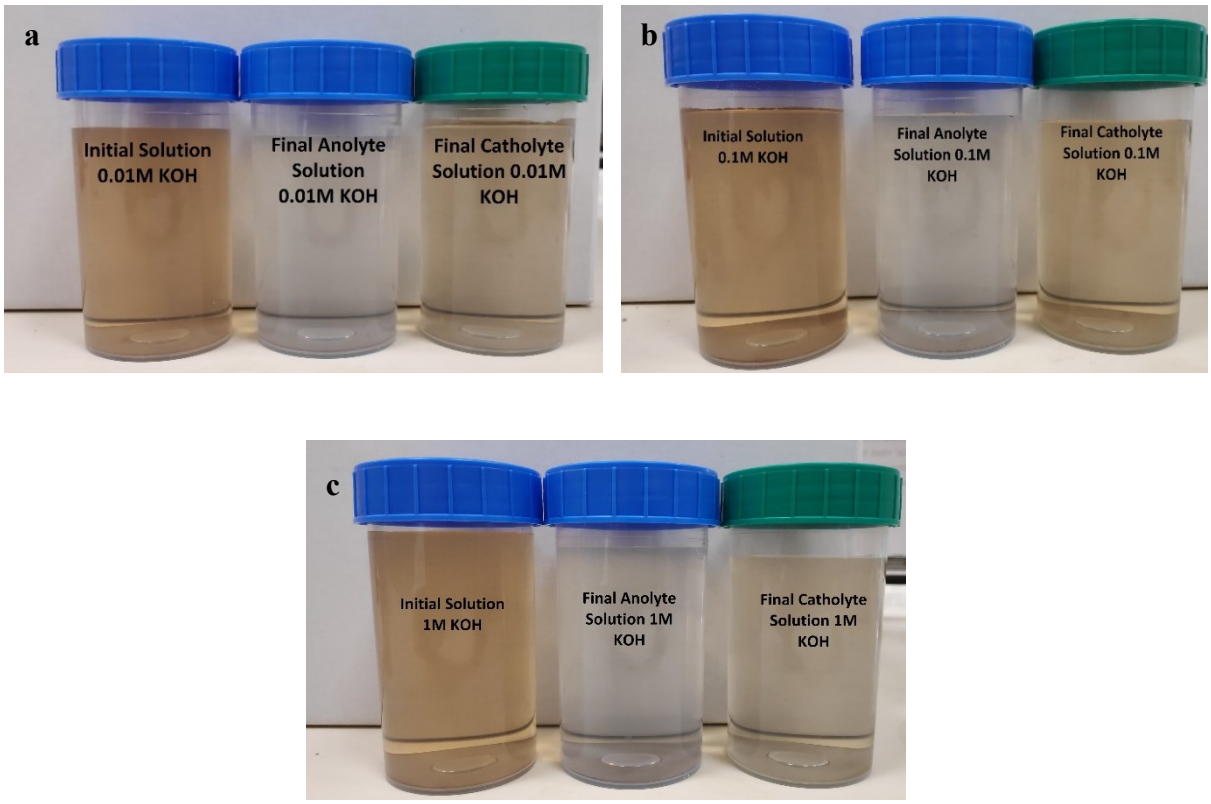

Figure 29 Effect of KOH: Images of the initial and final solutions a- 0.01M KOH; b-0.1M KOH ; C-1M KOH

It is observed from the spectrophotometric scans that there is a decrease in the humic acid concentration after electrolysis. For 0.01M KOH solution, it can be seen that the absorbance of the anolyte solution is considerably lower compared to the initial solution, i.e., the absorbance decreased from the initial 0.43 to 0.10 for the anolyte solution for 0.01M KOH. This trend was apparent for the 0.1M KOH and 1M KOH solutions, wherein the absorbance decreased from the initial 0.40 to 0.09 in the anolyte for 0.1M KOH and a decrease from the initial 0.38 to 0.17 in the anolyte for 1M KOH. Moreover, it is also evident from Figure 26 - Figure 28 that there is a decrease in the absorbance of the catholyte solution with respect to the initial solution, though not as significant. This observation is similar to that obtained in Figure 18, i.e., there is a transfer of some of the humic acid molecules from the catholyte chamber to the anolyte chamber attributed to the presence of an electric field and the anion exchange membrane similar to how the electrodialysis process works. Additionally, it was observed that after electrolysis, the colour of the solution used in the anolyte chamber is much lighter compared to the catholyte solution and the initial solution. This was subsequently verified via spectrophotometric analysis and is depicted in Figure 26, Figure 27 and Figure 28 for 0.01M KOH, 0.1M KOH, and 1M KOH solutions, respectively. The difference in colour was also evident from the images of the solutions taken before and after electrolysis. This is illustrated in Figure 29.

To compare with the results obtained with the carbon fibre anode, samples were also analysed using size exclusion high-performance liquid chromatography (SEC-HPLC); the results for the same are described in Figure 30.

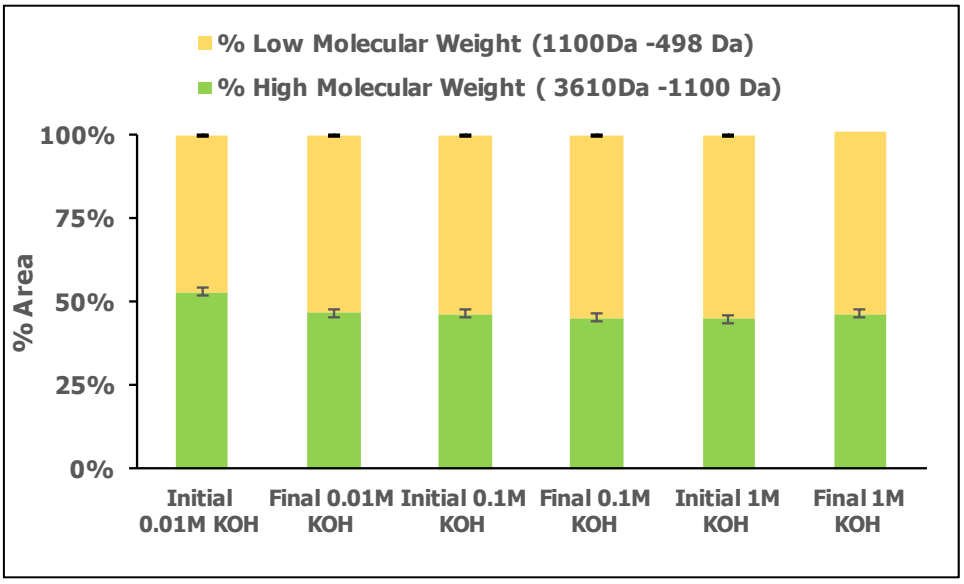

Figure 30 Effect of Electrolyte Concentration-Ni-Foam : SEC-HPLC(Area Under the Curve)

It is observed that after electrolysis with the Ni-Foam anode, the final solutions had a lower distribution of high molecular weight molecules compared to the initial solution and was followed by an increase in the distribution of low molecular weight molecules. This was apparent for the 0.01M and 0.1M KOH solutions; for instance, the % high Molecular weights decreased from 53% in the initial solution to 47% in the final solution, similarly for the 0.1M solution where the decrease was observed from 46 % at the initial to 45% in the final solution. Further, the % low Molecular weight increased from 47% at the initial to 53% in the final solution for 0.01M KOH, and for 0.1M KOH, the distribution of the lower molecular weight compounds increased from 53% in the initial to 55% in the final solution. However, the final solution after electrolysis for the 1M KOH solution exhibited an opposite trend wherein there was an increase in the distribution of higher molecular weight molecules with respect to the initial similar to what was observed in Figure 20 when the carbon fibre anode was used.

In general, the trend agrees with the COD and TOC removal efficiencies, i.e., the high COD removal accompanied by the low TOC removal efficiency in the final solutions indicates the formation of intermediates as the humic acid molecules undergo oxidation; this is supported by the subsequent increase in the % low molecular weight and decrease in the % high molecular weight contributions for the final solutions for 0.01M KOH and 0.1M KOH solutions.

4.3 Effect of Current Density

4.3.1 Carbon Fibre Anode

The experiments were conducted using synthetic wastewater containing 20 mg O_2/L humic acid as COD with 1M KOH as the electrolyte using the carbon fibre anode at constant current densities ranging from 25 A/m^2 to 150 A/m^2. The electrolysis experiments were conducted for a duration of 3hrs; the results are consequently represented in Figure 31 to Figure 37. Figure 31 illustrates the energy efficiency of hydrogen production for the carbon fibre anode using wastewater electrolysis and subsequently compared with conventional alkaline water electrolysis using the Ni-foam anode with 1M KOH as the electrolyte. It is observed from Figure 31 that the energy efficiency of H_2 production is relatively lower for synthetic wastewater with the carbon fibre anode compared to alkaline water electrolysis using the Ni-Foam anode. This can be explained by the fact that the Ni-foam electrode has a lower OER overpotential compared to the carbon fibre anode, i.e., 1.6V for the Ni-foam and 1.7V for the carbon fibre anode. In addition, prolonged electrolysis experiments with the carbon fibre anode resulted in its disintegration; further, the disintegration of the carbon electrode was exacerbated for current densities higher than 25 A/m^2. The loss of electrode material could potentially increase the contact resistance at the electrode/current collector interface resulting in higher ohmic losses.(Nourani et al., 2019). This is visually illustrated from the images of the electrode taken before and after electrolysis and is subsequently shown in Figure 32.

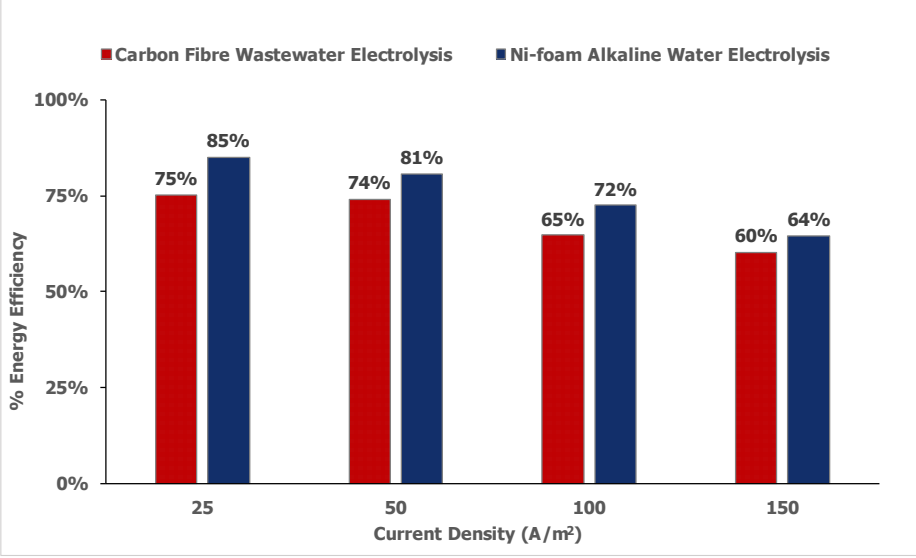

Figure 31 Effect of Current Density – Carbon Fibre Anode-Energy Efficiency

Moreover, in both cases, the energy efficiency follows a decreasing trend as the current densities are increased. This can be attributed to increased ohmic heating losses at higher

current densities and higher bubble formation on the surface of the anode and cathode, which can lead to increased resistance of the flow cell (Godula-Jopek, 2015; Wang et al., 2014).

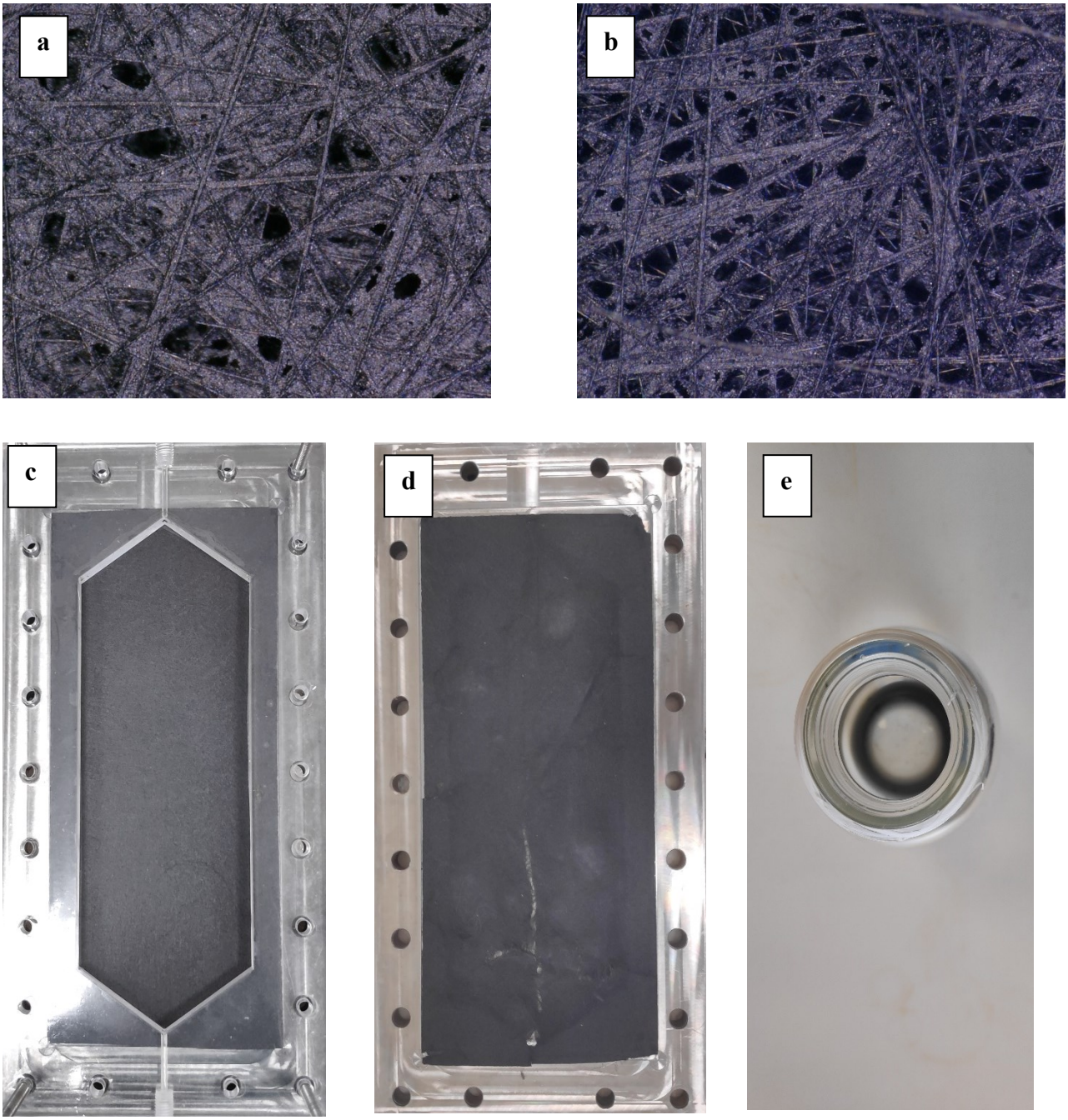

Figure 32 Effect of Current Density- Carbon Fibre Anode ; a - Before Electrolysis 200X Magnification; b – After Electrolysis 200X Magnification; c – Electrode in flow cell before Electrolysis ; d- Electrode in Flow Cell After Electrolysis at 100 A/m^2; e- Disintegrated electrode particles in the reservoir after electrolysis

The corresponding volumetric hydrogen production rate for the carbon fibre anode using synthetic wastewater and the Ni-foam electrode using alkaline water and compared with the theoretically calculated hydrogen production is depicted in Figure 33. It is observed that the

volumetric hydrogen production rate with the carbon fibre anode using the wastewater is comparable to that of the Ni-foam anode with alkaline water (1M KOH). Moreover, for both cases, the volumetric hydrogen production rate was more or less equal to the theoretically calculated rate based on faradays law. It can be seen that at a current density of 25 A/m^2 the H_2 production rate was approximately 1.60 ± 0.02 mL H_2 / min for both wastewater electrolysis using the carbon fibre anode and for alkaline water electrolysis using the Ni-foam anode, whereas the theoretically calculated rate was 1.53 mL H_2/min. This was also apparent for a current density of 50 A/m^{2,} but at higher current densities of 100 A/m^2 and 150 A/m^{2,} the hydrogen production rate of wastewater with the carbon fibre anode was slightly lower than the hydrogen production rate of the Ni-foam anode in alkaline water but still comparable to the theoretically calculated rate, i.e., for 100 A/m^2 the hydrogen production rate was 6.0 ± 0.19 mL H_2/min for the carbon fibre anode and 6.4 ± 0.08 mL H_2/min for the Ni-foam anode and the theoretical rate was 6.10 mL H_2/min.

The volumetric hydrogen production rate for wastewater did not appear to be impacted despite the disintegration of the carbon fibre anode. Nourani et al., 2019 also reported a similar

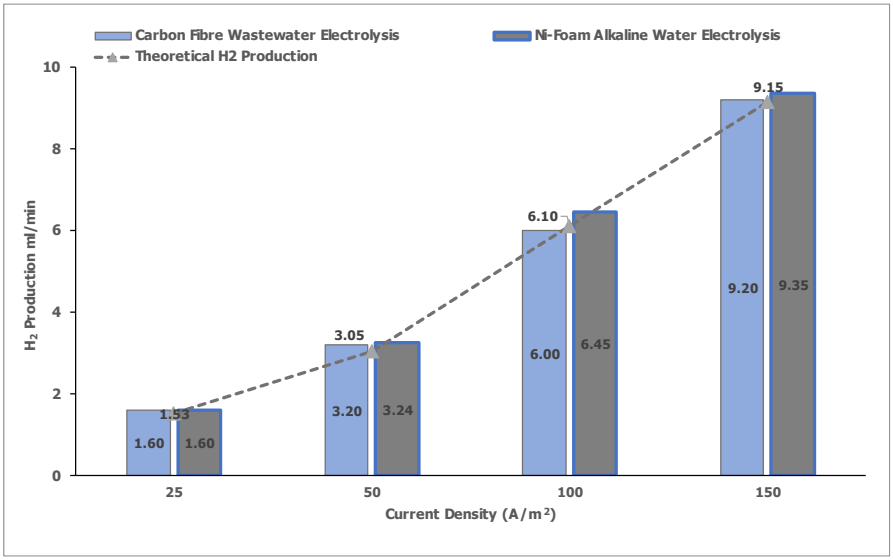

Figure 33 Effect of Current Density-Carbon Fibre Anode-Volumetric Hydrogen Production Rate (mL H_2/min)

observation, wherein the disintegration of the carbon fibre anode did not negatively impact the performance vanadium redox flow battery in which the electrode was employed. Bulk samples of the synthetic wastewater were collected after electrolysis from both anode and cathode chambers then equal volumes of the samples were taken and combined into a single solution.

Subsequently, COD and TOC analysis were conducted on the sample, and the results are illustrated in Figure 34 and Figure 35, respectively.

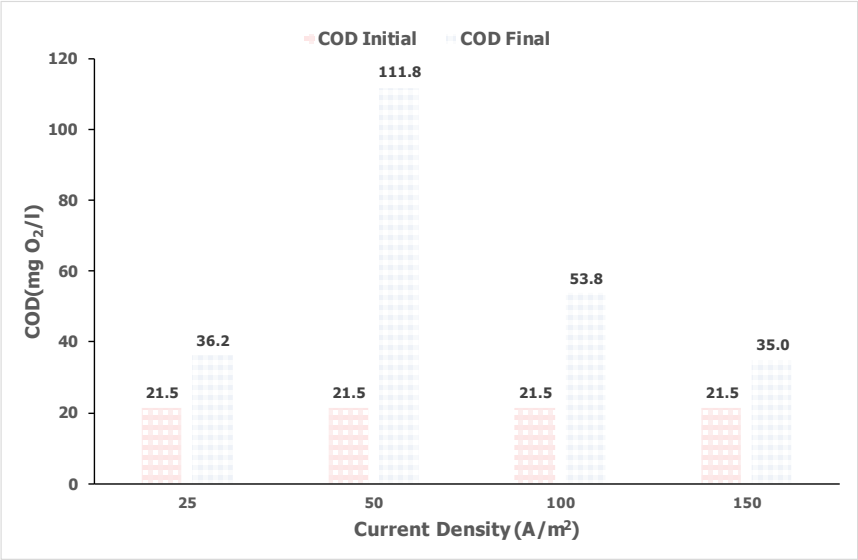

Figure 34 Effect of Current Density – Carbon Fibre Anode – Chemical Oxygen Demand (mg O_2/L)

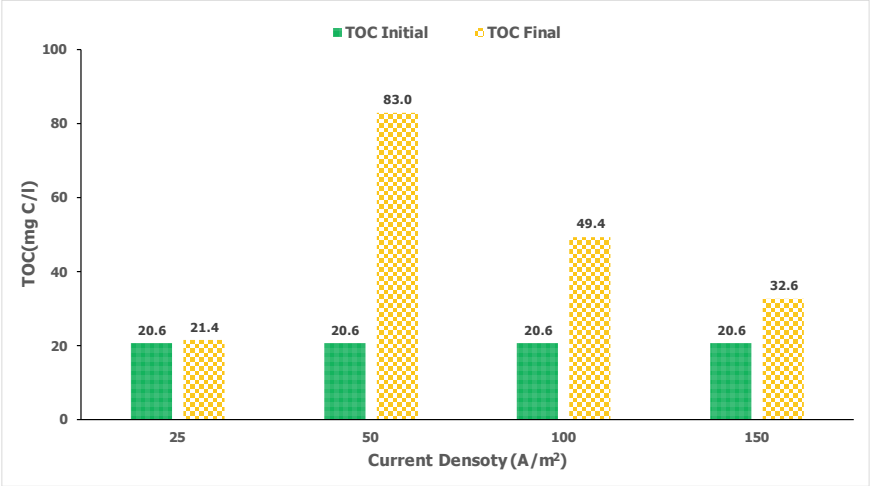

Figure 35 Effect of Current Density – Carbon Fibre Anode – Total organic Carbon (mg-C/L)

Similar to the results discussed in section 4.2.1 (Figure 11 and Figure 12), Again, it is observed that the final COD values were greater than the COD values of the initial solution. This was evident in the TOC results as well. This behaviour can again be explained by the adsorption of humics on the anode surface from the solution of the previous electrolysis batch and subsequent desorption when the electrolyte solutions are decanted and refilled with the next batch. Further,

the breakdown of electrode material into the solution could also result in an increase in the measured COD and TOC despite being filtered with a 0.45 um filter, as the carbon particle size can range from 0.1 µm to 7 µm(Holt & Horne, 1978; Ramulu & Kramlich, 2004).

It can be seen that the COD and TOC readings were maximum for 50 A/m^{2,} i.e., 111.8 ± 15.25 mg O_2/L and 83.0 ± 0.08 mg C/L. At higher current densities, for 100 A/m^2 and 150 A/m^2, it was observed that COD and TOC measurements after electrolysis were relatively lower compared to the values reported for 50 A/m^2. The exact reason for this behaviour is difficult to justify without knowing the rate of adsorption and desorption or the conditions under which the adsorption rate is maximum; this would require further research. Furthermore, this behaviour was also evident from both the spectrophotometric (Figure 36) analysis of the samples and images of the solutions taken after electrolysis(Figure 37). From Figure 36, it can be seen from the final absorbance peaks that after electrolysis, the peaks are much greater than the initial solution, i.e., the absorbance of the initial solution was approximately 0.42 at a wavelength of 288 nm, for 25 A/m^{2,} the absorbance at the peak was relatively similar at around 0.4, whereas the absorbance peak was much higher after electrolysis at 50 A/m^2, 100 A/m^2 and 150 A/m^2, with peak absorbances measured to be 2.3, 1.6 and 0.7, respectively.

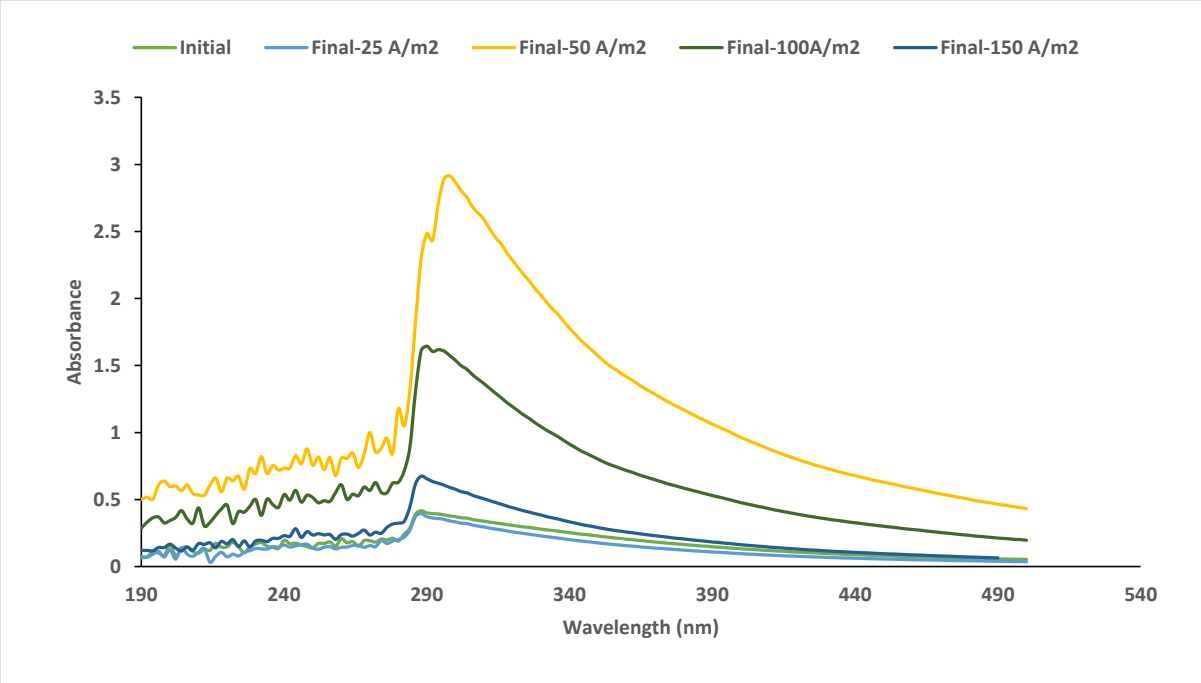

Figure 36 Effect of Current Density-Carbon Fibre Spectrophotometric Analysis

The variation in the colour of the solutions after electrolysis at various current densities is also clear from Figure 37. Evidence of electrode disintegration can also be seen in the final solution after electrolysis at a current density of 150 A/m^2 (black precipitate at the bottom of the container).

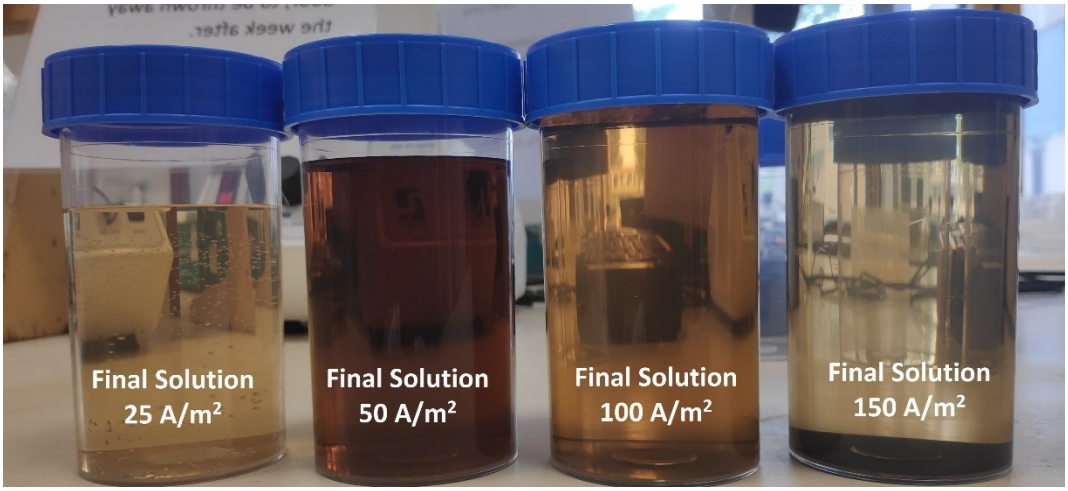

Figure 37 Effect of Current density – Carbon Fibre- Images of the Solutions After Electrolysis

4.3.2 Nickel Foam Anode

In light of the results obtained in section 4.2.2 using the Ni-foam as the anode, experiments were conducted to investigate the effect of increasing current density on the performance of the flow cell electrolyzer with synthetic wastewater and later compared with conventional alkaline water electrolysis with Ni-foam as the anode. The results are illustrated in Figure 38 to Figure 43. The experiments were conducted for a duration of 3 hrs. at applied current densities varying from 25 A/m^2 to 150 A/m^2 with 1M KOH as the supporting electrolyte. The corresponding energy efficiencies of hydrogen production for the Ni-foam electrode used for both the electrolysis of synthetic wastewater and alkaline water(only 1M KOH) are represented in Figure 38. It is observed from Figure 38 that the energy efficiency of hydrogen production

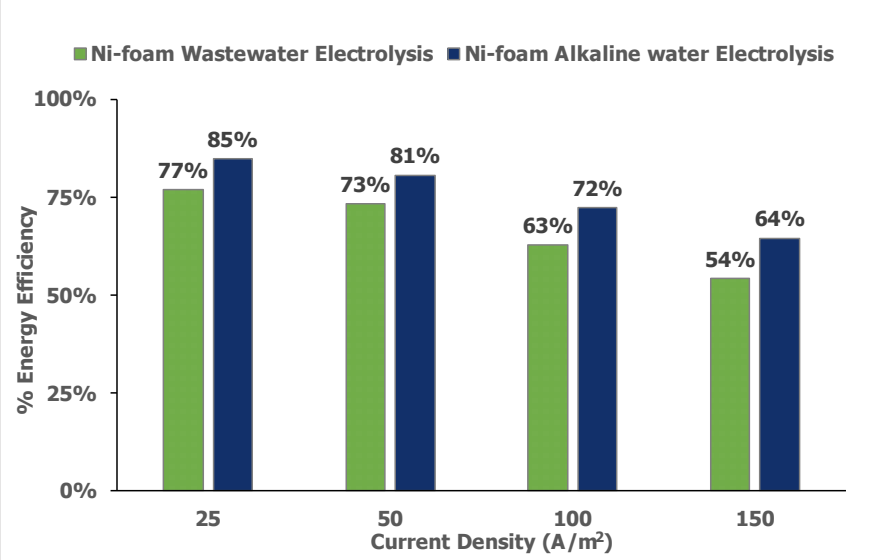

Figure 38 Effect of Current Density – Ni-Foam Anode- Energy Efficiency of Hydrogen Production

for wastewater electrolysis is relatively lower compared to the electrolysis of alkaline water (1M KOH), i.e., for a current density of 25 A/m^2, the efficiency was 77 ± 9.6 % for wastewater electrolysis and for alkaline water electrolysis the efficiency was 85 ± 3.53%. This was evident for higher applied current densities as well, that is, at 50 A/m^2, 100 A/m^{2,} and 150 A/m^2, respectively. The decrease in efficiency can once again be explained by the fact that in addition to water splitting, there is also anodic oxidation of the humic acid in the flow cell(Figure 40). Furthermore, because the experiments were conducted at a constant current density, it would seem that additional energy is required to maintain a constant current density while both water splitting and oxidation of humics occur at the anode(Cho, Kwon, et al., 2014; Cho & Hoffmann,

2017; Kargi & Arikan, 2013). This result agrees with the results described in Figure 22. Also, as mentioned previously in section 4.2.2, it is possible the that the fouling of the anion exchange membrane due to ongoing experiments with humic acid solutions could result in an increase in the membrane resistance, leading to higher ohmic losses in the cell.

In addition, the decreasing trend in the energy efficiency of hydrogen production is also noticeable as the current density is increased from 25 A/m^2 – 150 A/m^2; this can be attributed to two possible reasons. The first is due to increased ohmic losses as the current density is increased(Godula-Jopek, 2015), and the second can be linked to increased bubble formation and dispersion in the anolyte and catholyte chambers as a result of the increased rate of oxygen evolution reaction(OER) and hydrogen evolution reaction(HER). The bubbles can form both on the electrode surface and can disperse in the solution, which increases the resistance resulting in additional ohmic losses, which in turn translates to an increase in the cell potential for a given current density(Wang et al., 2014).

The resultant volumetric hydrogen production for wastewater electrolysis using Ni-foam anode compared with the conventional alkaline water electrolysis also using Ni-foam anode is depicted in Figure 39.

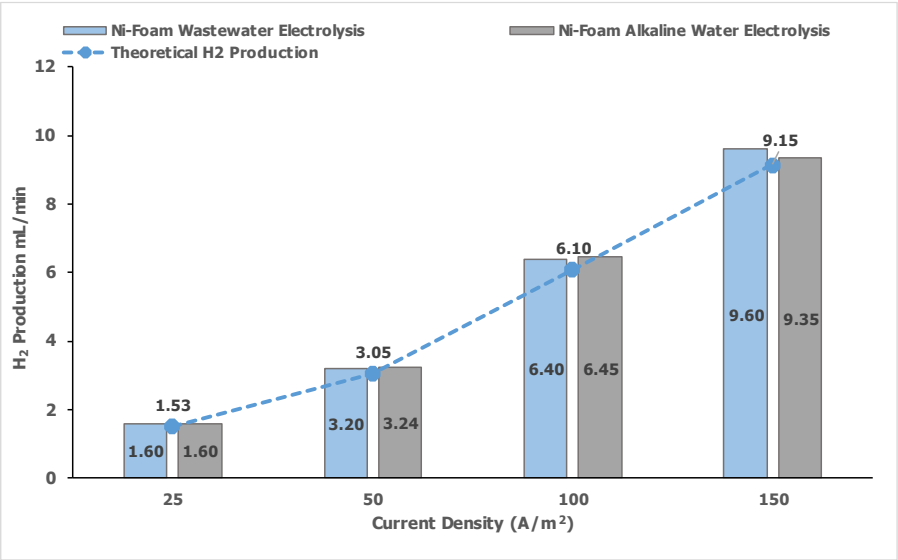

Figure 39 Effect of Current Density-Ni-Foam- Volumetric Hydrogen Production Rate (mL H_2/min)

It can be seen from Figure 39 that the volumetric hydrogen production rates for wastewater electrolysis are quite similar to the volumetric production rate of conventional water electrolysis, similar to the experiments in which carbon fibre was used as the anode(Fig 28). The major difference between the experiments conducted with carbon fibre as an anode and with Ni-foam as the anode is the fact that the energy efficiency is slightly lower for the carbon fibre compared to the Ni-foam anode(Figure 38). In addition, the durability of the Ni-foam anode was much better when used at higher current densities(100 A/m^2 and 150 A/m^2), whereas the carbon fibre anode exhibited material loss under these conditions.

The volumetric hydrogen production rate is comparable for synthetic wastewater and alkaline water at applied current densities of 25 A/m^2 and 50 A/m^2 i.e., 1.6 ± 0.02 mL H_2/min for both synthetic wastewater and alkaline water and 3.20 ± 0.03 mL H_2/min for synthetic wastewater and 3.24 ± 0.03 mL H_2/min for alkaline water. At higher applied current densities, that is, for 100 A/m^2 and 150 A/m^2, it was observed that the volumetric hydrogen production rate when synthetic wastewater was used was slightly higher than when conventional alkaline water was used. It is possible that the oxidation of humics at the anode could potentially enhance the hydrogen production rate(Eker & Kargi, 2010; Kargi et al., 2011). Further, the oxidation of humics was also evident from the COD and TOC removal efficiencies, which are represented in Figure 40 and Figure 41, respectively.

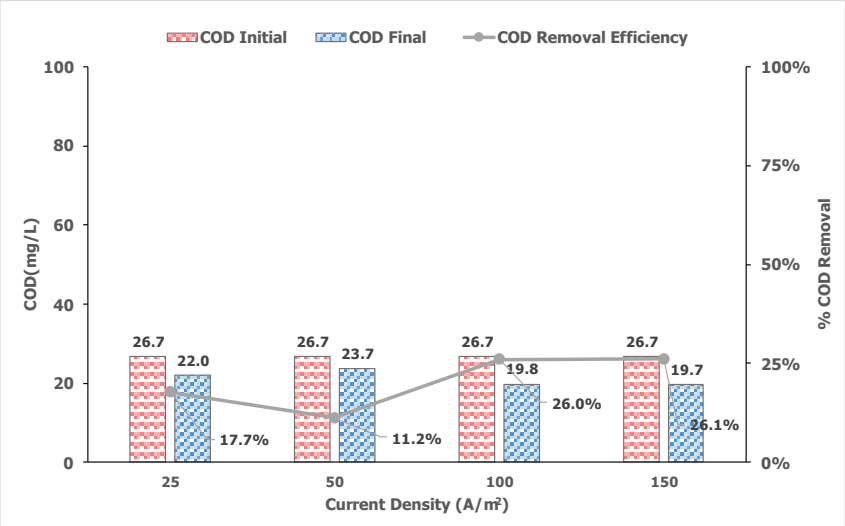

Figure 40 Effect of Current Density- Ni Foam Anode – COD Removal Efficiency

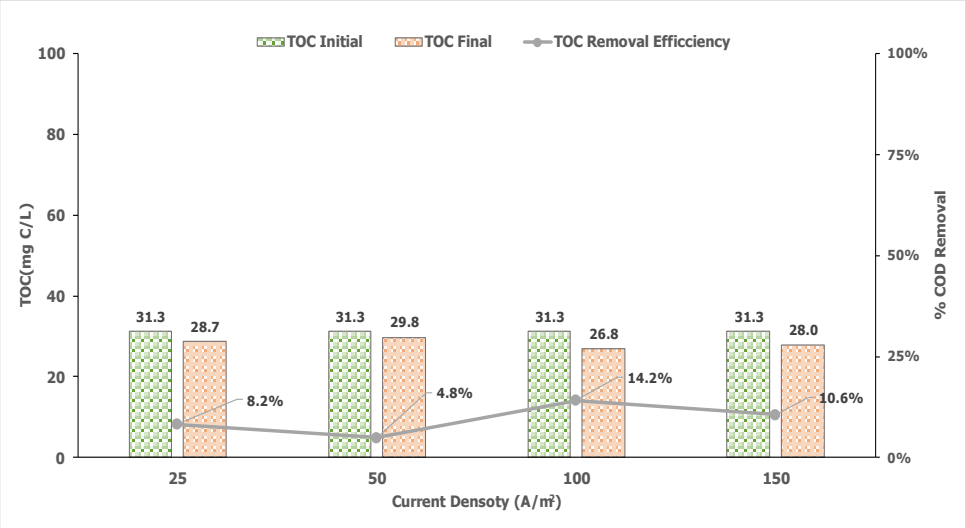

Figure 41 Effect of Current Density – Ni Foam Anode- TOC Removal Efficiency

However, based on the COD removal efficiency, it could be that the contribution of organics oxidation to the hydrogen production rate may not be that substantial since the maximum COD removal obtained was 26 ± 2.7% and 26.1 ± 6.6% at applied current densities of 100 A/m^2 and 150 A/m^2. This was also evident from the coulombic efficiencies obtained for the oxidation of humics(Eq 33), i.e., for applied current densities of 100 A/m^2 and 150 A/m^2 the coulombic efficiencies were 0.5 ± 0.15% and 0.4 ± 0.01 %, respectively. Based on the COD and TOC removal efficiencies, it is evident that the TOC removal efficiencies were noticeably lower than the COD removal efficiencies; for example, for applied current densities of 100 A/m^2 and 150 A/m^2 the corresponding TOC removal efficiencies were only 14.2 ± 1.4% and 10.6 ±1.5%, respectively. This indicates that the oxidation of humic acid molecules at the anode is accompanied by the formation of intermediates as a result of ring breakage due to the complex structure of the molecule(Chiang et al., 2000; Tang et al., 2014; Vlaicu et al., 2011). The formation of intermediates by an was also evident in the HPLC analysis discussed in section 4.2.2 as an increase in the distribution of % low molecular weights was observed compared to the contribution of % high molecular weights(Figure 30). Moreover, It is observed that as the applied current density is increased, there is also an increasing trend observed in the COD removal efficiencies; similar results were also reported by Chiang et al., 2000 and Vlaicu et al., 2011.

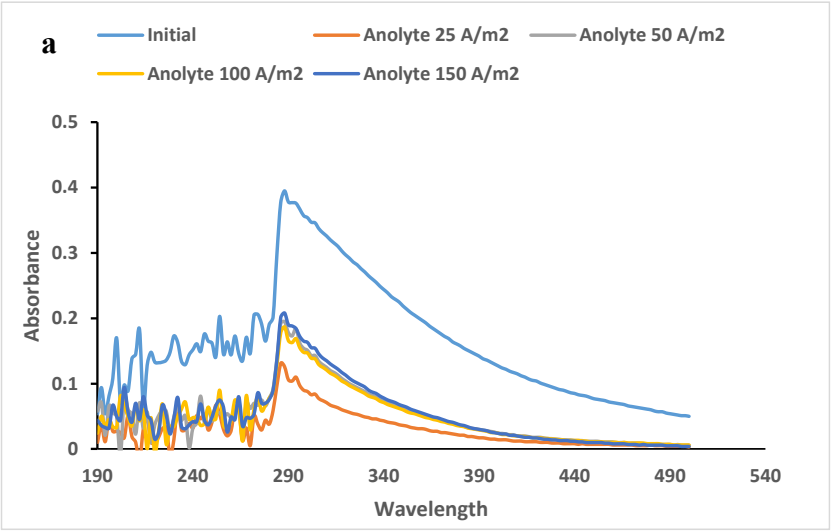

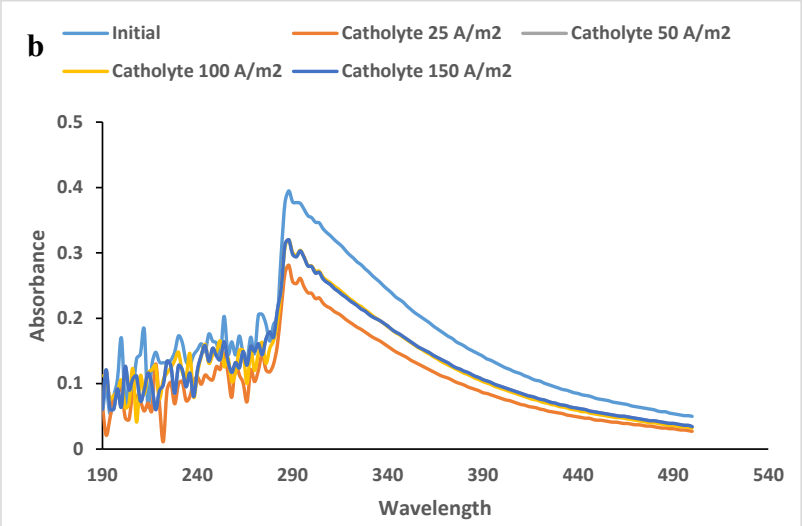

Figure 42 Effect of Current Density-Ni-Foam-Spectrophotometric Analysis

Furthermore, changes in the effluent colour were also noticeable after electrolysis; this could indicate that there could be a decrease in the concentration of humics in the synthetic wastewater after electrolysis. This was observable visually from the photographs of the solutions taken after electrolysis(Figure 43) and was also via spectrophotometric analysis; the corresponding scans are illustrated in Figure 42. The scan was performed for solutions from both the anolyte and catholyte chambers. It can be seen from the anolyte scans in Figure 42a that there is a decrease in the intensity of the absorbance of the solutions after electrolysis with respect to the initial, i.e., the intensity of absorbance at 290 nm decreases from the initial 0.37 to 0.10 after electrolysis. At an applied current density of 25 A/m^2, whereas for applied current densities of 50 A/m^2, 100A/m^2, and 150 A/m^2, the intensity of absorbance decreased to 0.17,

0.16 and 0.18, respectively. Moreover, scans of the catholyte solutions(Figure 42b) after electrolysis also show a decrease in the concentration of humic. A decrease in the intensity of absorbance at 290nm was observed with respect to the initial solution, i.e., the absorbance decreased from the initial 0.39 to 0.28 for a current density of 25 A/m^2 and at an applied current density of 50 A/m^2, 100 A/m^2 and 150 A/m^2 the absorbance decreased to 0.32. This agrees with the results obtained in Figure 17 and Figure 18, i.e., there is the transport of humate molecules from the anolyte chamber to the catholyte chamber.

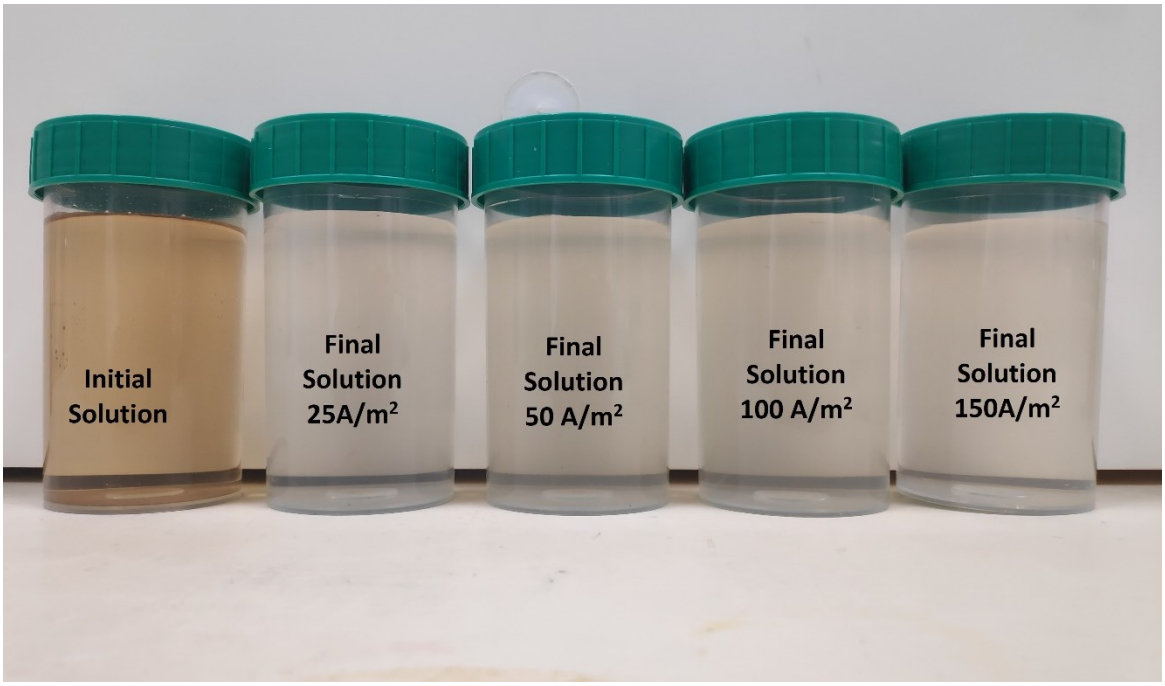

Figure 43 Effect of Current density – Ni-foam - Images of the Solutions After Electrolysis

4.4 Effect of Humic Acid Concentration

4.4.1 Carbon Fibre Anode

In an effort to oxidize the humics at the anode, experiments were conducted using synthetic wastewater with 1M KOH as the supporting electrolyte for 20 mgO_2/L, 50 mgO_2/L, and 100 mg O_2/L HA concentration. In this experiment, the synthetic wastewater was used only in the anolyte chamber, and in the catholyte chamber, only 1M KOH solution was used. The experiments were conducted under potentiostatic conditions for a duration of 24 hrs at an applied voltage of 1.5V and a corresponding current density of 0.46 A/m^2. The corresponding results are depicted in Figure 44 – Figure 49. The potential was selected such that the water splitting at the anode is minimized, i.e., the OER potential of the carbon fibre anode is between 1.7-1.78 V based on the cyclic voltammetry and linear sweep analysis discussed(Figure 4, Figure 5, Figure 6 and Figure 7). The applied potential of 1.5 V was within the water stability region and ensured that water splitting was minimized.

The results of the COD analysis after electrolysis are shown in Figure 44. In accordance with previously reported data for the electrolysis of synthetic wastewater using the carbon fibre anode(sections 4.2.1 and 4.2.2), it is observed that the COD of the solution is once again considerably higher after electrolysis with respect to the initial solution. This was also apparent from the corresponding TOC results in Figure 45. It is observed that for an initial COD of 30.5 ± 1.2 mg O_2/L of humic acid, the final COD was approximately 125.7 ± 1.15 mg O_2/L.

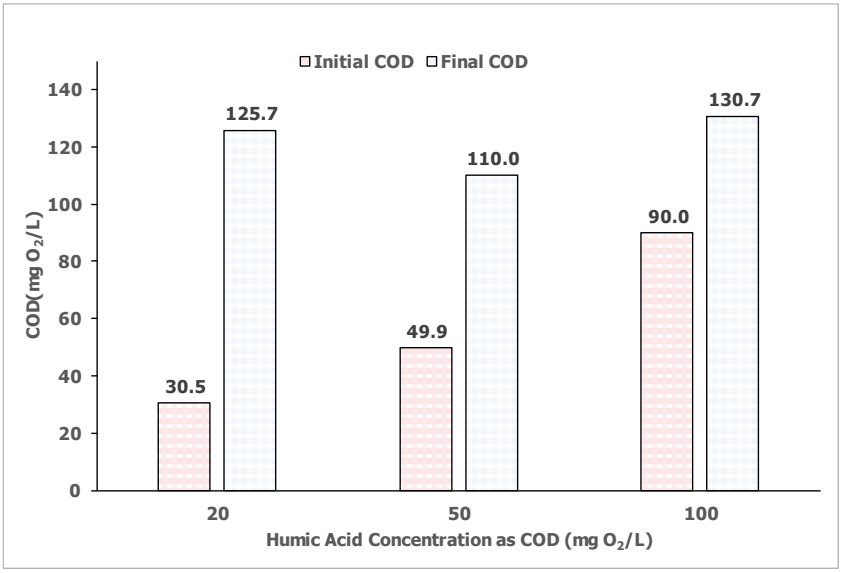

Figure 44 Effect of Humic Acid Concentration- Carbon Fibre Anode – Chemical Oxygen Demand mg O_2/L

similarly, for an initial COD of 49.9 ± 1 mg O_2/L; the COD after electrolysis was 110.0 ± 1.0 mg O_2/L. Regarding TOC results, it was observed that the TOC also increased considerably after electrolysis, i.e., the TOC increased from 21.3 ± 0.2 mg-C/L to 111.70 ± 0.1 mg-C/L for synthetic wastewater prepared with 20 mg O_2/L humic acid, in the same way, the TOC after electrolysis increased to 161.4 ± 0.3 mg-C/L from the initial 52.1 ± 0.15 mg-C/L for synthetic wastewater prepared with 50 mg O_2/L of humic acid.

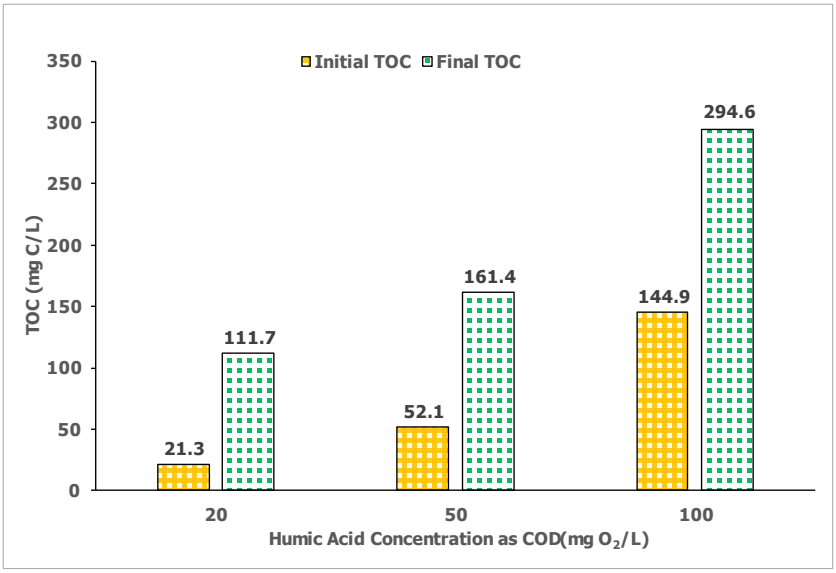

Figure 45 Effect of Humic Acid Concentration-Carbon Fibre Anode – TOC mg-C/L

These observations can be related to the electro-sorption/adsorption of humic acid molecules on the surface of the carbon fibre anode from previous experiment batches and subsequent desorption after the solutions were decanted (Bán et al., 1998). moreover, since there was considerable loss of the electrode material due to electrode disintegration. It is possible that some of these carbon particles may be interfering with the COD and TOC measurements; this could be likely because the carbon particles can range in size from 0.1 µm to 7 µm while the samples were filtered using 0.45 µm filters. Despite this interference, spectrophotometric analysis of the anolyte samples revealed an increase in the intensities of absorbance after electrolysis (Figure 46, Figure 47 and Figure 48). This indicates that the anolyte samples have an increase in the concentration of humic acid. This was also observed visually from the photographs of the anolyte solutions taken after electrolysis. It would seem that under both potentiostatic and galvanostatic conditions (4.3.1 and 4.2.1), the carbon electrode was unable to oxidize the humic acid molecules effectively.

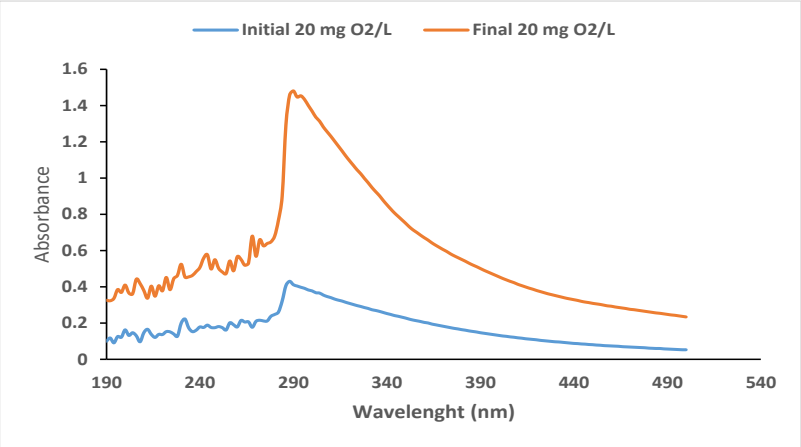

Figure 46 Effect of Humic Acid Concentration – Carbon Fibre Anode- Spectrophotometric Analysis- 20 mg O_2/L Humic Acid

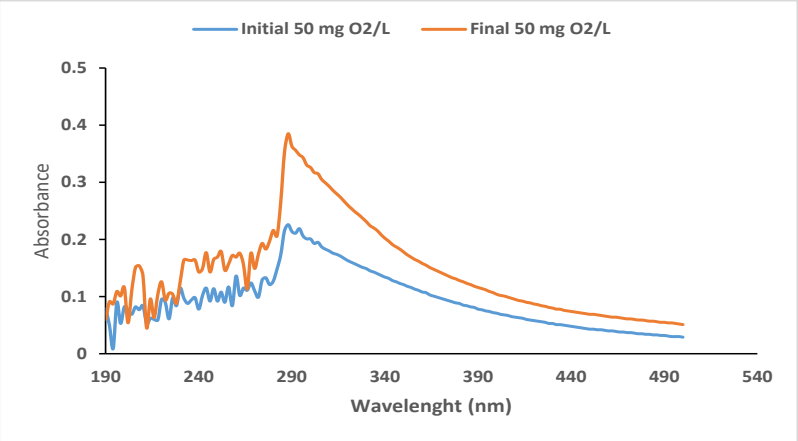

Figure 47 Effect of Humic Acid Concentration – Carbon Fibre Anode- Spectrophotometric Analysis- 50 mg O_2/L Humic Acid

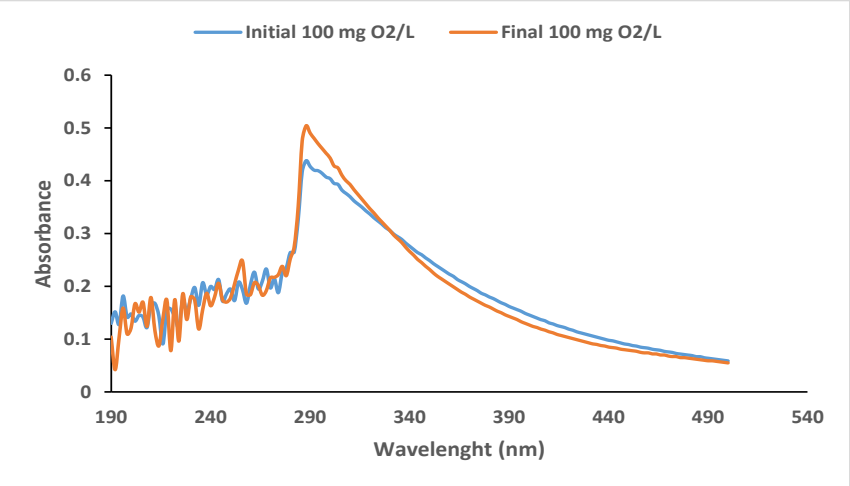

Figure 48 Effect of Humic Acid Concentration – Carbon Fibre Anode- Spectrophotometric Analysis- 100 mg O_2/L Humic Acid

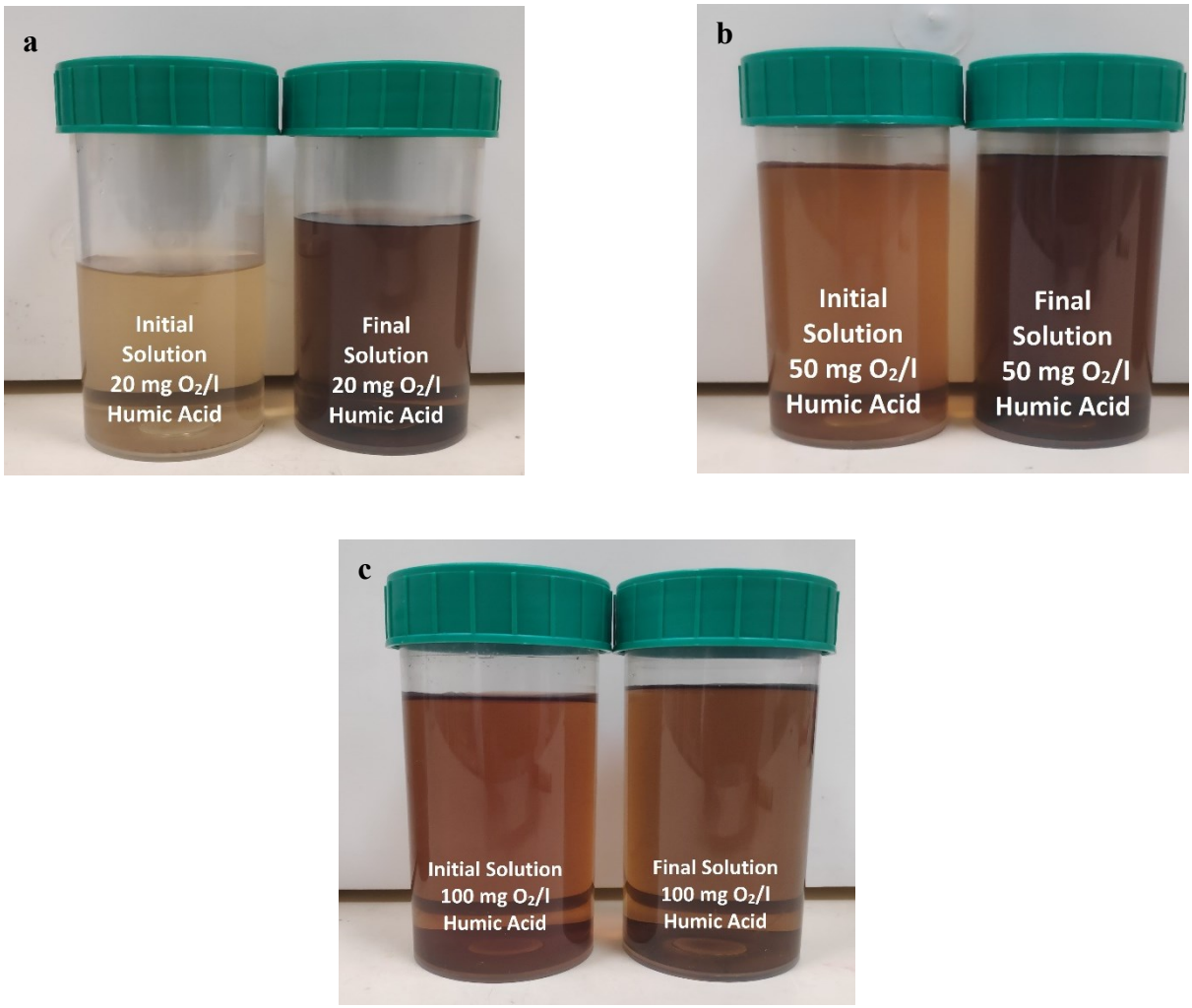

Figure 49 Effect of Humic Acid Concentration – Carbon Fibre Anode- Photographs of the solutions before and after electrolysis ; a) 20 mg O_2/L ; b) 50 mg O_2/L ; c) 100 mg O_2/L

4.4.2 Nickel Foam Anode

For the Ni-foam anode, the effect of humic acid concentration was investigated under galvanostatic conditions for synthetic wastewater containing humic acid concentrations of 20 mg O_2/L, 50 mg O_2/L, and 100 mg O_2/L with 1M KOH as the supporting electrolyte. The current density was selected based on the calculated limiting current density(Eq 28) for the respective concentrations of humic acid, i.e., for 20 mg O_2/L, 50 mg O_2/L and 100 mg O_2/L; the applied current density was 12.55 A/m^2, 31.39 A/m^2 and 62.90 A/m^2. Similar to the experiments conducted with the carbon fibre anode(4.4.1), the synthetic wastewater was only used as the anolyte, whereas 1M KOH was used as the catholyte. The results of this experiment are illustrated in Figure 50- Figure 57.

The corresponding energy efficiency of hydrogen production for the experiments with different humic acid concentrations is represented in Figure 50. The observations agree with the results described in 4.2.2 and 4.3.2; it is observed that the energy efficiency of H_2 production is relatively lower compared to conventional water electrolysis, which can once again be linked to the additional energy required for the side reaction, i.e., oxidation of humics occurs in addition water splitting at the anode and also due to increased resistance of the anionic exchange membrane due to fouling. The oxidation of humics was evident from the COD removal efficiencies as well (Figure 51), in which there was a considerable reduction in the chemical oxygen demand of the anolyte after electrolysis. In addition, a decreasing trend in energy efficiency is observed as the concentration of the humic acid was increased. This can be linked to higher ohmic heating losses as a result of higher applied current densities for the 50 mg O_2/L and 100 mg O_2/L. The colour of the anolyte served as an indicator of COD removal,

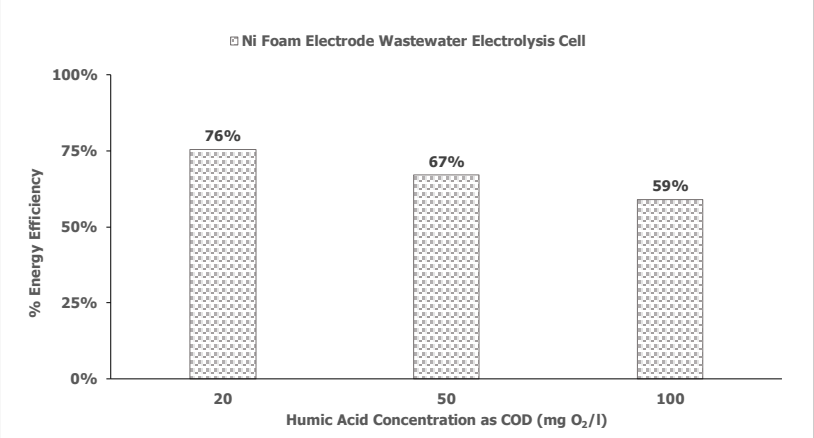

Figure 50 Effect of Humic Acid Concentration- Ni-Foam- Energy Efficiency of Hydrogen Production

i.e., the duration that the anolyte was selected such that when the electrolysis was complete, the colour of the solution turned colourless to very light brown from the initial dark brown. For this to happen, the 50 mg O_2/L solution had to be electrolysed for 6 hrs, and the 100 mgO_2/L solutions had to be electrolysed for 8 hrs.

It is also observed from the COD removal efficiencies that there seems to be an increasing

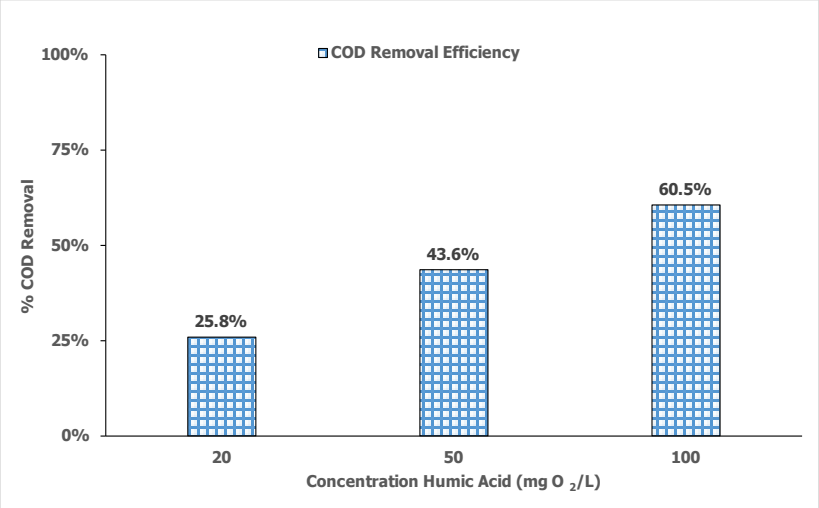

Figure 51 Effect of Humic Acid Concentration- Ni-Foam- COD Removal Efficiency

trend in the removal efficiency as the humic acid concentration is increased. The increase is due to the longer duration of electrolysis required for higher concentrations of humic acid, i.e., an increase in the removal efficiency was observed from 25.8 ± 9% for 20 mg O_2/L to 43.6 ± 5% for 50 mg O_2/L to 60.5 ± 4.2 % for 100 mg O_2/L. Furthermore, the applied current densities were also higher for 50 mg O_2/L and 100 mg O_2/L, based on the results obtained in section 4.3.2(Figure 40) and also from literature (Vlaicu et al., 2011); higher current densities generally result in better removal efficiencies.

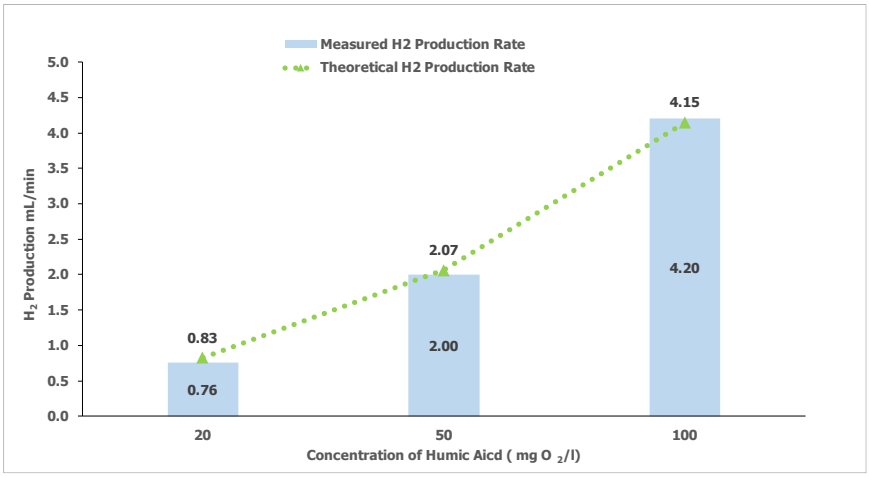

Figure 52 Effect of Humic Acid Concentration- Ni-Foam- Volumetric Hydrogen Production Rate

Due to the oxidation of humic acid, an increase in the volumetric hydrogen production rate would be expected. However, the measured volumetric hydrogen production rates were very close to the theoretically calculated rate (Figure 52). This can be further elaborated by considering the TOC results(Figure 53) in which it is observed that compared to the COD removal efficiency, the TOC removal efficiencies were not that considerable, i.e., for synthetic wastewater prepared with 20 mg O_2/L, the TOC removal efficiency was only 17 ± 0.3% whereas for the 50 mg O_2/L and 100 mg O_2/L solutions the removal efficiencies were 11.8 ± 0.2% and 27.3 ± 0.5 %, respectively. This indicates that there is only partial oxidation of humics, which is further accompanied by the formation of intermediates resulting in lower TOC removal efficiencies. Thus, the contribution of organics oxidation to the hydrogen may

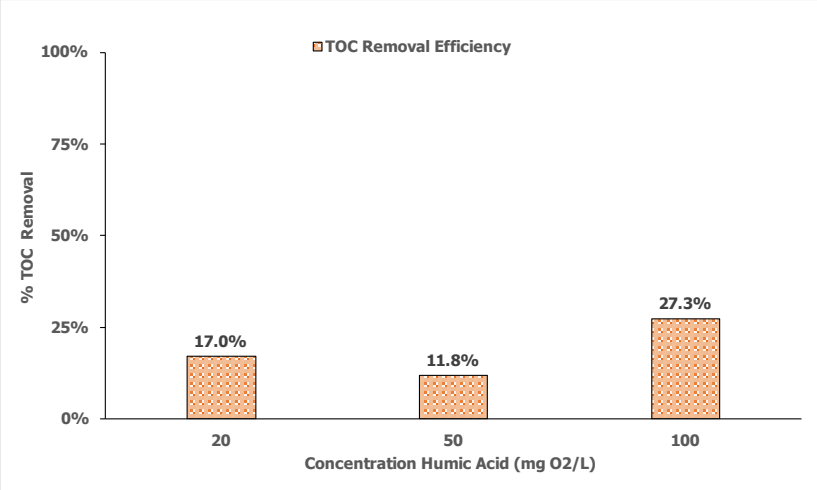

Figure 53 Effect of Humic Acid Concentration- Ni-Foam- TOC Removal Efficiency

not be that significant. This was also clear from the calculated coulombic efficiencies for the oxidation of humics over the duration of electrolysis, i.e., for the oxidation of 20 mg O_2/L the coulombic efficiency was 4.0 ± 0.5%, similarly for 50 mg O_2/L and 100 mg O_2/L, the calculated current efficiencies were 1.2 ± 0.04% and 0.9 ± 0.02%, respectively. In comparison, the corresponding coulombic efficiencies for the oxygen evolution reaction at the anode for the solutions containing 20 mg O_2/L, 50 mg O_2/L, and 100 mg O_2/L averaged 97.5 ± 3.3%(Appendix A.4).

Even though the electrolysis of synthetic wastewater resulted in low TOC removal efficiencies, the spectrophotometric analysis revealed that there was still some reduction in the humic acid concentrations after electrolysis. This is better illustrated in Figure 54 - Figure 57. It can be

seen from the scans that there is a decrease in the intensity of absorbance at 290 nm for all the tested concentrations of humic acid. For instance, when considering the scans for the solution containing 20 mg O_2/L of humic acid, the intensity of absorbance decreases from 0.395 to 0.195 after electrolysis. Similarly, for the solutions containing 50 mg O_2/L and 100 mg O_2/L of humic acid wherein the intensity of absorbance decreased from 0.97 to 0.39 and from 1.80 to 0.52, respectively. The change in colour of the solutions after electrolysis was also apparent from the photographs of the solutions (Figure 57). This observation is also in accordance with the spectral scans described in section 4.2.2 (Figure 26 - Figure 28) and section 4.3.2(Figure 42).

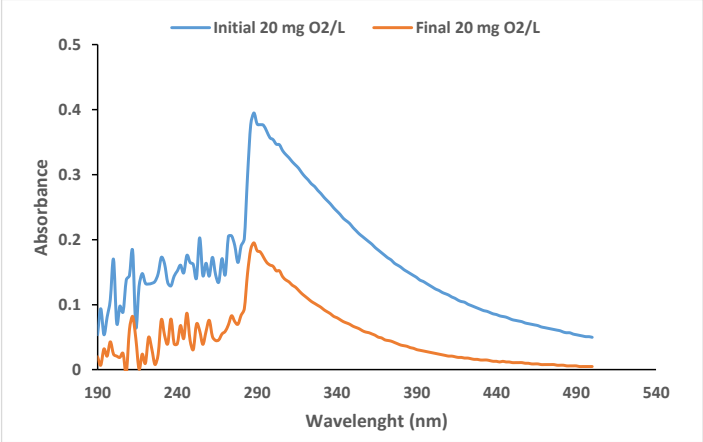

Figure 54 Effect of Humic Acid Concentration – Ni-Foam Anode- Spectrophotometric Analysis- 20 mg O_2/L Humic Acid

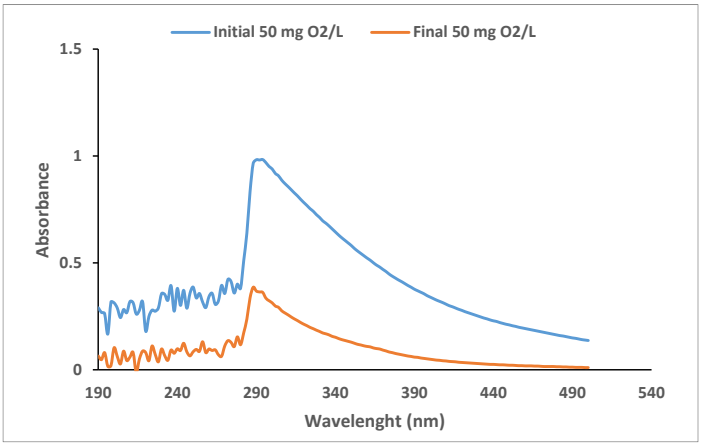

Figure 55 Effect of Humic Acid Concentration – Ni-Foam Anode- Spectrophotometric Analysis- 50 mg O_2/L Humic Acid

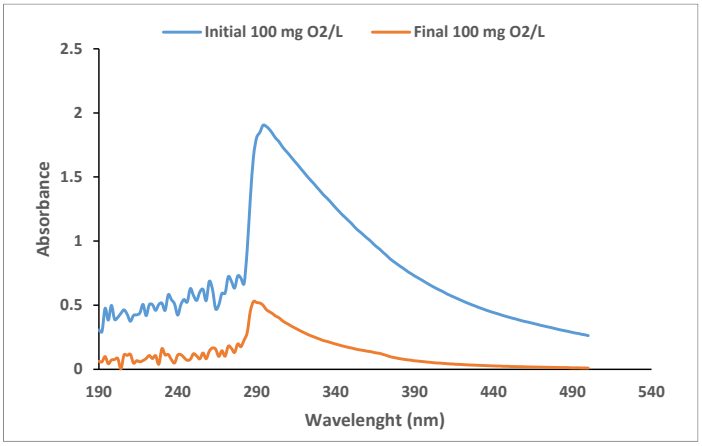

Figure 56 Effect of Humic Acid Concentration – Ni-Foam Anode- Spectrophotometric Analysis- 100 mg O_2/L Humic Acid

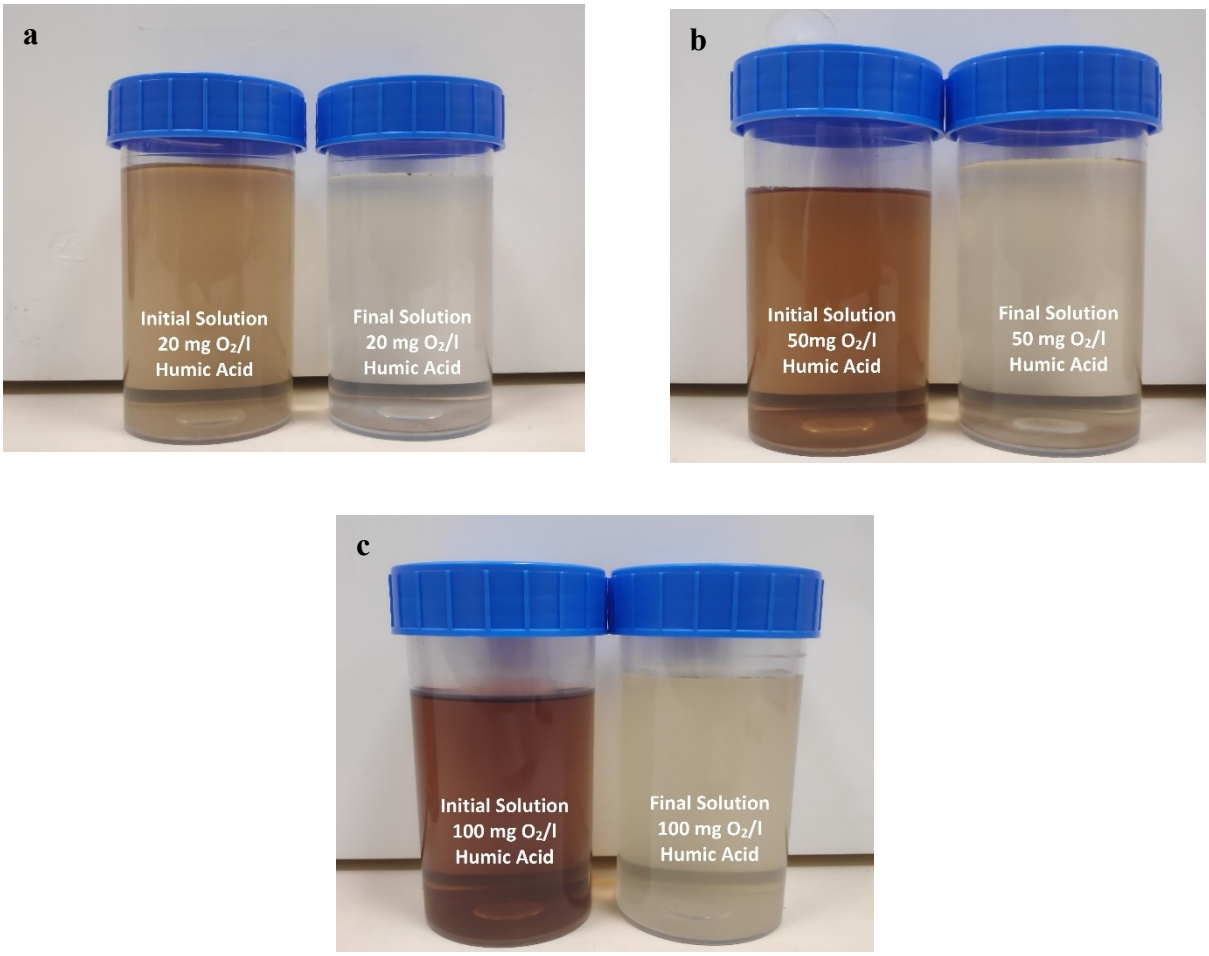

Figure 57 Effect of Humic Acid Concentration – Ni-Foam Anode- Photographs of the solutions before and after electrolysis ; a) 20 mg O_2/L ; b) 50 mg O_2/L ; c) 100 mg O_2/L

4.5 Experiments with Real Municipal Effluent

Based on the results discussed in the previous sections with synthetically prepared. Further experiments were conducted with real municipal effluent obtained from the Harnaschpolder water treatment plant. The corresponding water quality of municipal effluent is represented in Table 3, respectively. The experiments were conducted to investigate the effects of electrolyte concentration (KOH) and applied current density on the volumetric hydrogen production, energy efficiency of hydrogen production, and COD removal efficiency. For all experiments, municipal effluent was employed as the anolyte, and the catholyte used was only a KOH

Table 3 Quality of Effluent at Harnaschpolder Wastewater Treatment Plant(Rietveld et al., 2011).

Parameter	Unit	Average
C	µS/cm	989
TSS	mg/L	7.38
TKN	mg/L	2.13
NH_4-N	mg N/L	0.58
BOD_5	mg O_2/L	3.28
COD	mg O_2/L	36.89
NO_3-N	mg N/L	4.7
PO_4-P	mg/L	0.49
Total P	mg/L	0.8
Total N	mg/L	6.83
Pb	µg/L	2.48
Zn	µg/L	23.75
Cr	µg/L	1.21
As	µg/L	1.23
Cu	µg/L	0.83
Cd	µg/L	0.05
Hg	µg/L	0.03
Cl	mg/L	133.7
Ca	mg/L	63.6
SO_4	mg/L	62.5
Na	mg/L	96.9
Mg	mg/L	8.56
K	mg/L	23
Hardness	mmol/L	2.12

solution prepared in demi water. This was done firstly to prevent the cathodic deposition of Ca^{2+} and Mg^{2+} species, which is present in the municipal effluent(Table 2), and secondly to prevent crossover of anions, more specifically the humate anions from the catholyte chamber to the anolyte chamber. Moreover, prior to solution preparation, the municipal effluent was filtered with 0.45 µm filter paper to remove suspended and large particulate matter. The experiments were conducted for both the carbon fibre and the Ni-foam anode and are discussed in the subsequent sections.

4.5.1 Effect of Electrolyte Concentration

Analogous to the experiments conducted in section 4.3, electrolysis of municipal effluent was conducted for KOH concentrations ranging from 0.01M to 1M. The experiments were conducted at an applied current density of 12.55 A/m^2 for a duration of 3hrs. Figure 59 represents the energy efficiency of hydrogen production and represents the corresponding volumetric hydrogen production rate; the results are compared for both Ni-foam and carbon fibre anodes.

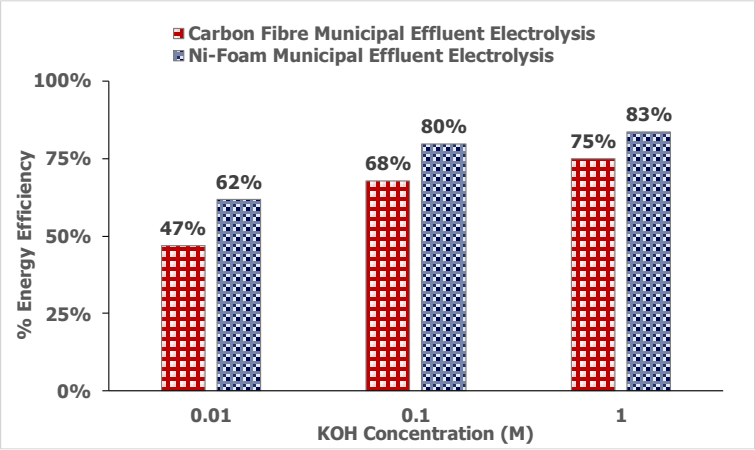

Figure 58 Effect of KOH Concentration -Municipal Effluent – Energy Efficiency of Hydrogen Production- Carbon Fibre and Ni- Foam Anode

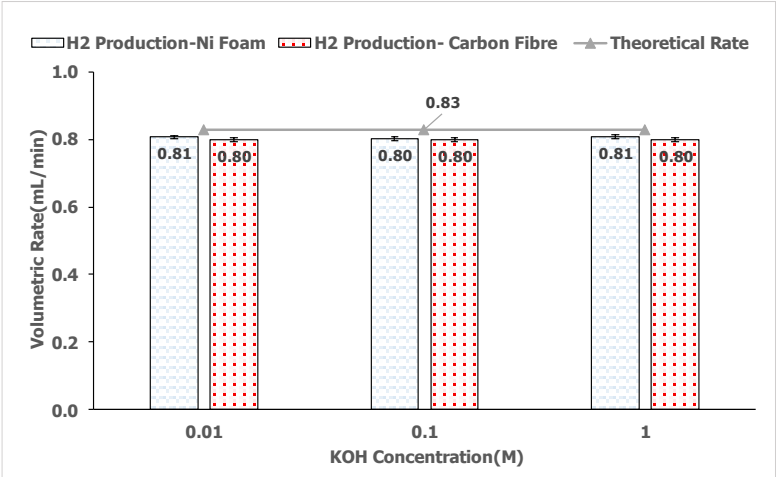

Figure 59 Effect of KOH Concentration -Municipal Effluent – Volumetric Hydrogen Production Rate - Carbon Fibre and Ni- Foam Anode

In accordance with the results discussed in section 4.3, it is observed that the energy efficiency of hydrogen production using municipal effluent is higher for the Ni-Foam electrode compared to the Carbon fibre anode. For instance, if we consider the municipal effluent solution with 1M KOH as the supporting electrolyte, the corresponding energy efficiency for the carbon fibre anode is 75 ± 3%, and for the Ni-foam anode, the energy efficiency was 83 ± 3%. This can be related to the higher overpotential of the carbon-fibre anode compared to the Ni-foam anode(Figure 7).

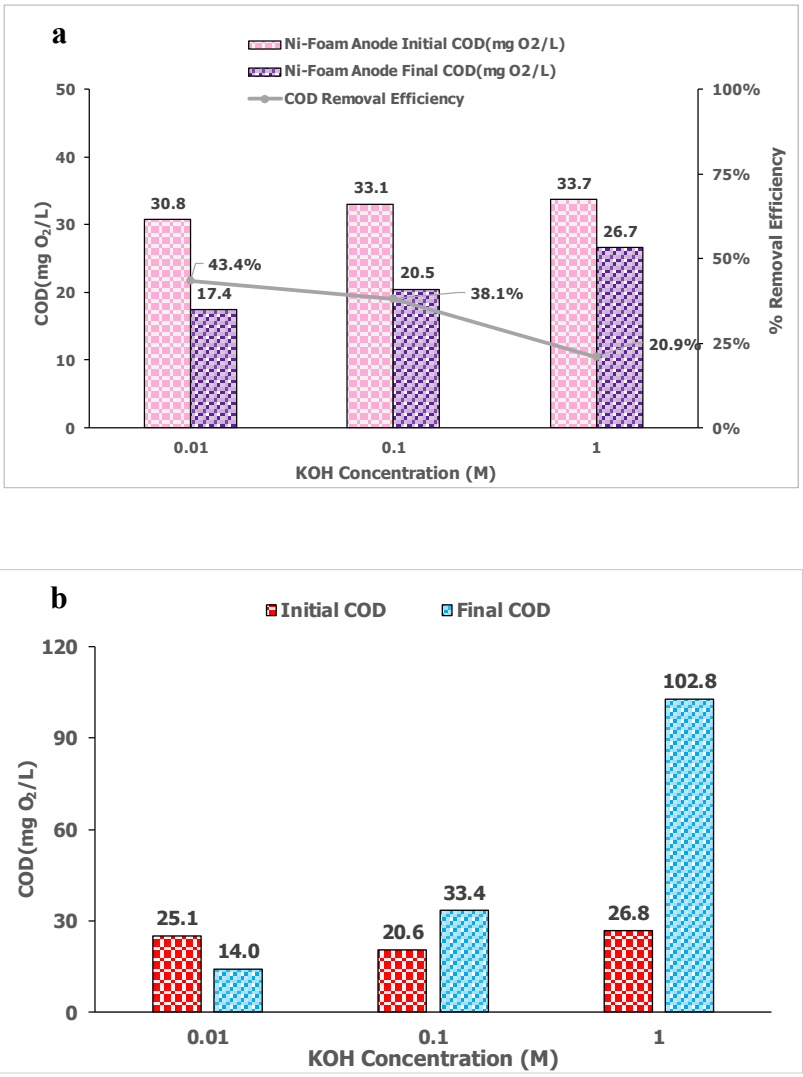

Figure 60 Effect of KOH Concentration- Municipal Effluent- Chemical Oxygen Demand (mg O_2/L) a) Ni-Foam Anode b) Carbon Fibre Anode

Moreover, the energy efficiencies of hydrogen production via electrolysis of municipal effluent were also lower versus conventional alkaline water electrolysis, i.e., For the Ni-foam anode in 1M KOH solution, a maximum efficiency of 85 ± 7% was recorded. When considering the municipal effluent electrolysis using the Ni-foam anode, the drop in the energy efficiency can be explained by other side reactions that can occur on the anode in addition to water splitting. Based on the water quality for municipal effluent (Table 3), the possible side reactions that can occur could be due to the oxidation of chloride ions (chlorine evolution reaction, CLER), the oxidation of sulfate ions(Dresp et al., 2019) and also because of the oxidation of organics in the solution, which was evidenced by the decrease in the COD after electrolysis(Cho, Kwon, et al., 2014; Cho & Hoffmann, 2017). The same can be expected to occur for the carbon fibre anode; however, the contribution of organics oxidation may not be that considerable due to the low COD removal efficiencies.

The volumetric hydrogen production rates of municipal effluent electrolysis for both the Ni-foam anode and the carbon fibre anode are represented in Figure 59. It is observed that despite the use of municipal effluent, the hydrogen production for both the Ni-foam and the carbon fibre anode were similar; that is, the measured volumetric hydrogen production rates for municipal effluent for all concentrations of electrolyte(KOH) for both the electrodes was approximately 0.800 ± 0.13 mL H_2/ min comparable to the theoretical rate of 0.83 mL H_2/min all be it at lower energy efficiency.

It is observed from Figure 60a that the electrolysis of the municipal effluent using Ni-Foam anode can lead to considerable removal of COD after electrolysis for all concentrations of KOH ranging from 0.1 - 1M KOH, respectively. Furthermore, it can be seen that as the concentration of KOH increases, the corresponding COD removal decreases, i.e., the COD removal efficiency for 0.01M KOH solution is 43.4 ± 3% and decreases to 38.1 ± 7.0% and 20.9 ± 5% for the 0.1M KOH and 1M KOH solutions, respectively. This is similar to the observations obtained for synthetically produced wastewater described in section 4.3.2 (Figure 22). Moreover, the spectrophotometric scans represented in Figure 61 also agreed with this, where the intensity of absorbance of the solution after electrolysis was higher for 0.1M and 1M KOH compared to 0.01M KOH, i.e., the absorbance for the 0.01M KOH solution after electrolysis was 0.03, for the 0.1M KOH solution the absorbance was 0.04 and for 1M KOH solution the absorbance was 0.065(Figure 61a, Figure 61b, and Figure 61c).

In contrast, the carbon fibre anode only showed a decrease in the COD for 0.01M KOH solution, but for 0.1M and 1M KOH solutions, a subsequent increase in the COD concentration was observed after electrolysis for 0.1M and 1M KOH solutions(Figure 61d, Figure 61and Figure 61f). There could likely be a reduction in COD after electrolysis using the carbon fibre anode in light of the reduction of COD observed in the 0.01M KOH solution; however, due to the electro-sorption/adsorption of humics during electrolysis and the subsequent desorption after electrolysis the, change in COD can be difficult assess for the subsequent solutions. Moreover, the spectrophotometric scans also conform to the pattern of the final COD measured, where it can be seen that for the 0.01M KOH solution, the intensity of absorbance at 290 nm

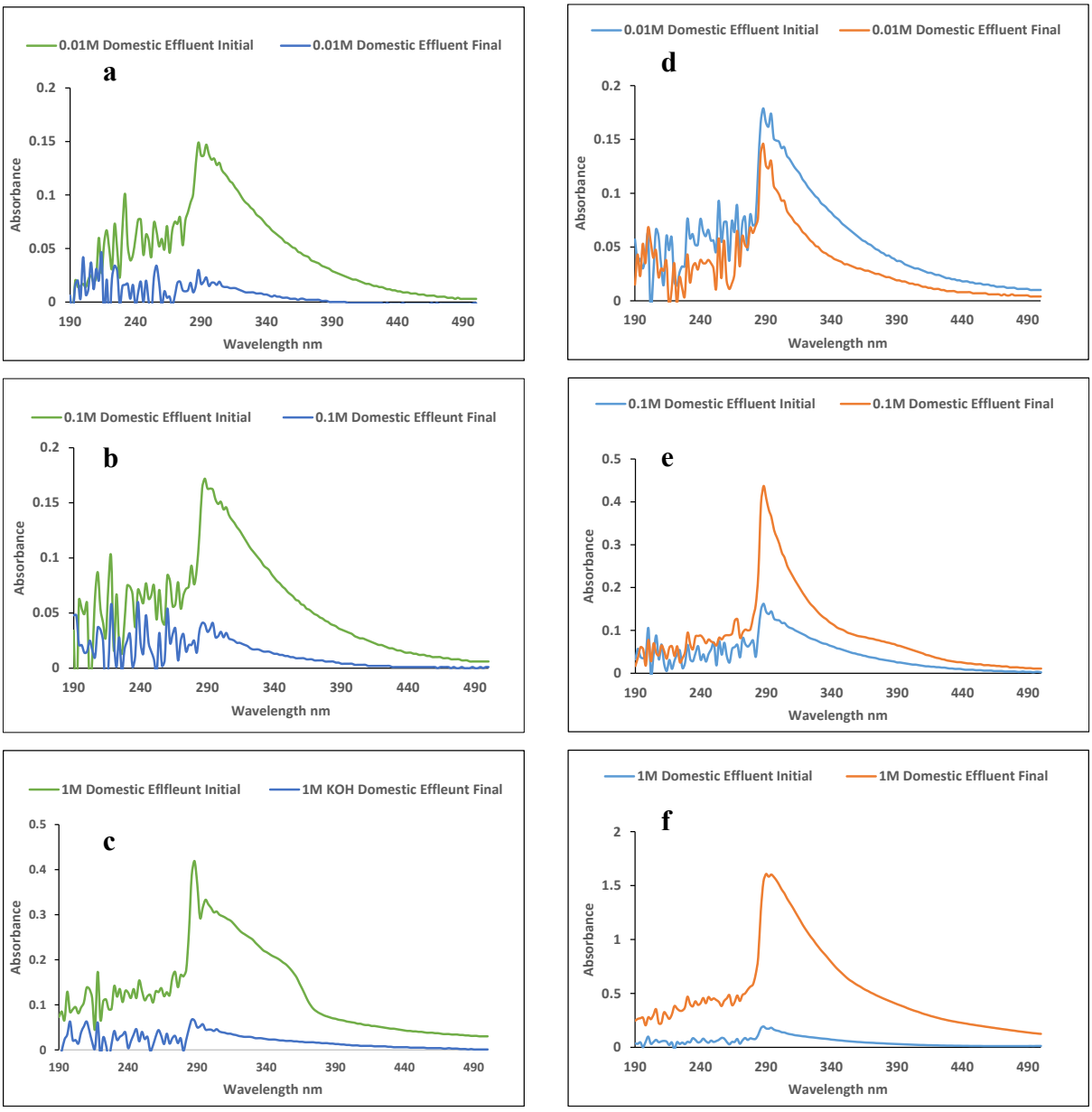

Figure 61 Effect of KOH- Municipal Effluent- Spectrophotometric Scans- 0.01M - 1MKOH.

a, b, and c – Ni-Foam Anode ; d, e, and f – Carbon Fibre Anode.

decreased from 0.18to 0.15 after electrolysis, whereas the intensity absorbance at 290 nm increased at higher concentrations of KOH, i.e., the absorbance at 290 nm increased from 0.16 to 0.43 for the 0.1M KOH solution and an increase from 0.19 to 1.54 for 1M KOH solution. This is also evident from the photographs of the solutions taken before and after electrolysis and is illustrated in Figure 62.

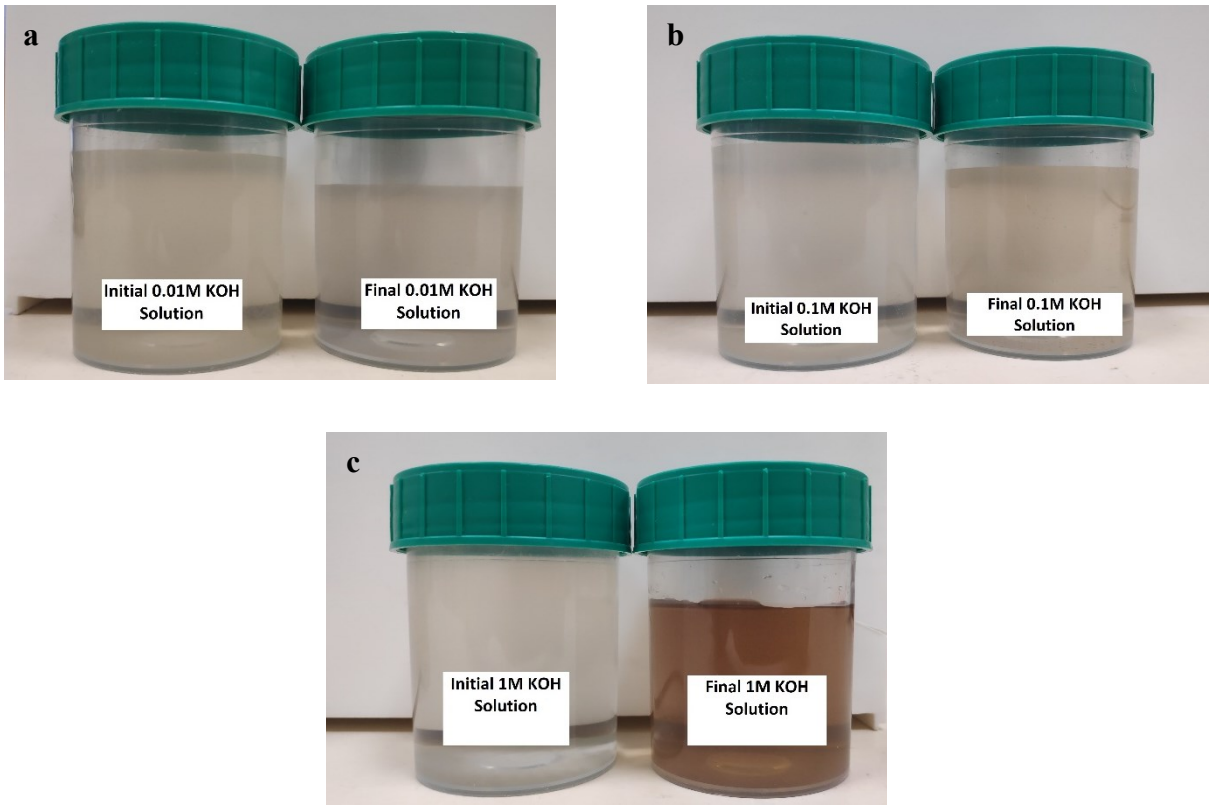

Figure 62 Effect of KOH-Municipal Effluent-Carbon Fibre Anode - Initial and Final solutions a- 0.01M KOH; b-0.01M KOH ; c-0.01M KOH

4.5.2 Effect of Current Density

The effect of applied current density was also investigated using municipal effluent for both the Ni-Foam and the carbon fibre anode. Based on the results described in section 4.6.1, the municipal effluent was used with 1M KOH as the supporting electrolyte. Experiments were conducted for applied current densities ranging from 25 A/m^2 to 150 A/m^2 for a duration of 3hrs, similar to previously conducted experiments described in section 4.3. The corresponding energy efficiencies of hydrogen production are illustrated in Figure 63.

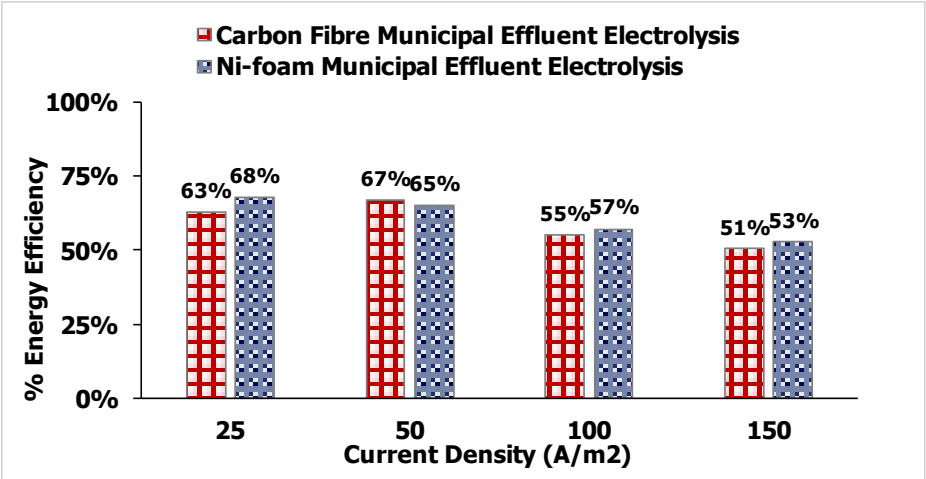

Figure 63 Effect of Current Density -Municipal Effluent – Energy Efficiency of Hydrogen Production- Carbon Fibre and Ni- Foam Anode

From Figure 63, it is evident that the energy efficiency of hydrogen production is slightly higher for the Ni-foam electrode compared to the carbon fibre electrode; this is to be expected owing to the lower OER overpotential of Ni-Foam compared to the carbon fibre electrode, i.e., 1.6V for Ni-foam and 1.7V for Carbon Fibre(Figure 7).

Moreover, similar to the observations described in section 4.3, it is observed that the energy efficiency progressively decreases as the current density is increased; as previously discussed, this is linked to ohmic losses at higher current densities, increased resistance due to bubble formation at the electrode surface and bubble dispersion in the solution which is enhanced at higher current densities(Holladay et al., 2009; Zeng & Zhang, 2010). When compared to the energy efficiency of hydrogen production using synthetic effluent, it is observed that the energy efficiency of hydrogen production using municipal effluent is relatively lower for both the Ni-foam and the carbon fibre anode; further, the efficiency was also lower compared to conventional water electrolysis. For instance, if we consider an applied current density of 25

A/m^2, it can be seen that the energy efficiency of hydrogen production using synthetic wastewater for the Ni-foam and carbon fibre anode was 77 ± 10% and 75 ± 2.3%, respectively(Figure 38 and Figure 31). In contrast, the energy efficiency of hydrogen production using municipal effluent for the Ni-foam and the carbon Fibre anodes were 68 ± 8% and 63 ± 7.3%, respectively(Figure 63), and for conventional alkaline water electrolysis using Ni-foam anode, the energy efficiency was close to 85 ± 6.9%.

When considering the Ni-foam anode, the decrease in energy efficiency with respect to conventional alkaline can be explained by the additional side reaction, that is, the oxidation of humics in the system during electrolysis. This is also evidenced by the decrease in the COD measured after electrolysis compared to the initial (Figure 64a). This behaviour was also observed for the electrolysis of synthetic wastewater using the Ni-foam anode described previously in section 4.3.2. When considering the carbon fibre anode, it is difficult to say whether the oxidation of organics actually occurs because the measured COD after electrolysis was always greater than the initial (Figure 64b) owing to the adsorption of humate on the surface of the carbon fibre electrode.

Moreover, it was observed that the carbon fibre electrode would tend to disintegrate during the electrolysis process, and at current densities greater than 25 $A/m^{2,}$ the surface disintegration of the electrode was accelerated. The loss of material can increase the contact resistance between the current collector and the electrode, thereby decreasing the overall energy efficiency of hydrogen production(Nourani et al., 2019). Further, the energy efficiency was still lower for both the Ni-foam and the carbon fibre anode for the electrolysis of municipal effluent compared to the electrolysis of synthetic wastewater; this behaviour may be attributed to an increase in the resistance of the anion exchange membrane due to increased fouling by the humic acid molecules.

It can be seen that the electrolysis of municipal effluent using the Ni-foam anode resulted in a decrease in the COD of the solution after electrolysis (Figure 64). Based on the COD removal efficiencies, an increasing trend is observed as the applied current density is increased, i.e., the COD removal efficiency increased from 17.5 ± 9% at an applied current density of 25 A/m^2 to 19.1 ± 4 % at an applied current density of 100 A/m^2 with a slight decrease to 18.4 ± 4 % at 150 A/m^2. The calculated coulombic efficiency also indicated that during the electrolysis

process, not much current is diverted towards the oxidation of organics, i.e., for the applied current densities of 25 A/m^2, 50 A/m^2, 100 A/m^{2,} and 150 A/m^2 the corresponding coulombic efficiencies for organics oxidation were 0.9 ± 0.7%, 0.51 ± 0.4 %, 0.3 ± 0.2%, and 0.17 ± 0.2 %, respectively whereas the coulombic efficiency for the OER was on average 91 ± 5% for all the applied current densities(Appendix A.4).

In contrast, the electrolysis of the municipal effluent using the carbon fibre anode showed only an increase in the COD of the solution after electrolysis; moreover, compared to the experiments conducted with carbon fibre anode described in the previous sections the disintegration of the electrode was observably higher; during the electrolysis, the colour of the solution would change from light brown to dark brownish/black(Figure 65).

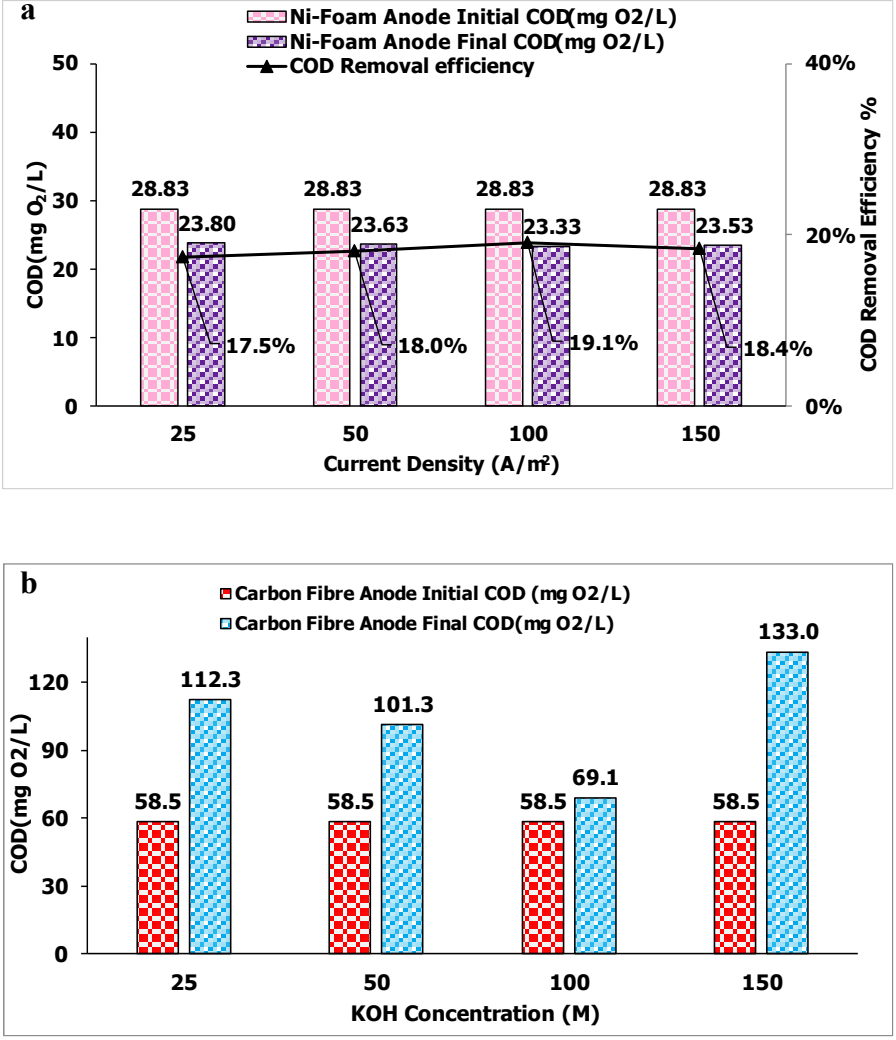

Figure 64 Effect of Current Density- Municipal Effluent- Chemical Oxygen Demand (mg O_2/L) a) Ni-Foam Anode b) Carbon Fibre Anode

As a result of the increased carbon concentration in the solution, it is likely that some of these particles could be oxidized in accordance with Eq 46, Eq 47, and Eq 48, respectively(Nourani et al., 2019).

$$C + 2OH^- \rightarrow CO_2 + 2H^+ + 2e^- \quad \text{Eq 34}$$

$$C + OH^- \rightarrow CO + H^+ + 2e^- \quad \text{Eq 35}$$

$$CO + OH^- \rightarrow CO_2 + H^+ + 2e^- \quad \text{Eq 36}$$

Figure 65 Image of The Final Solution Just After Electrolysis of The Municipal Effluent at an Applied Current Density Of 100 A/m^2

This is also evident from the coulombic efficiency for the OER using the carbon fibre anode, i.e., the OER coulombic efficiency averaged 69 ± 7.4%, which is significantly lower than the coulombic efficiencies obtained in section 4.3.1 using just synthetic wastewater wherein the coulombic efficiency averaged 96 ± 3.0%. Based on the volumetric hydrogen production rates (Figure 66), it is observed that the hydrogen production rates for municipal effluent using both the Ni-foam and carbon fibre anodes are very close to the theoretical production. This behaviour is logical based on the HER coulombic efficiencies, which averaged 91 ± 3.5% for both the Ni-foam and carbon fibre anode(Appendix A.4). Despite the carbon fibre anode exhibiting lower OER coulombic efficiencies, there is still a generation of H^+ as a result of carbon oxidation (Eq 46-48) which would satisfy the H^+ requirement at the cathode.

Further, based on the results reported by Kargi & Arikan, 2013. it would be expected that hydrogen production would be enhanced. However, this was not observed mainly due to the fact that the COD removal efficiencies were not that considerable(Figure 64a) and also compared to the study conducted by Eker & Kargi, 2010; Kargi & Arikan, 2013; Kargi & Catalkaya, 2011; the initial COD was much lower since their study employed the use of raw wastewater with COD in the range 5000 to 25000 mg/L and in this study treated wastewater(Municipal effluent) was used with a residual COD in the range 28- 58 mg/L.

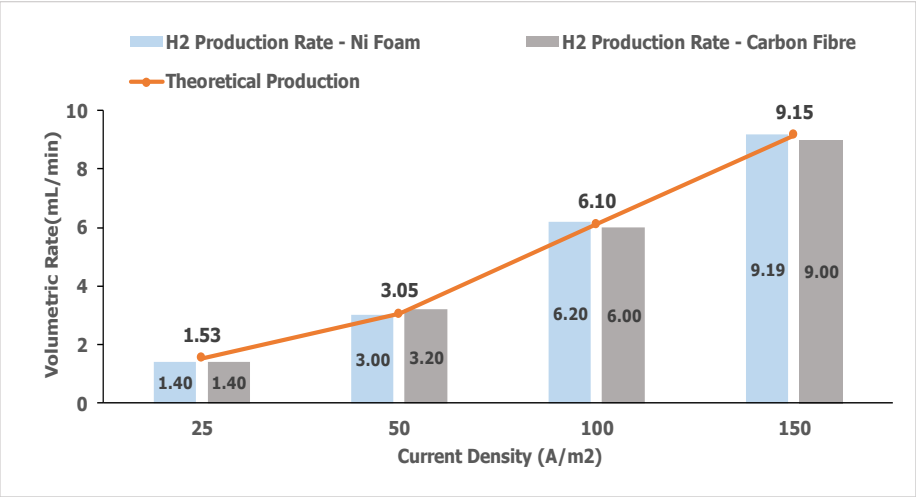

Figure 66 Effect of Current Density – Municipal Effluent – Volumetric Hydrogen Production Rates – Ni-Foam and Carbon Fibre Anode

Samples after electrolysis were also scanned spectrophotometrically to assess the extent of humic acid removal after electrolysis. The spectral scans and photos taken after electrolysis of Municipal effluent using Ni-foam anode are represented in Figure 67, whereas the same for the carbon fibre anode is represented in Figure 68.

It is observed from Figure 67a that there is a reduction in the intensity of absorbance at 290 nm after electrolysis of municipal effluent for all applied current densities, i.e., the absorbance decreased from the initial 0.157 to 0.101 for 25 A/m^2, 0.09 for 50 A/m^2 and 0.08 for applied current densities 100 A/m^2 and 150 A/m^2, respectively. The decrease in the intensity of absorbance is indicative of oxidation of the humic acid after electrolysis. Moreover, from Figure 67b, the change in colour of the solution was also apparent; the solution colour changed from the initial light brown to colourless for all applied current densities. This trend was also observed when synthetic wastewater was electrolysed with Ni-foam(section 4.3.2, Figure 43).

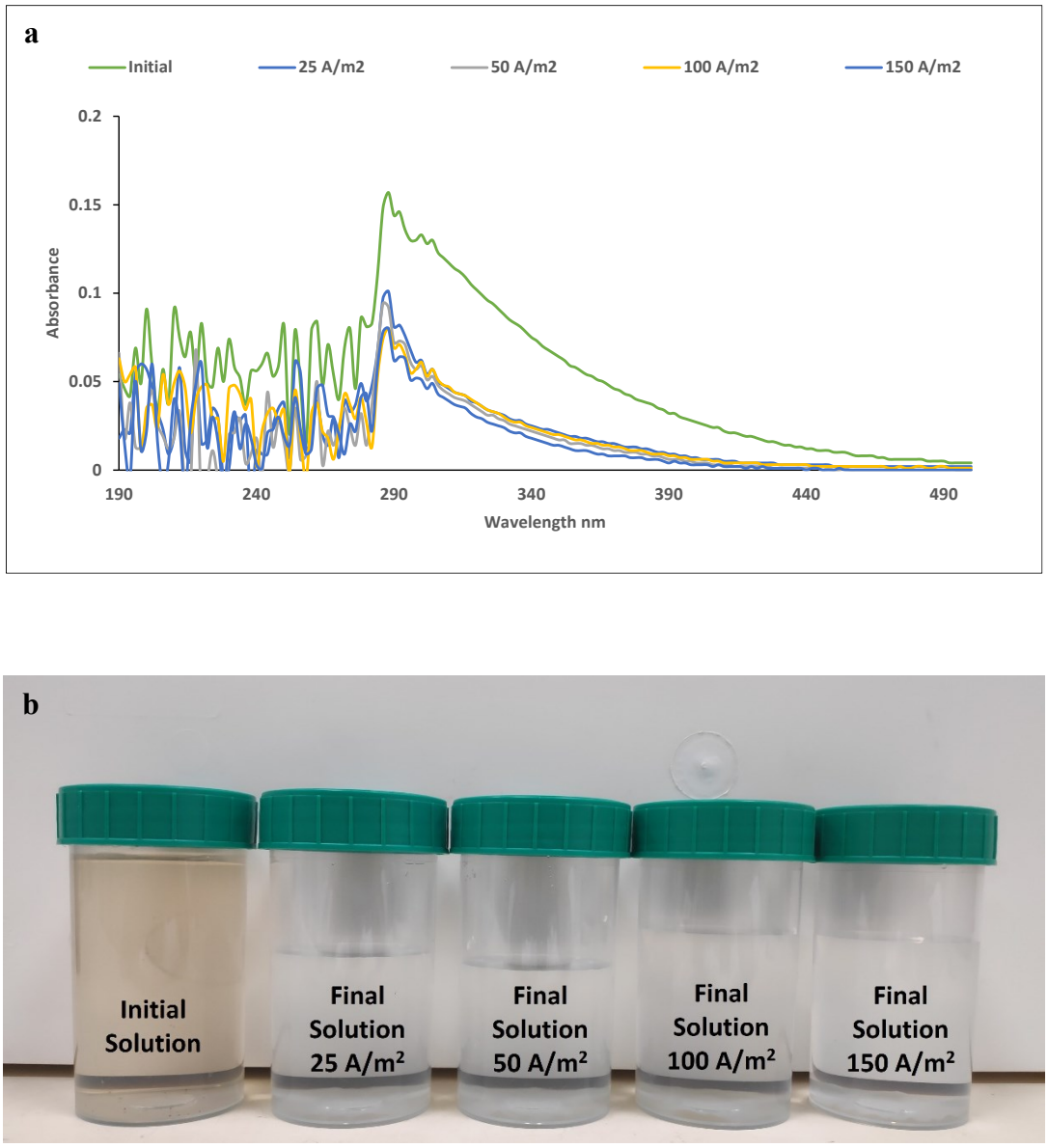

Figure 67 Effect of Current Density – Municipal Effluent - Ni-Foam; a) Spectral Scans ; b) Photographs of Solutions After Electrolysis

In contrast, the increase in the intensity of absorbance at 290 nm was apparent after electrolysis using the carbon fibre anode. It can be seen from Figure 68a that the absorbance increased from the initial 0.17 to 1.02 after electrolysis at 25 A/m$^{2;}$ similarly, the intensity absorbance increased to 0.85, 0.33, and 1.16 for applied current densities of 50 A/m^2, 100 A/m^{2,} and 150 A/m^2, respectively. It is observed that the absorbance increases after electrolysis at 25 A/m^{2,} then decreases at 50 A/m^2 and 100 A/m^{2,} then increases again after electrolysis at 150 A/m^2. This is suggestive of the adsorption/electro-sorption and desorption of humic acid molecules on the

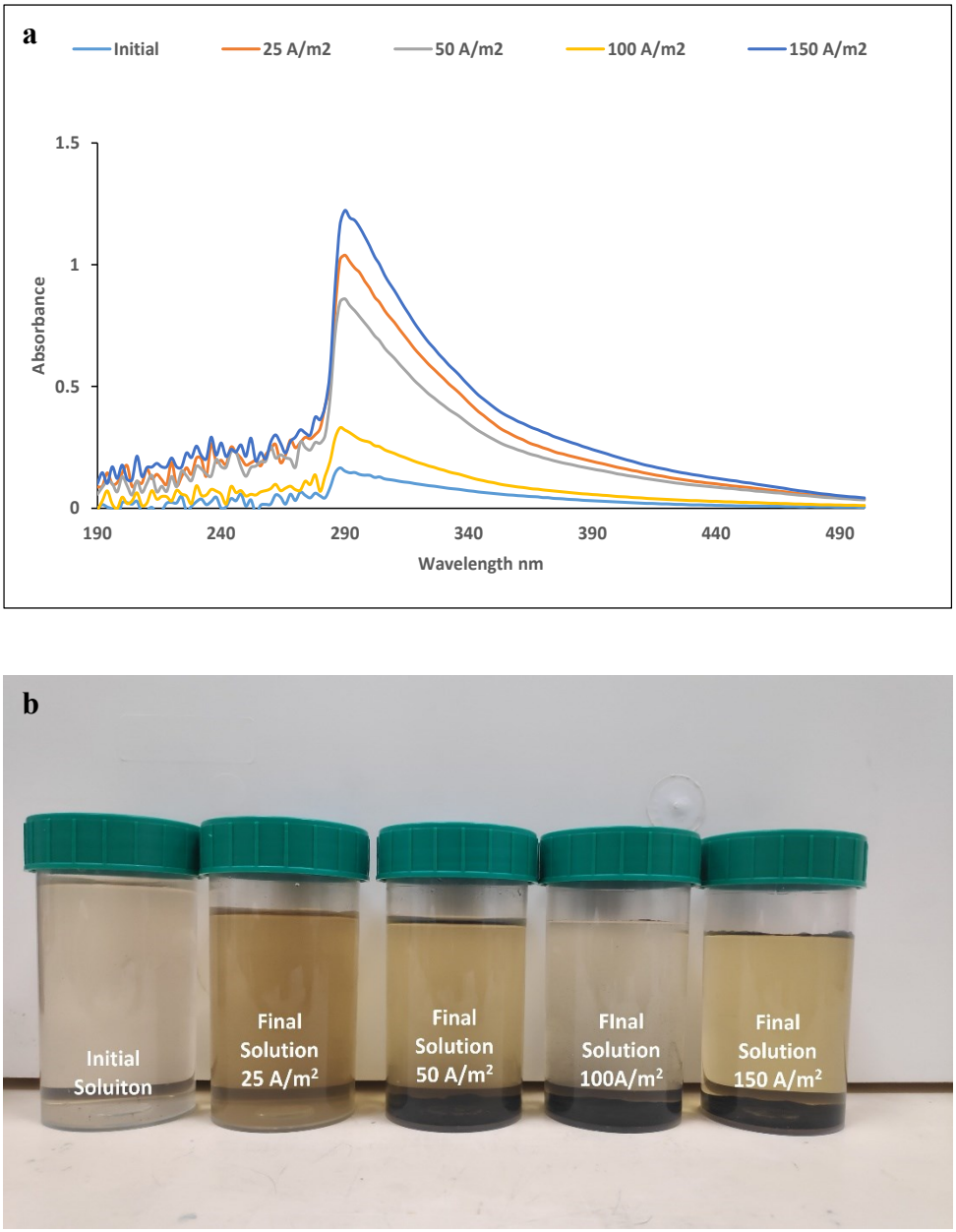

Figure 68 Effect of Current Density – Municipal Effluent - Carbon Fibre; a) Spectral Scans ; b) Photographs of Solutions After Electrolysis

surface of the carbon anode. This was also observed as a change in the colour of the solutions after electrolysis, as depicted in Figure 68b, respectively.

Figure 68b also shows the effect of current density on the stability of the carbon electrode; it can be seen that for current densities greater than 25 A/m^2, the disintegration of the electrode was apparent. This is clear from the black precipitate (carbon particles) observed after electrolysis at 50 A/m^2, 100 A/m^2 and 150 A/m^2, respectively.

4.6 Discussion

In light of the results described previously, it is apparent that the electrolysis of synthetic effluent and real effluent can result in hydrogen production with reasonable energy efficiency (Figure 9, Figure 22, Figure 31, Figure 38, Figure 58 and Figure 63). The electrolysis experiments revealed that the energy efficiency was most satisfactory for 1M KOH concentration due to its high conductivity (208-211 mS/cm). For instance, for the electrolysis of synthetic effluent, the energy efficiency was 82 ± 1.2% and 83 ± 3.40% at an applied current density of 12.55 A/m^2 for the carbon fibre anode and Ni-foam anode, respectively(Figure 9). The energy efficiency was also comparable to that of conventional alkaline water electrolysis under the same conditions with Ni-foam as both the anode and cathode, wherein the energy efficiency was 85 ± 6.9%. The trend was similar for municipal effluent electrolysis as well wherein the energy efficiency was 75 ± 3.0 % for the 83 ± 3.0% carbon fibre and Ni-foam anode, respectively(Figure 58). In addition, when investigating the effect of increasing the current density, a decreasing trend in the energy efficiency for electrolysis of synthetic effluent, real municipal effluent and conventional alkaline water electrolysis was observed due to increased ohmic heating losses, mass transport resistance and bubble dispersion(Godula-Jopek, 2015; Wang et al., 2014).

Cho & Hoffmann, 2017 reported a maximum energy efficiency of hydrogen production of 23% at an applied current density of 200 A/m^2 for the electrolysis of real wastewater samples with NaCl as the supporting electrolyte using a BiO_x/TiO_2 anode. In comparison, the energy efficiency observed in this investigation with 1M KOH solution at an applied current density of 150 A/m^2 for electrolysis of synthetic effluent and real municipal effluent was 60 ± 2.8% and 51 ± 5.0% for the carbon fibre anode and 54 ± 3.2% and 53 ± 5.1% for the Ni-foam anode, respectively. It is apparent that considerable improvements in energy efficiency were obtained from the current investigation in comparison to Cho & Hoffmann, 2017. The difference in the energy can be primarily attributed to the fact that they employed an undivided cell with NaCl as the electrolyte, which can promote the CLER at the anode and subsequent CLRR at the cathode(Eq 8 – Eq 10), thereby inhibiting the hydrogen evolution reaction; further, the CLER tends to have faster electrode kinetics since only $2e^-$ are involved in comparison to the OER which involves $4e^-$(Amikam et al., 2018; Dresp et al., 2019). Further, the consumption of protons at the cathode for the HER can lead to a localised pH increase promoting the formation of hypochlorite ions.

Consequently, HER and CLRR occur at the cathode; this is clear from coulombic efficiency for the HER and CLRR reported by Cho & Hoffmann, 2017 which was 41% and 29%, respectively. Moreover, when Ma et al. 2014, investigated hydrogen gas production due to electrochemical oxidation of phenol, they also reported a similar observation in which the hydrogen production rate was lower with NaCl as the electrolyte compared to Na_2SO_4 despite having better COD removal efficiencies. The coulombic efficiency for the HER in the current study was in the range 91 - 97% and 92 - 98% for municipal and synthetic effluent electrolysis, respectively(Appendix A.4). This was primarily due to the use of KOH as the supporting electrolyte. Even though chloride was present in the municipal effluent (Table 3), the presence of oxyanions such as OH^- impede the mass transfer of Cl^- ions on the anode surface, thereby inhibiting the CLER (Amikam et al., 2018); as a result the HER and OER would not be influenced the CLRR and the CLER at the cathode and anode respectively.

Table 4 Summary of Research on Hydrogen Production by Wastewater Electrolysis

Type of Wastewater	Voltage (V)	Current (A)	Time (h)	Vol. H_2(L)	H_2 Rate (mL/ min)	% COD Removal	% Energy Efficiency	Ref.
Olive Mill WW	3	0.06	96	3.02	0.52	44	65	(Kargi & Catalkaya, 2011b)
Landfill Leachate	4	0.18	96	5	0.87	77	26	(Kargi & Catalkaya, 2011a)
Cheese Whey WW	5	0.05	158	5.5	0.59	22	67	(Kargi & Uzunc, 2012)
Vinegar Fermentation WW	4	0.10	72	2.8	0.67	10.5	74	(Kargi & Arikan, 2013)
Phenol (synthetic wastewater)	3	0.5	504	35	1.17	100	50	(Ma et al., 2014)

Previously researched electrolysis of various types of industrial wastewater by Kargi and co-researchers are represented in Table 4.

The studies described in Table 4 show that the energy efficiencies are relatively improved compared to the study conducted by Cho & Hoffman., 2017 and more comparable to the efficiencies reported in this investigation. Note that the studies described in Table 4 were more focused on the oxidation of organics under potentiostatic conditions rather than water splitting; as a result, the energy efficiencies reported were based on the average current intensities and cumulative hydrogen production due to the decomposition of organics throughout the

experiment. With respect to the applied voltages in the studies by Kargi et al. and Ma et al., 2014, the voltages were significantly higher (≥ 3 V), whereas the voltages rarely exceeded 2.6 V for the electrolysis of synthetic and municipal effluent conducted in this investigation. This could be explained by taking into account the solution conductivities; in the studies described in Table 4, the conductivities of the raw wastewaters ranged from 1.60 – 5.60 mS/cm; in contrast, the conductivities in this investigation was a minimum of 2.77 mS/cm for 0.01M KOH and a maximum of 211 mS/cm for 1M KOH. Moreover, for the 1M KOH solutions, the voltage exceeded 2.6 V when the applied current density was 150A/m^2(approx. 1.314A for an anode area of 87.6 cm^2), whereas, from Table 4, it can be seen that the maximum current obtained was only 0.18 A. at an applied voltage of 5V. Moreover, when comparing the rates of H_2 production , the rates in general were higher in the current investigation when compared to Table 4. For instance, at an applied current of 0.1 A , Kargi & Arikan, 2013 reported a H_2 production rate of 0.67 mL/min whereas in the current investigation the corresponding rate was 0.8 mL/min for an applied current of density of 12.55 A/m^2(0.1A for an anode area of 87.6 cm^2) similarly, when compared to Ma et al., 2014 at an applied current of 0.5 A the H_2 production rate was 1.17 mL/min and in this investigation for an applied current 50 A/m^2(approx. 0.44 A for an anode area of 87.6 cm^2) the H_2 production rate was 3.20 mL/min(Figure 10, Figure 23, Figure 33 and Figure 39). This was the case since water splitting was dominant compared to oxidation of organics.

Further, regarding the volumetric hydrogen production rates, the data showed that the hydrogen production rates converged closely with the theoretical values(Figure 10, Figure 23, Figure 33 and Figure 39); this would be expected for the electrolysis experiments with carbon fibre anodes because no COD degradation was observed. Nevertheless, for electrolysis of synthetic effluent using the Ni-foam, because there was COD removal, it would be anticipated to be reflected in the volumetric hydrogen production (Eq 37). Note that MO_x in Eq 37 is a metal oxide anode which is generally used to represent DSA anodes such as IrO_2, RuO_2, BiO_x and TiO_2; considering Ni-foam whose chemical formula $NiFeO_x$ or NiO_x the 'M' indicates the NiFe/Ni metal segment of the molecule(Mischa M. Bakker & Vermaas, 2019; Diaz-Morales et al., 2016).

From Eq 37, the additional electrons produced due to the oxidation of organics can result in an can result in the cathodic evolution of hydrogen in the flow cell electrolyzer(Ma et al., 2014); this can be better visualized by Figure 69.

Oxidation of organics on the Ni-foam anode (alkaline conditions)

$MO_{x+1} + R \rightarrow MO_x + CO_2 + OH^- + e^-$ *Eq 37*

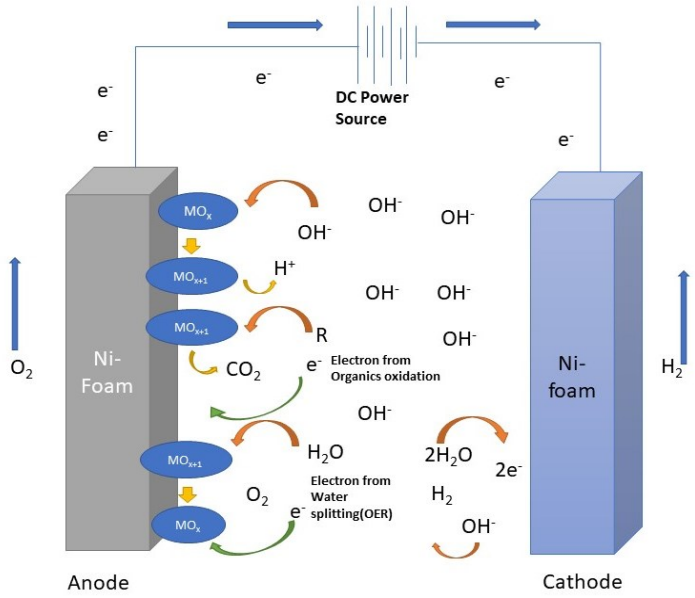

Figure 69 Mechanism of organic oxidation and water splitting for H_2 production on Ni-foam anode

In addition, according to Table 4, their research hypothesized the potential of hydrogen production due to the oxidation of organics present in wastewater. Furthermore, investigations by Eker & Kargi, 2010 reported that the hydrogen production due to the wastewater electrolysis was greater than conventional water splitting, and the extent of hydrogen production would depend on the concentration of organics in the wastewater, that is a higher COD would result in higher hydrogen production. Eker & Kargi, 2010 reported that for conventional water electrolysis the hydrogen production rate of 0.37 mL/min whereas for the electrolysis of industrial wastewater the rate was 3 mL/min (Eker & Kargi, 2010). In the investigation by Eker & Kargi, 2010 they employed industrial wastewater with a COD of 10000 mg/L, after electrolysis the final COD was 9333 mg/L, i.e., approximately 667 mg/L of COD was oxidized, and the corresponding protons generated resulted in a higher hydrogen production rate. In contrast, the synthetic effluent prepared in this investigation had a COD concentration of only 26.7 mg /L. Considering the electrolysis experiments with the Ni-foam anode, even though the COD removal efficiency of 24.6 ± 8 % was obtained at a current density of 150 A/m^2 with 1M

KOH as the supporting electrolyte only 6.92 mg/L was oxidized to produce electrons for hydrogen evolution at the cathode. Based on stoichiometric calculations, 6.92 mg/L of COD could theoretically give 8.7mL of H_2 after electrolysis. This would again be dependent on the volume of wastewater electrolysed; in this investigation the total volume of wastewater electrolysed was 0.5 L and the corresponding stoichiometric calculations were done for the same, in contrast the experiments by Kargi et al. (Table 4) electrolysed 1L of wastewater. Additionally, since the TOC removal obtained was at maximum only 6.2 ± 0.3% the actual contribution of the organics degradation to the hydrogen production may not be that substantial as intermediates are formed due aromatic ring cleavage(Dong et al., 2016; Guo et al., 2018) and also demonstrated by the HPLC-SEC analysis conducted.

Considering the variation in the energy efficiency between the Ni-foam anode and the carbon fibre anode, the contrast can be associated with the lower OER potential for the Ni-foam anode compared to the carbon fibre anode(Figure 8). Additionally, the difference in the energy efficiency with respect to alkaline water electrolysis could be linked to side reactions occurring on the anode in addition to water splitting. Considering the carbon fibre anode, HPLC analysis of the synthetic effluent after electrolysis showed an increase in the distribution of high molecular weight compounds of the humic acid molecule indicating the occurrence of a polymerisation reaction(Figure 20). A similar observation was reported by Cozzolino & Piccolo, 2002 and Piccolo et al., 2000, wherein they reported that the polymerization of humic structures was stabilized by the formation of C-O-C and C-C covalent bonds catalysed by peroxidase enzyme. On account of this, a similar explanation can be suggested for the electrochemically catalysed polymerisation of humic acid observed in this research. In addition to the polymerization reaction occurring on the carbon fibre anode, the conjugate base of the humic acid (humate) would tend to adsorb on the surface of the anode, followed by subsequent desorption when the flow cell was decanted for the next batch. A direct consequence of this phenomenon is that the solution after electrolysis with the carbon fibre anode would exhibit a higher COD compared to the initially prepared solution. This was also clear from the spectral scans of the solutions before and after electrolysis(Figure 15 and Figure 36). Further, the carbon fibre anode would tend to disintegrate at current densities greater than 25 A/m^2, even though the solutions were filtered with 0.45 μm filters; it is also likely that the carbon particles less than 0.45 μm size could interfere with the COD analysis resulting in a higher measured value

compared to the initial since their size can range from 0.1 µm to 7 µm(Holt & Horne, 1978; Ramulu & Kramlich, 2004).

Concerning the Ni-foam anode, it was observed that the humic acid was degraded to some extent, though complete mineralization was not observed. This is evidenced by the COD and TOC removal efficiencies for the electrolysis of synthetic effluent after electrolysis(Figure 24, Figure 25, Figure 40, Figure 41 and Figure 64). For 1M KOH solution at an applied current density of 12.55 A/m^2, a COD removal of 24.6 ± 8 % and a corresponding TOC removal of 6.2 ± 0.3% were detected. The low TOC removal, in contrast to the higher COD removal, is linked to the formation of intermediates as a result of the breakdown of the aromatic rings on the humic acid molecules. This observation was also evidenced by the HPLC analysis, where the chromatogram indicated an increase in the fraction of the low molecular weight compounds followed by a decrease in the high molecular weight compounds(Figure 30).

5. Integration of Water Electrolysis with Aerobic Wastewater Treatment Plant

Based on the results obtained for the electrolysis of domestic effluent, it is possible to use wastewater (in this case, municipal effluent) as a water source for the production of hydrogen via alkaline water electrolysis. A possible scenario would be to have an electrolyzer installed within the wastewater treatment plant and allow some of the treated water to be diverted for the generation of hydrogen and oxygen. The produced hydrogen can have many applications, these include the generation of electricity via a fuel cell or gas turbine, and the hydrogen can be used as a chemical feedstock for the production of ammonia and can also be used to reduce the CO_2 to CH_4 in anaerobic digestion plants further increasing the biogenic methane production. The oxygen produced can be used within the wastewater treatment plant for the aeration of the bioreactors. To gain an advantage of the high purity O_2, the aeration tanks should be modified to have a closed configuration which can allow for an O_2-rich atmosphere. In addition, the solubility of the O_2 gas in the reactor is determined by its partial pressure and to maximize the solubility, the partial pressure has to be increased. The modified aeration tanks should also be able to accommodate the higher pressures in their design for efficient functioning. Moreover, because traditional aerobic wastewater treatment plants require oxygen, which is provided by the atmosphere using air pumps and diffusers, the maximum purity of oxygen that can be obtained is only 21%. Replacing this with high-purity oxygen can potentially reduce the energy consumption of the wastewater treatment plant because the flow rate of air required would be significantly lower as less volume of gas would be pumped to supply the same amount of oxygen, provided the relevant modifications are incorporated into

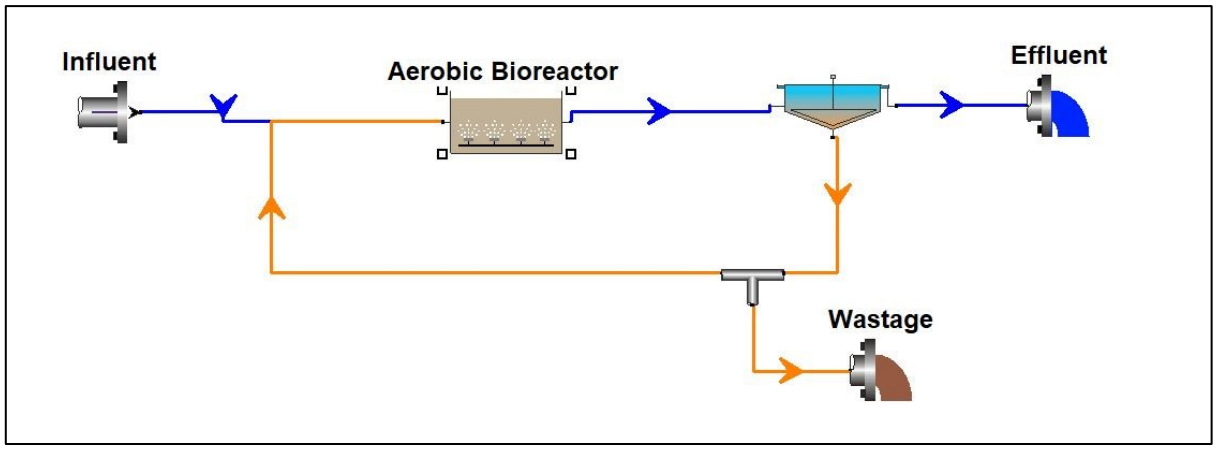

Figure 70 BioWin Plant Schematic

the design. To give a better perspective, basic plant simulations were conducted using BioWin 6.2. Two simulations were conducted; The first simulation was conducted using conventional aeration with atmospheric oxygen and was used as a baseline for comparison, and the second simulation was conducted using 95% pure oxygen with a surface pressure of 200 kPa(1.9 atm). The basic schematic of the plants is shown in Figure 70. The plant was designed for a flow of 10,000 m^3/day with a reactor volume of 5000 m^3. The influent and effluent water quality values are described in Table 5.

Table 5 Water Quality Parameters used in the BioWin Simulations

Parameter	Influent	Effluent
COD (mg O2/L)	500	33
Total Nitrogen (mg N/L)	40	24
Phosphorous (mg P/L)	10	5
Sulfur (mg S/L)	0	0
Nitrate (mg N/L)	0	0
pH	7.3	6.8
Alkalinity mmol/L	6	-
ISS (mgISS/L)	45	0.7
Ca (mg/L)	80	80
Mg (mg/L)	15	14

The results of the steady-state simulations are shown in Table 6. It can be seen from table 5 that there is a substantial difference with respect to the amount of energy used by the air pumps. Further, the reduction in the air flow requirement is also clear, i.e., with respect to the energy requirement, there is a reduction of 1.2 kWh(4320 kJ), and with respect to the air flow requirements, a reduction of 2156 m^3/hr.

Table 6 Biowin Simulation Results

Parameters	Conventional Aeration	High Purity O_2 Plant (95% O_2)
HRT (h)	10.5	10.5
DO set point (mg O_2/l)	2.1	2.1
Oxygen Uptake Rate (mgO_2/l/hr)	23.6	23.4
Oxygen Transfer Rate(kg O_2/hr)	119	116
Air Flow Rate (m^3/hr)	3706	1550
Total Plant Power Requirement (W)	88	40
Daily Energy Requirement (kWh)	2.1	0.9
Daily Energy Requirement (kJ)	7680	3494

Based on the Oxygen Transfer Rate(OTR), an estimate can be made for the amount of water needed to be electrolyzed to meet the oxygen demand of the wastewater treatment plant. From Table 6, the OTR for the high-purity oxygen plant was 116 kg O_2/hr; from the stoichiometry of water splitting, it is known that 0.89 kg O_2 is produced per litre of water electrolysed, this gives a water requirement of approximately 3.1 m^3/day. The BioWin simulation showed that approximately 9708 m^3/day of treated water is discharged. The amount of water that is needed for electrolysis is only about 0.03% of the discharged effluent, which indicates that water availability may not be an issue for electrolysis in wastewater treatments if the production of pure O_2 to meet the oxygen requirement is the objective. The overall design of the electrolyzer is given in Table 7. For the electrolyzer design, the water conversion efficiency is selected based on the average coulombic efficiency of the oxygen evolution reaction obtained for the electrolysis of municipal effluent using Ni-foam as the anode (section 4.5).

Table 7 Design Parameters Electrolyser

Parameter	Value
Oxygen Transfer Rate (OTR) WWTP (kg O_2/h)	116
Oxygen To be Supplied (kg O_2/day)	2784
Amount of Water Required (m^3/day)	3.1
WWTP Effluent Flow (m^3/day)	9708
Fraction of water Needed	0.03%
Water Conversion Efficiency	91%
Water flow into electrolyser (m^3/h)	0.14
Volumetric H_2 Production (m^3/h)	162
H_2 production(kg H_2/day)	348
Volumetric O_2 Production (m^3/h)	81
O_2 production (kg O_2/day)	2784
Energy requirement electrolysis (MW)	0.7
Current Requirement (A)	389
Applied Current Density (A/cm^2)	0.10
Electrode area Requirement (m^2)	0.4

From Table 7, it can be seen that the electrolyzer needs about 0.7 MW of energy to produce sufficient oxygen for the bioreactor. Further, for practicality purposes, it would be better to install a 1MW electrolyzer due to its commercial availability. A likely candidate would be the McPhy 200-30 electrolyzer. This electrolyzer is rated at 1MW and can produce approximately 200 m^3 H_2/h at a pressure of 30 bar. A typical representation is given in Figure 71. Moreover,

based on the effluent water quality, sufficient preliminary treatment may be required to remove the Ca^{2+} and Mg^{2+} ions. The treatment technologies that can be employed can include pellet softening, Nanofiltration or Ultrafiltration. This should be done to prevent the deposition of $Ca(OH)_2$ or $Mg(OH)_2$ on the cathode surfaces of the electrolyzer, as this can lead to poor efficiency of hydrogen production and, eventually failure of the electrochemical cell due to excessive scale formation.

Figure 71 McPhy 200-30 Alkaline Water Electrolyser

6. Conclusions

In this study, the possibility of hydrogen production using municipal effluent using two different anodes, carbon fibre and Ni-foam, was investigated. The experiments were conducted in a two-compartment electrolyzer flow cell with another Ni-foam electrode used as the cathode. The electrolysis experiments were conducted with synthetically prepared effluent containing 20 mg O_2/L humic acid and with real municipal effluent. For each experiment, the corresponding energy efficiency of hydrogen production, volumetric hydrogen production rate, COD, and TOC removal efficiencies were determined. The experiments were conducted to investigate the effects of electrolyte(KOH) concentration and applied current density and are subsequently summarized in relation to the research questions discussed in section 2.3

RQ1: How is hydrogen production affected in a KOH electrolysis cell if synthetic and real municipal effluent are used?

- The volumetric hydrogen production rates obtained using synthetic and municipal effluent did not appear to be significantly affected. In all experiment sets investigating the effect of electrolyte concentration and the effect of applied current density, the volumetric hydrogen production rate obtained was very close to the theoretically calculated value; moreover, the coulombic efficiencies for the hydrogen evolution reaction exceeded 90% for all these experiments. (RQ1)

RQ2: What is the extent of humic acid oxidation at the carbon fibre and Ni-foam anode when used in an STP effluent electrolysis cell?

- The initial hypothesis suggested that the increased activity of the hydroxide ions would generate hydroxyl radicals on the anode surface as a precursor to the oxygen evolution reaction, which could oxidize the humic acid molecules in the effluent. However, the results for experiments with the Ni-foam anode indicated otherwise because increasing the electrolyte concentration resulted in a decrease in the COD removal efficiencies. For the experiments with the carbon fibre anode, it was observed that the COD of the solutions after electrolysis was significantly higher than the COD in the initially prepared solutions. This was thought to occur due to the adsorption/electro-sorption of the humic acid molecules on the surface of the carbon electrode(RQ2).
- Considering the effect of COD and TOC removal efficiencies for increasing applied current densities, an increase in the overall removal efficiencies was observed for the Ni-foam anode for both synthetic effluent and real municipal effluent. When the carbon fibre anode was used,

the COD of the solution after electrolysis was greater than the COD of the initially prepared solution. In addition, the disintegration of the carbon fibre anode was also evident as the applied current density exceeded 25 A/m^2. Moreover, since both the carbon fibre anode and the Ni-foam anode have relatively low OER overpotentials, they are active toward oxygen evolution rather than the oxidation of organics in the solution. This was evidenced by the low coulombic efficiencies obtained for the oxidation of organics, i.e., a coulombic efficiency of organics oxidation obtained was 1.8 ± 0.2% at 25 A/m^2, whereas the coulombic efficiency for the oxygen evolution reaction was on average 96 ± 2.8%. (RQ2)

RQ3: What is the fate of the humic acid molecules in the solution after electrolysis?

- HPLC analysis of the final solutions after electrolysis using the carbon fibre anode revealed an interesting occurrence. The chromatograms showed that there was a subsequent increase in the contribution of high molecular weight molecules(1100 Da -3610 Da) after electrolysis compared to the initial solution. This suggests that a polymerization reaction may have occurred on the electrode surface. In contrast, the chromatograms of the solutions electrolyzed with the Ni-foam anode showed a decrease in the contribution of high molecular weight molecules and an increase in lower molecular weight molecules indicating that the humic acid molecules were broken down into smaller fragments during electrolysis.

RQ4:How does the electrolysis performance compare with conventional alkaline water electrolysis with Ni-foam as both the anode and cathode in the electrolysis cell?
RQ5:How is the energy efficiency for hydrogen production affected when carbon fibre or Ni-foam is used as the anode to electrolyze synthetic effluent and real municipal effluent?

- For the experiments that involved investigating the effect of electrolyte concentration ranging from 0.1-1M KOH, an increase in energy efficiency was observed for experiments with both the carbon fibre anode and the Ni-foam anode. This is to be expected as the solution conductivity is subsequently increased. For the 1M KOH solutions, the energy efficiency using synthetic effluent for the carbon fibre anode was approximately 82 ± 1.2% and for the Ni-foam anode was 83 ± 3.4%. When municipal effluent was employed, the energy efficiency was 74 ± 2.7% for the carbon fibre anode and 82 ± 2.8% for the Ni-Foam anode at an applied current density of 12.55 A/m^2.(RQ4 And RQ5)
- The effect of increasing the applied current density revealed a decreasing trend in the energy efficiency observed for both the carbon fibre anode and the Ni-foam anode. The trend was apparent when for the synthetic effluent as well as the real municipal effluent. For the synthetic effluent, the energy efficiency was slightly higher for the Ni-foam anode compared to the carbon fibre anode, i.e., for an applied current density of 25 A/m^2 the energy efficiency for the

carbon fibre anode, and the Ni-foam was 75 ± 2.8% and 77 ± 9.6%, respectively. In comparison, the energy efficiency for conventional alkaline water electrolysis using the Ni-foam anode was 85 ± 3.5 %. When municipal effluent was employed, the decrease in the energy efficiency was much more substantial; for an applied current density of 25 $A/m^{2,}$ the energy efficiency was 63 ± 7.3% for the carbon fibre anode and 68 ± 7.9% for the Ni-foam(RQ4 and RQ5).

RQ6: How can this electrolysis technique be integrated with existing wastewater treatment plants?

- As discussed in Section 5, it is possible to divert some of the treated effluents from a wastewater treatment plant for the production of hydrogen and oxygen via electrolysis. Moreover, the results indicated that only 0.03% of effluent was needed to produce enough O_2 to meet the treatment plant requirements. This was also followed by energy savings of approximately1.2 kWh(4320 kJ) due to reduced load on the air pumps as pure oxygen is supplied instead of atmospheric oxygen. It should also be noted that the energy savings can change depending on the size of the water treatment plant and its subsequent oxygen requirements.

To conclude, the use of municipal effluent as a source of wastewater is a viable alternative for the production of hydrogen. With regards to the anode that can be used, Ni-Foam seems to be the best candidate due to its high durability. Carbon fibre, on the other hand, exhibited disintegration during the electrolysis experiments and could not effectively oxidize the humic acid molecules in both synthetic and municipal effluent.

7. Recommendations

Further studies can be conducted to improve our understanding of the electrolysis of wastewater. A few recommendations for further research are described below.

- This study revealed that the carbon fibre anode was not very durable under the conditions of alkaline water electrolysis; additionally, the electrode was not able to effectively oxidize the humic acid molecules in both synthetic effluent and real municipal effluent. Future research can be conducted to improve the durability of the carbon electrode and also to develop a hybrid electrode with catalysts that favour the oxygen evolution reaction and allow for the efficient oxidation of pollutants. For instance, combining an active and non-active anode, i.e., BDD(non-active) and Ni-foam(Active).
- Throughout the study, the adsorption/electro-sorption of the humic acid molecules on the surface of the carbon fibre anode was prevalent. Moreover, for the experiments involving the carbon fibre anode, HPLC analysis indicated a possible polymerization reaction. Further research may be required to understand the mechanism of the adsorption and polymerization reactions taking place at the carbon fibre anode.
- Regarding the composition of the spent electrolyte, further research can be done to investigate the reason behind the colour change of the solution and the effect of the carbon particles on the humic acid molecules in the solution.
- Concerning the incorporation of an electrolyser into an existing wastewater treatment plant for the generation of pure oxygen, additional investigations can be conducted using Aspen plus to understand the overall energy balance and feasibility of the process. In addition, lab-scale investigations can also be conducted to investigate techniques to integrate and manage the tandem functioning of an electrolyser and an aerobic bioreactor.

8. References

Amikam, G., Nativ, P., & Gendel, Y. (2018). Chlorine-free alkaline seawater electrolysis for hydrogen production. *International Journal of Hydrogen Energy*, *43*(13), 6504–6514. https://doi.org/10.1016/j.ijhydene.2018.02.082

Bakker, M M. (2018). *On the optimization of hydrogen production by pressure swing induced alkaline water electrolysis*.

Bakker, Mischa M., & Vermaas, D. A. (2019). Gas bubble removal in alkaline water electrolysis with utilization of pressure swings. *Electrochimica Acta*, *319*, 148–157. https://doi.org/10.1016/j.electacta.2019.06.049

Bán, A., Schäfer, A., & Wendt, H. (1998). Fundamentals of electrosorption on activated carbon for wastewater treatment of industrial effluents. *Journal of Applied Electrochemistry*, *28*(3), 227–236. https://doi.org/10.1023/A:1003247229049

Becker, F. G., Cleary, M., Team, R. M., Holtermann, H., The, D., Agenda, N., Science, P., Sk, S. K., Hinnebusch, R., Hinnebusch A, R., Rabinovich, I., Olmert, Y., Uld, D. Q. G. L. Q., Ri, W. K. H. U., Lq, V., Frxqwu, W. K. H., Zklfk, E., Edvhg, L. V, Wkh, R. Q. (2010). Electrochemistry for the Environment. In C. Comninellis & G. Chen (Eds.), *Syria Studies* (Vol. 7, Issue 1). Springer New York. https://doi.org/10.1007/978-0-387-68318-8

Bennett, J. E. (1980). Electrodes for generation of hydrogen and oxygen from seawater. *International Journal of Hydrogen Energy*, *5*(4), 401–408. https://doi.org/10.1016/0360-3199(80)90021-X

Bock, C., & MacDougall, B. (1999). The Anodic Oxidation of p-Benzoquinone and Maleic Acid. *Journal of The Electrochemical Society*, *146*(8), 2925–2932. https://doi.org/10.1149/1.1392030

Bourne, S. (2012). *The future of fuel: The future of hydrogen* (Issue 1). https://doi.org/10.1016/S1464-2859(12)70027-5

Cañizares, P., Domínguez, J. A., Rodrigo, M. A., Villaseñor, J., & Rodríguez, J. (1999). Effect of the current intensity in the electrochemical oxidation of aqueous phenol wastes at an activated carbon and steel anode. *Industrial and Engineering Chemistry Research*, *38*(10), 3779–3785. https://doi.org/10.1021/ie9901574

Cavaliere, P. D., Perrone, A., & Silvello, A. (2021). Water electrolysis for the production of hydrogen to be employed in the ironmaking and steelmaking industry. *Metals*, *11*(11). https://doi.org/10.3390/met11111816

CBS. (2022). *Urban waste water treatment per province and river basin district*.

https://opendata.cbs.nl/#/CBS/en/dataset/7477eng/table?dl=72A95

Chiang, L. C., Chang, J. E., & Wen, T. C. N. (2000). Destruction of refractory humic acid by electromechanical oxidation process. *Water Science and Technology*, *42*(3–4), 225–232. https://doi.org/10.2166/wst.2000.0384

Cho, K., & Hoffmann, M. R. (2017). Molecular hydrogen production from wastewater electrolysis cell with multi-junction BiOx/TiO2 anode and stainless steel cathode: Current and energy efficiency. *Applied Catalysis B: Environmental*, *202*(2017), 671–682. https://doi.org/10.1016/j.apcatb.2016.09.067

Cho, K., Kwon, D., & Hoffmann, M. R. (2014). Electrochemical treatment of human waste coupled with molecular hydrogen production. *RSC Advances*, *4*(9), 4596–4608. https://doi.org/10.1039/c3ra46699j

Cho, K., Qu, Y., Kwon, D., Zhang, H., Cid, C. A., Aryanfar, A., & Hoffmann, M. R. (2014). Effects of anodic potential and chloride ion on overall reactivity in electrochemical reactors designed for solar-powered wastewater treatment. *Environmental Science and Technology*, *48*(4), 2377–2384. https://doi.org/10.1021/es404137u

Cozzolino, A., & Piccolo, A. (2002). Polymerization of dissolved humic substances catalyzed by peroxidase. Effects of pH and humic composition. *Organic Geochemistry*, *33*(3), 281–294. https://doi.org/10.1016/S0146-6380(01)00160-7

De Melo, B. A. G., Motta, F. L., & Santana, M. H. A. (2016). Humic acids: Structural properties and multiple functionalities for novel technological developments. *Materials Science and Engineering C*, *62*, 967–974. https://doi.org/10.1016/j.msec.2015.12.001

Diaz-Morales, O., Ferrus-Suspedra, D., & Koper, M. T. M. (2016). The importance of nickel oxyhydroxide deprotonation on its activity towards electrochemical water oxidation. *Chemical Science*, *7*(4), 2639–2645. https://doi.org/10.1039/c5sc04486c

Dincer, I., & Acar, C. (2014). Review and evaluation of hydrogen production methods for better sustainability. *International Journal of Hydrogen Energy*, *40*(34), 11094–11111. https://doi.org/10.1016/j.ijhydene.2014.12.035

Dong, G., Lu, J., & Lai, W. (2016). *Insights into the Mechanism of Aromatic Ring Cleavage of Noncatecholic Compound 2 - Aminophenol by Aminophenol Dioxygenase: A Quantum Mechanics/Molecular Mechanics Study*. https://doi.org/10.1021/acscatal.6b00372

Dresp, S., Dionigi, F., Klingenhof, M., & Strasser, P. (2019). Direct electrolytic splitting of seawater: Opportunities and challenges. *ACS Energy Letters*, *4*(4), 933–942. https://doi.org/10.1021/acsenergylett.9b00220

Dubey, P. K., Sinha, A. S. K., Talapatra, S., Koratkar, N., Ajayan, P. M., & Srivastava, O. N. (2010). Hydrogen generation by water electrolysis using carbon nanotube anode. *International Journal of Hydrogen Energy*, *35*(9), 3945–3950. https://doi.org/10.1016/j.ijhydene.2010.01.139

Eker, S., & Kargi, F. (2010). Hydrogen gas production from electrohydrolysis of industrial wastewater organics by using photovoltaic cells (PVC). *International Journal of Hydrogen Energy*, *35*(23), 12761–12766. https://doi.org/10.1016/j.ijhydene.2010.08.101

El-Emam, R. S., & Özcan, H. (2019). Comprehensive review on the techno-economics of sustainable large-scale clean hydrogen production. *Journal of Cleaner Production*, *220*, 593–609. https://doi.org/10.1016/j.jclepro.2019.01.309

Elgrishi, N., Rountree, K. J., McCarthy, B. D., Rountree, E. S., Eisenhart, T. T., & Dempsey, J. L. (2018). A Practical Beginner's Guide to Cyclic Voltammetry. *Journal of Chemical Education*, *95*(2), 197–206. https://doi.org/10.1021/acs.jchemed.7b00361

Fan, L., Zhou, Y., Yang, W., Chen, G., & Yang, F. (2008). Electrochemical degradation of aqueous solution of Amaranth azo dye on ACF under potentiostatic model. *Dyes and Pigments*, *76*(2), 440–446. https://doi.org/10.1016/j.dyepig.2006.09.013

Godula-Jopek, A. (2015). *Hydrogen Production by Electrolysis*. WIley-VCH.

Grigoriev, S. A., Porembsky, V. I., & Fateev, V. N. (2006). Pure hydrogen production by PEM electrolysis for hydrogen energy. *International Journal of Hydrogen Energy*, *31*(2), 171–175. https://doi.org/10.1016/j.ijhydene.2005.04.038

Guo, Y., Xue, Q., Zhang, H., Wang, N., Chang, S., Wang, H., Pang, H., & Chen, H. (2018). *Treatment of real benzene dye intermediates wastewater by the Fenton method : characteristics*. 80–90. https://doi.org/10.1039/c7ra09404c

Ho, P. C., Palmer, D. A., & Gruszkiewicz, M. S. (2001). Conductivity measurements of dilute aqueous hcl solutions to high temperatures and pressures using a flow-through cell. *Journal of Physical Chemistry B*, *105*(6), 1260–1266. https://doi.org/10.1021/jp0029818

Holladay, J. D., Hu, J., King, D. L., & Wang, Y. (2009). An overview of hydrogen production technologies. *Catalysis Today*, *139*(4), 244–260. https://doi.org/10.1016/j.cattod.2008.08.039

Holt, P. F., & Horne, M. (1978). Dust from carbon fibre. *Environmental Research*, *17*(2), 276–283. https://doi.org/10.1016/0013-9351(78)90030-0

Huang, X., Qu, Y., Cid, C. A., Finke, C., Hoffmann, M. R., Lim, K., & Jiang, S. C. (2016). Electrochemical disinfection of toilet wastewater using wastewater electrolysis cell.

Water Research, *92*, 164–172. https://doi.org/10.1016/j.watres.2016.01.040

Hyunwoong, P., Vecitis, C. D., Wonyong, C., Weres, O., & Hoffmann, M. R. (2008). Solar-powered production of molecular hydrogen from water. *Journal of Physical Chemistry C*, *112*(4), 885–889. https://doi.org/10.1021/jp710723p

IEA. (2021). Net Zero by 2050: A Roadmap for the Global Energy Sector. *International Energy Agency*, 224.

IPCC. (2022). *Climate Change 2022: Mitigation of Climate Change. Contribution of Working Group III to the Sixth Assessment Report of the Intergovernmental Panel on Climate Change*. https://doi.org/10.1017/9781009157926

Ji, M., & Wang, J. (2021). Review and comparison of various hydrogen production methods based on costs and life cycle impact assessment indicators. *International Journal of Hydrogen Energy*, *46*(78), 38612–38635. https://doi.org/10.1016/j.ijhydene.2021.09.142

Jiang, J., Chang, M., & Pan, P. (2008). Simultaneous hydrogen production and electrochemical oxidation of organics using boron-doped diamond electrodes. *Environmental Science and Technology*, *42*(8), 3059–3063. https://doi.org/10.1021/es702466k

Kargi, F., & Arikan, S. (2013). Improved hydrogen gas production in electrohydrolysis of vinegar fermentation wastewater by scrap aluminum and salt addition. *International Journal of Hydrogen Energy*, *38*(11), 4389–4396. https://doi.org/10.1016/j.ijhydene.2013.01.191

Kargi, F., & Catalkaya, E. C. (2011a). Electrohydrolysis of landfill leachate organics for hydrogen gas production and COD removal. *International Journal of Hydrogen Energy*, *36*(14), 8252–8260. https://doi.org/10.1016/j.ijhydene.2011.04.197

Kargi, F., & Catalkaya, E. C. (2011b). Hydrogen gas production from olive mill wastewater by electrohydrolysis with simultaneous COD removal. *International Journal of Hydrogen Energy*, *36*(5), 3457–3464. https://doi.org/10.1016/j.ijhydene.2010.12.078

Kargi, F., Catalkaya, E. C., & Uzuncar, S. (2011). Hydrogen gas production from waste anaerobic sludge by electrohydrolysis: Effects of applied DC voltage. *International Journal of Hydrogen Energy*, *36*(3), 2049–2056. https://doi.org/10.1016/j.ijhydene.2010.11.087

Kargi, F., & Uzunc, S. (2012). *Simultaneous hydrogen gas formation and COD removal from cheese whey wastewater by electrohydrolysis*. *7*. https://doi.org/10.1016/j.ijhydene.2012.05.019

Kartikaningsih, D., Huang, Y. H., & Shih, Y. J. (2017). Electro-oxidation and characterization

of nickel foam electrode for removing boron. *Chemosphere*, *166*, 184–191. https://doi.org/10.1016/j.chemosphere.2016.09.091

Khan, M. A., Zhao, H., Zou, W., Chen, Z., Cao, W., Fang, J., Xu, J., Zhang, L., & Zhang, J. (2018). Recent Progresses in Electrocatalysts for Water Electrolysis. In *Electrochemical Energy Reviews* (Vol. 1, Issue 4). Springer Singapore. https://doi.org/10.1007/s41918-018-0014-z

Kim, J., Choi, W. J. K., Choi, J., Hoffmann, M. R., & Park, H. (2013). Electrolysis of urea and urine for solar hydrogen. *Catalysis Today*, *199*(1), 2–7. https://doi.org/10.1016/j.cattod.2012.02.009

Li, X. Y., Cui, Y. H., Feng, Y. J., Xie, Z. M., & Gu, J. D. (2005). Reaction pathways and mechanisms of the electrochemical degradation of phenol on different electrodes. *Water Research*, *39*(10), 1972–1981. https://doi.org/10.1016/j.watres.2005.02.021

Liao, A. A., Spitzer, M., Motheo, A. J., & Bertazzoli, R. (2008). Electrocombustion of humic acid and removal of algae from aqueous solutions. *Journal of Applied Electrochemistry*, *38*(5), 721–727. https://doi.org/10.1007/s10800-008-9502-x

Lu, S., Zhao, B., Chen, M., Wang, L., Fu, X. Z., & Luo, J. L. (2020). Electrolysis of waste water containing aniline to produce polyaniline and hydrogen with low energy consumption. *International Journal of Hydrogen Energy*, *45*(43), 22419–22426. https://doi.org/10.1016/j.ijhydene.2020.06.116

Ma, W., Cheng, Z., Gao, Z., Wang, R., Wang, B., & Sun, Q. (2014). Study of hydrogen gas production coupled with phenol electrochemical oxidation degradation at different stages. *Chemical Engineering Journal*, *241*, 167–174. https://doi.org/10.1016/j.cej.2013.12.031

Marcel Pourbaix. (1974). *Atlas of electrochemical equilibria in aqueous solutions - Marcel Pourbaix - Google Books* (p. 644).

Marzo, E., Gali, A., Lefevre, B., Bouchy, L., Vidal, A., Cortina, J. L., & Fabre, A. (2012). Hydrogen and oxygen production using wastewater effluent treated with ultra-filtration and membrane distillation (greenlysis). *Procedia Engineering*, *44*, 1744–1746. https://doi.org/10.1016/j.proeng.2012.08.932

Muradov, N. Z., & Veziroğlu, T. N. (2005). From hydrocarbon to hydrogen-carbon to hydrogen economy. *International Journal of Hydrogen Energy*, *30*(3), 225–237. https://doi.org/10.1016/j.ijhydene.2004.03.033

Nourani, M., Zackin, B. I., Sabarirajan, D. C., Taspinar, R., Artyushkova, K., Liu, F., Zenyuk, I. V., & Agar, E. (2019). Impact of Corrosion Conditions on Carbon Paper Electrode

Morphology and the Performance of a Vanadium Redox Flow Battery. *Journal of The Electrochemical Society*, *166*(2), A353–A363. https://doi.org/10.1149/2.1041902jes

Ojaomo, K. E., Erinle, T. J., Oladebeye, D. H., & Olakolegan, O. D. (2020). Hydrogen Generation through Electrolysis of Brine for Clean Energy Development in a Depressed Economy. *Iarjset*, *7*(4), 94–101. https://doi.org/10.17148/iarjset.2020.7415

Panizza, M., Michaud, P. A., Cerisola, G., & Comninellis, C. H. (2001). Electrochemical treatment of wastewaters containing organic pollutants on boron-doped diamond electrodes: Prediction of specific energy consumption and required electrode area. *Electrochemistry Communications*, *3*(7), 336–339. https://doi.org/10.1016/S1388-2481(01)00166-7

Panizza, Marco, & Cerisola, G. (2009). Direct and mediated anodic oxidation of organic pollutants. *Chemical Reviews*, *109*(12), 6541–6569. https://doi.org/10.1021/cr9001319

Park, Hana, Choo, K. H., Park, H. S., Choi, J., & Hoffmann, M. R. (2013). Electrochemical oxidation and microfiltration of municipal wastewater with simultaneous hydrogen production: Influence of organic and particulate matter. *Chemical Engineering Journal*, *215–216*, 802–810. https://doi.org/10.1016/j.cej.2012.11.075

Park, Hyunwoong, Bak, A., Ahn, Y. Y., Choi, J., & Hoffmannn, M. R. (2012). Photoelectrochemical performance of multi-layered BiO x-TiO 2/Ti electrodes for degradation of phenol and production of molecular hydrogen in water. *Journal of Hazardous Materials*, *211–212*, 47–54. https://doi.org/10.1016/j.jhazmat.2011.05.009

Park, Hyunwoong, Vecitis, C. D., & Hoffmann, M. R. (2009). Electrochemical water splitting coupled with organic compound oxidation: The role of active chlorine species. *Journal of Physical Chemistry C*, *113*(18), 7935–7945. https://doi.org/10.1021/jp810331w

Pathak, A. K., Kothari, R., Tyagi, V. V., & Anand, S. (2020). Integrated approach for textile industry wastewater for efficient hydrogen production and treatment through solar PV electrolysis. *International Journal of Hydrogen Energy*, *45*(48), 25768–25782. https://doi.org/10.1016/j.ijhydene.2020.03.079

Piccolo, A., Cozzolino, A., Conte, P., & Spaccini, R. (2000). Polymerization of humic substances by an enzyme-catalyzed oxidative coupling. *Naturwissenschaften*, *87*(9), 391–394. https://doi.org/10.1007/s001140050747

Polcaro, A. M., & Palmas, S. (1997). Electrochemical Oxidation of Chlorophenols. *Industrial and Engineering Chemistry Research*, *36*(5), 1791–1798. https://doi.org/10.1021/ie960557g

Ramulu, M., & Kramlich, J. (2004). Machining of fiber reinforced composites: Review of environmental and health effects. *International Journal of Environmentally Conscious Design & Manufacturing*, *11*(4), 1–19.

Rietveld, L. C., Norton-Brandão, D., Shang, R., Van Agtmaal, J., & Van Lier, J. B. (2011). Possibilities for reuse of treated domestic wastewater in The Netherlands. *Water Science and Technology*, *64*(7), 1540–1546. https://doi.org/10.2166/wst.2011.037

Rijnaarts, T., Moreno, J., Saakes, M., de Vos, W. M., & Nijmeijer, K. (2019). Role of anion exchange membrane fouling in reverse electrodialysis using natural feed waters. *Colloids and Surfaces A: Physicochemical and Engineering Aspects*, *560*(October 2018), 198–204. https://doi.org/10.1016/j.colsurfa.2018.10.020

Rodrigo, M. A., Electrochem, J., Soc, D., Rodrigo, M. A., Michaud, P. A., Duo, I., Panizza, M., & Cerisola, G. (2001). *Oxidation of 4-Chlorophenol at Boron-Doped Diamond Electrode for Wastewater Treatment Oxidation of 4-Chlorophenol at Boron-Doped Diamond Electrode for Wastewater Treatment*. 59–64. https://doi.org/10.1149/1.1362545

Roser, H. R. ; M., & Rosado, P. (2022). *CO_2 and Greenhouse Gas Emissions*. Our World in Data. https://ourworldindata.org/grapher/annual-co2-emissions-per-country?time=1750..2020&country=AUS~NLD~GBR

Sharmila, V. G., Banu, J. R., Kim, S. H., & Kumar, G. (2020). A review on evaluation of applied pretreatment methods of wastewater towards sustainable H2 generation: Energy efficiency analysis. *International Journal of Hydrogen Energy*, *45*(15), 8329–8345. https://doi.org/10.1016/j.ijhydene.2020.01.081

Struyk, Z., & Sposito, G. (2001). Redox properties of humic acids. *Geoderma*, *102*(3–4), 329–346.

Tang, C., Yan, W., & Zheng, C. (2014). Electrochemical oxidation of humic acid at the antimony- and nickel-doped tin oxide electrode. *Frontiers of Environmental Science and Engineering*, *8*(3), 337–344. https://doi.org/10.1007/s11783-013-0545-9

Tufa, R. A., Hnát, J., Němeček, M., Kodým, R., Curcio, E., & Bouzek, K. (2018). Hydrogen production from industrial wastewaters: An integrated reverse electrodialysis - Water electrolysis energy system. *Journal of Cleaner Production*, *203*, 418–426. https://doi.org/10.1016/j.jclepro.2018.08.269

Vlaicu, I., Pop, A., Manea, F., & Radovan, C. (2011). Degradation of humic acid from water by advanced electrochemical oxidation method. *Water Science and Technology: Water Supply*, *11*(1), 85–95. https://doi.org/10.2166/ws.2011.013

Wang, M., Wang, Z., Gong, X., & Guo, Z. (2014). The intensification technologies to water electrolysis for hydrogen production - A review. *Renewable and Sustainable Energy Reviews*, *29*, 573–588. https://doi.org/10.1016/j.rser.2013.08.090

Yacouba, Z. A., Mendret, J., Lesage, G., Zaviska, F., & Brosillon, S. (2021). Removal of organic micropollutants from domestic wastewater: The effect of ozone-based advanced oxidation process on nanofiltration. *Journal of Water Process Engineering*, *39*(July 2020), 101869. https://doi.org/10.1016/j.jwpe.2020.101869

Yeo, I. H., Wen, S., & Mho, S. il. (2010). Effect of interfacial oxides on the electrochemical activity of lead dioxide film electrodes on a ti substrate. *Analytical Sciences*, *26*(1), 39–44. https://doi.org/10.2116/analsci.26.39

Yi, F., & Chen, S. (2008). Electrochemical treatment of alizarin red S dye wastewater using an activated carbon fiber as anode material. *Journal of Porous Materials*, *15*(5), 565–569. https://doi.org/10.1007/s10934-007-9134-2

Zeng, K., & Zhang, D. (2010). Recent progress in alkaline water electrolysis for hydrogen production and applications. *Progress in Energy and Combustion Science*, *36*(3), 307–326. https://doi.org/10.1016/j.pecs.2009.11.002

Zhou, D., Li, P., Xu, W., Jawaid, S., Mohammed-Ibrahim, J., Liu, W., Kuang, Y., & Sun, X. (2020). Recent Advances in Non-Precious Metal-Based Electrodes for Alkaline Water Electrolysis. *ChemNanoMat*, *6*(3), 336–355. https://doi.org/10.1002/cnma.202000010

A. Appendix

A.1 Arduino Sensor Components

For safety reasons, a DIY Arduino sensor was constructed to measure the hydrogen concentration in the workspace. The components required to construct the sensor are as follows:-

- MQ-8 Gas Sensor
- Arduino UNO microcontroller
- Jumper cables

The circuit diagram is shown in Figure 73a and Figure 73b

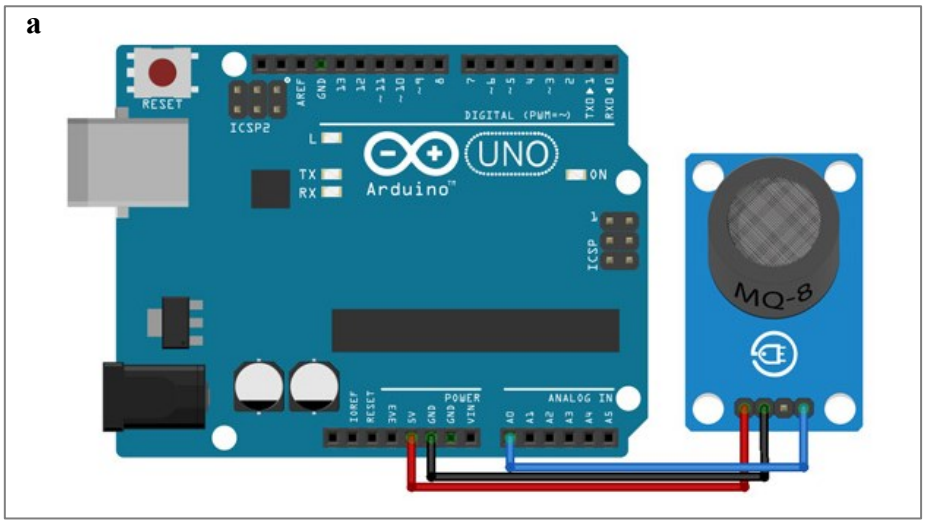

Figure 72 Arduino Sensor Circuit Diagram

A.2 Arduino Sensor Code

```
#define        MQ_PIN                       (0)     //define which analog input channel you are going to use
#define        RL_VALUE                     (10)    //define the load resistance on the board, in kilo ohms
#define        RO_CLEAN_AIR_FACTOR          (70)    //RO_CLEAR_AIR_FACTOR=(Sensor resistance in
clean air)/RO,
                                            //which is derived from the chart in datasheet

/***********************Software Related Macros************************************/
#define        CALIBARAION_SAMPLE_TIMES     (50)    //define how many samples you are going to
take in the calibration phase
#define        CALIBRATION_SAMPLE_INTERVAL  (500)   //define the time interal(in milisecond)
between each samples in the
                                            //cablibration phase
#define        READ_SAMPLE_INTERVAL         (50)    //define how many samples you are going to take
in normal operation
#define        READ_SAMPLE_TIMES            (5)     //define the time interal(in milisecond) between
each samples in
                                            //normal operation

/*********************Application Related Macros**********************************/
#define        GAS_H2                       (0)

/*****************************Globals***********************************************/
float          H2Curve[3]  =  {2.3, 0.93,-1.44};    //two points are taken from the curve in datasheet.
                                            //with these two points, a line is formed which is "approximately
equivalent"
                                            //to the original curve.
                                            //data format:{ x, y, slope}; point1: (lg200, lg8.5), point2: (lg10000,
lg0.03)

float          Ro          =  10;                //Ro is initialized to 10 kilo ohms

void setup()
{
  Serial.begin(9600);                       //UART setup, baudrate = 9600bps
  Serial.print("Calibrating...\n");
  Ro = MQCalibration(MQ_PIN);                       //Calibrating the sensor. Please make sure the sensor
is in clean air
                                            //when you perform the calibration
  Serial.print("Calibration is done...\n");
  Serial.print("Ro=");
  Serial.print(Ro);
  Serial.print("kohm");
  Serial.print("\n");

  Serial.print("Sensor analog output:");
  Serial.print(analogRead(MQ_PIN));
  Serial.print("\n");
}

void loop()
{

   Serial.print("H2:");
   Serial.print(MQGetGasPercentage(MQRead(MQ_PIN)/Ro,GAS_H2) );
   Serial.print( "ppm" );
   Serial.print("\n");

   Serial.print("Sensor analog output: ");
   Serial.print(analogRead(MQ_PIN));
   Serial.print("\n");

   Serial.print("Rs Value: ");
```

```
  Serial.print(MQRead(MQ_PIN));
  Serial.print("kohm");
  Serial.print("\n");
  Serial.print("\n");

  delay(200);
}

/****************** MQResistanceCalculation *************************************
Input:   raw_adc - raw value read from adc, which represents the voltage
Output:  the calculated sensor resistance
Remarks: The sensor and the load resistor forms a voltage divider. Given the voltage
         across the load resistor and its resistance, the resistance of the sensor
         could be derived.
************************************************************************************/
float MQResistanceCalculation(int raw_adc)
{
  return ( ((float)RL_VALUE*(1023-raw_adc)/raw_adc));
}

/***************************** MQCalibration ****************************************
Input:   mq_pin - analog channel
Output:  Ro of the sensor
Remarks: This function assumes that the sensor is in clean air. It use
         MQResistanceCalculation to calculates the sensor resistance in clean air
         and then divides it with RO_CLEAN_AIR_FACTOR. RO_CLEAN_AIR_FACTOR is about
         10, which differs slightly between different sensors.
************************************************************************************/
float MQCalibration(int mq_pin)
{
  int i;
  float val=0;

  for (i=0;i<CALIBARAION_SAMPLE_TIMES;i++) {            //take multiple samples
    val += MQResistanceCalculation(analogRead(mq_pin));
    delay(CALIBRATION_SAMPLE_INTERVAL);
  }
  val = val/CALIBARAION_SAMPLE_TIMES;                   //calculate the average value

  val = val/RO_CLEAN_AIR_FACTOR;                        //divided by RO_CLEAN_AIR_FACTOR yields the
Ro
                                        //according to the chart in the datasheet

  return val;
}
/*****************************  MQRead *********************************************
Input:   mq_pin - analog channel
Output:  Rs of the sensor
Remarks: This function use MQResistanceCalculation to caculate the sensor resistenc (Rs).
         The Rs changes as the sensor is in the different consentration of the target
         gas. The sample times and the time interval between samples could be configured
         by changing the definition of the macros.
************************************************************************************/
float MQRead(int mq_pin)
{
  int i;
  float rs=0;

  for (i=0;i<READ_SAMPLE_TIMES;i++) {
    rs += MQResistanceCalculation(analogRead(mq_pin));
    delay(READ_SAMPLE_INTERVAL);
  }

  rs = rs/READ_SAMPLE_TIMES;
```

```
  return rs;
}

/***************************  MQGetGasPercentage **********************************
Input:   rs_ro_ratio - Rs divided by Ro
         gas_id      - target gas type
Output:  ppm of the target gas
Remarks: This function passes different curves to the MQGetPercentage function which
         calculates the ppm (parts per million) of the target gas.
************************************************************************************/
int MQGetGasPercentage(float rs_ro_ratio, int gas_id)
{
  if ( gas_id == GAS_H2) {
     return MQGetPercentage(rs_ro_ratio,H2Curve);
  }
  return 0;
}

/***************************  MQGetPercentage **********************************
Input:   rs_ro_ratio - Rs divided by Ro
         pcurve      - pointer to the curve of the target gas
Output:  ppm of the target gas
Remarks: By using the slope and a point of the line. The x(logarithmic value of ppm)
         of the line could be derived if y(rs_ro_ratio) is provided. As it is a
         logarithmic coordinate, power of 10 is used to convert the result to non-logarithmic
         value.
************************************************************************************/
int  MQGetPercentage(float rs_ro_ratio, float *pcurve)
{
  return (pow(10,( ((log(rs_ro_ratio)-pcurve[1])/pcurve[2]) + pcurve[0])));
}
```

A.3 Images of the Flow Cell and Setup

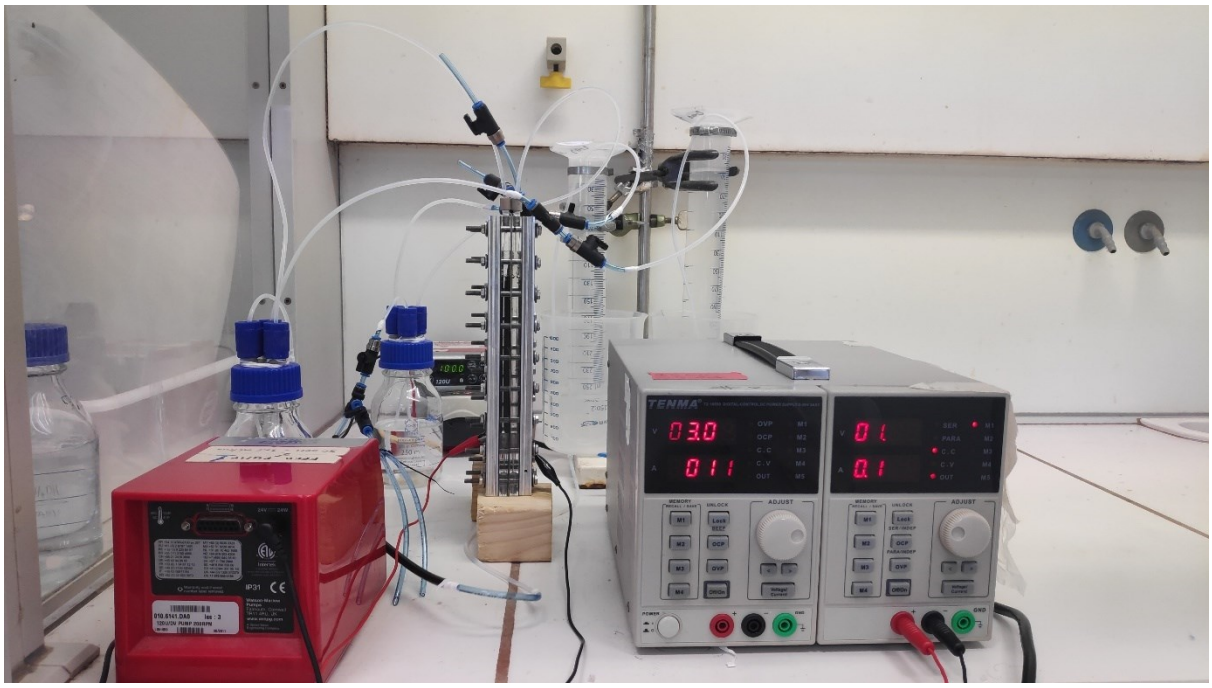

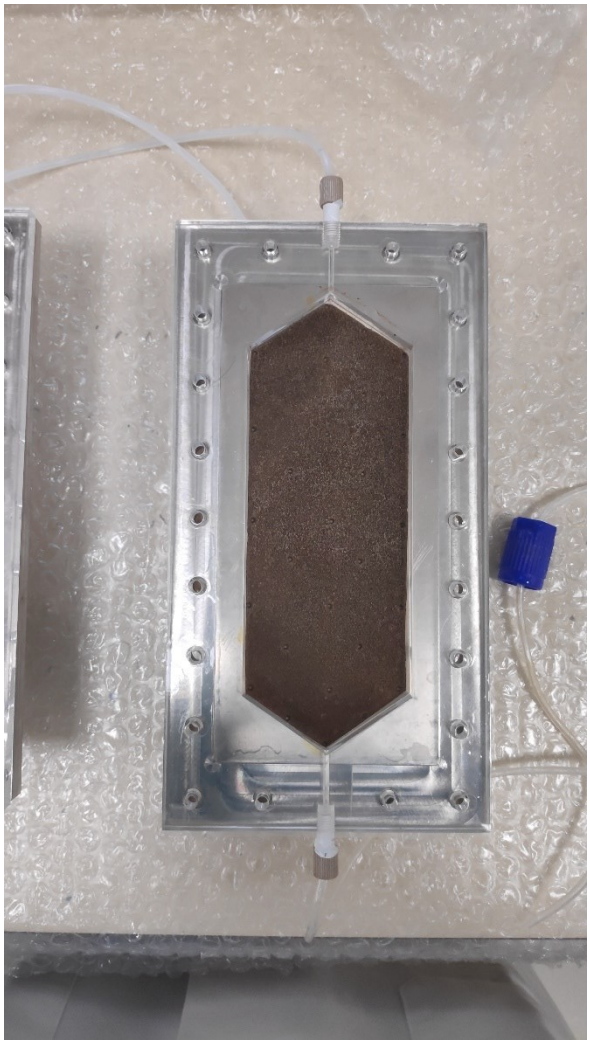

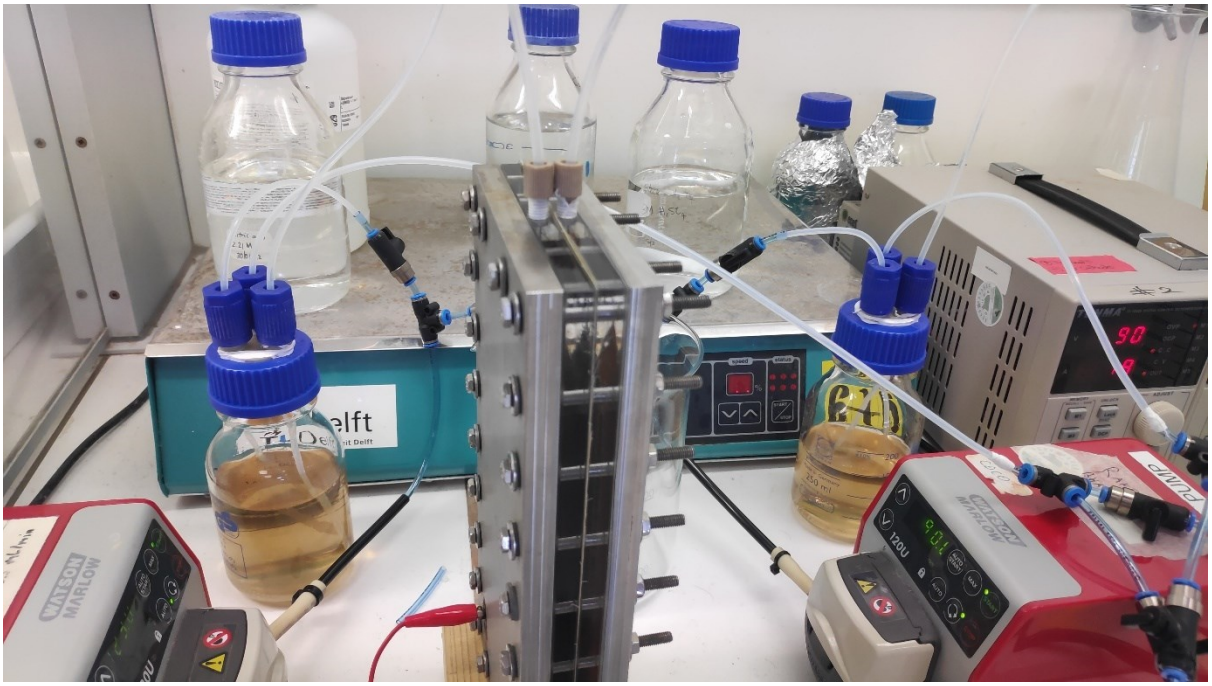

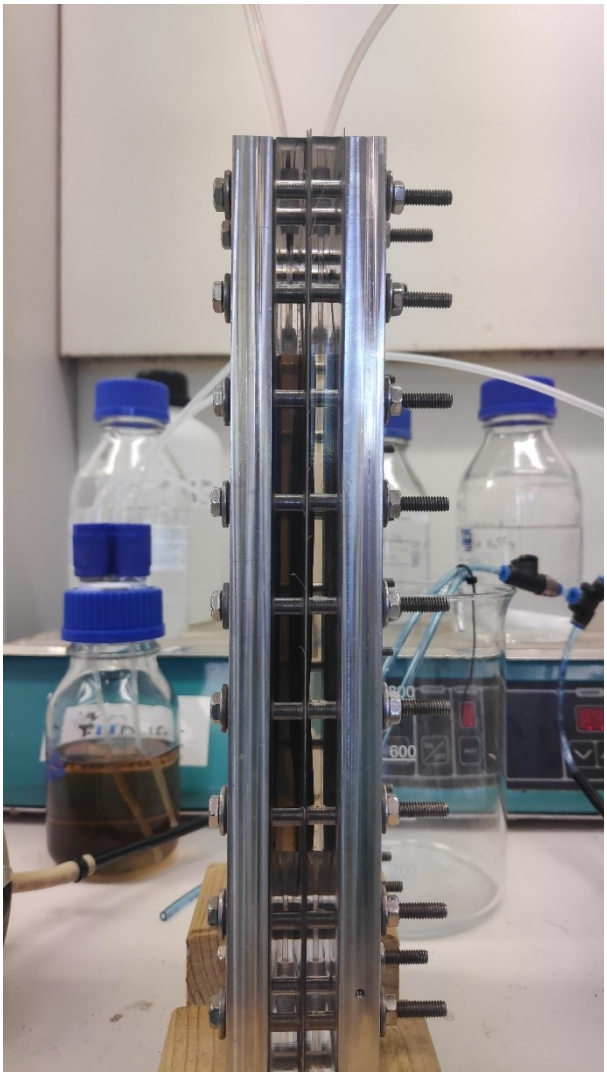

A.4 Coulombic Efficiency

Effect of KOH- Electrolysis of Synthetic Effluent

Carbon Fibre

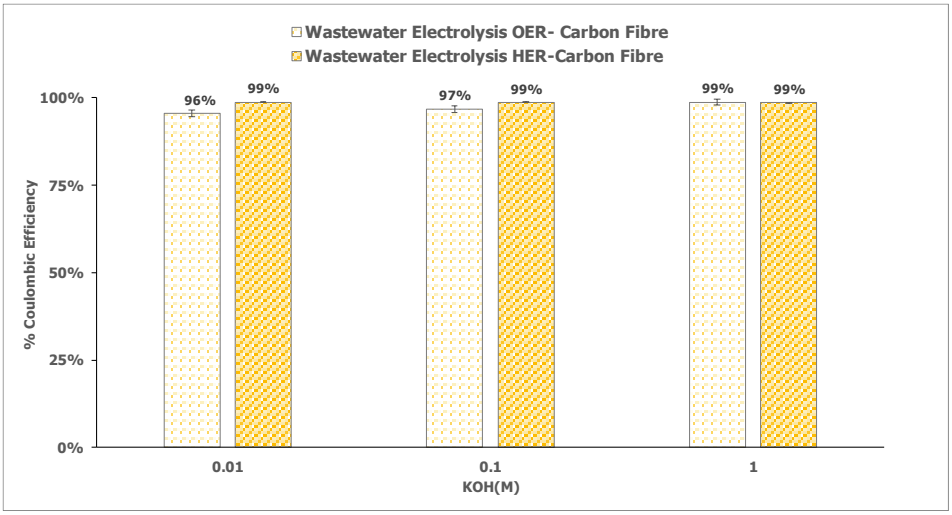

Ni-Foam

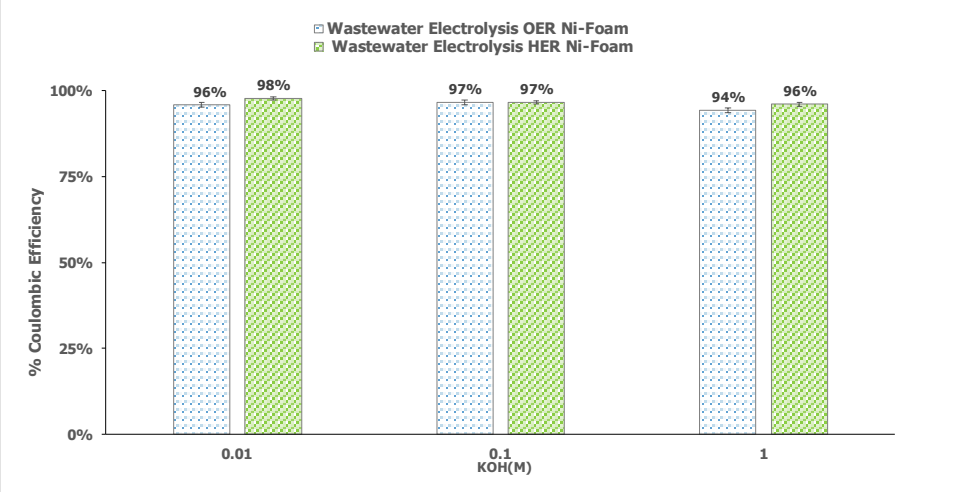

Effect of Current Density-Electrolysis of Synthetic Effluent

Carbon Fibre

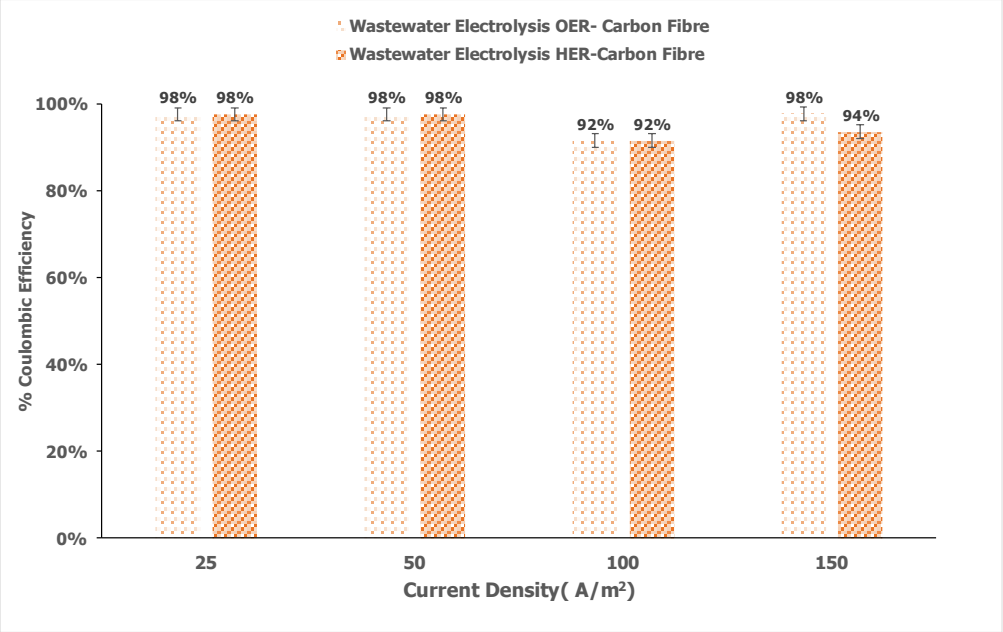

Ni-Foam

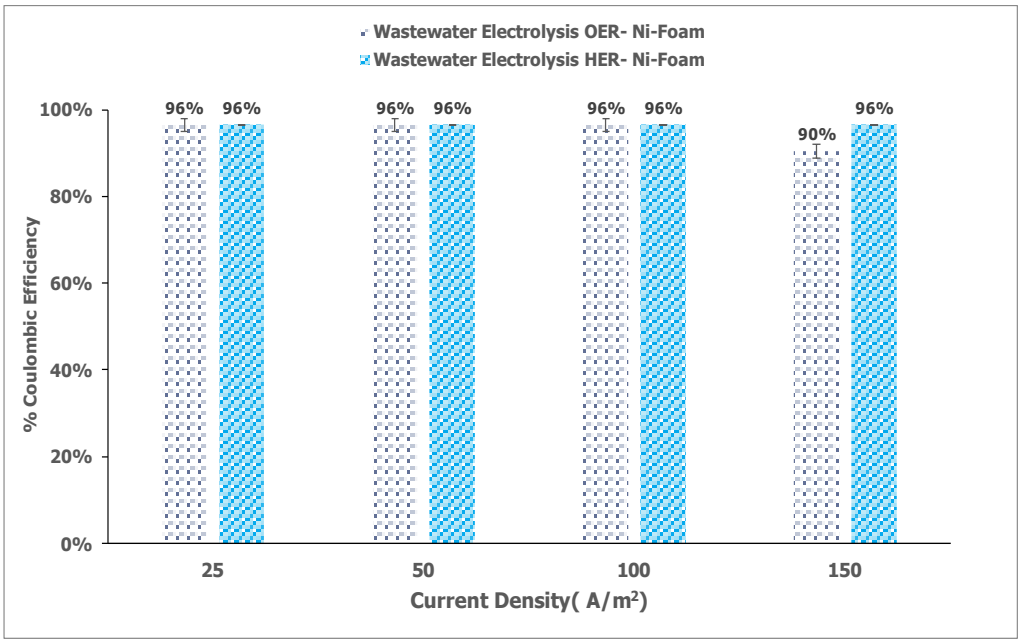

Effect of Humic Acid Concentration -Electrolysis of Synthetic Effluent

Ni-Foam

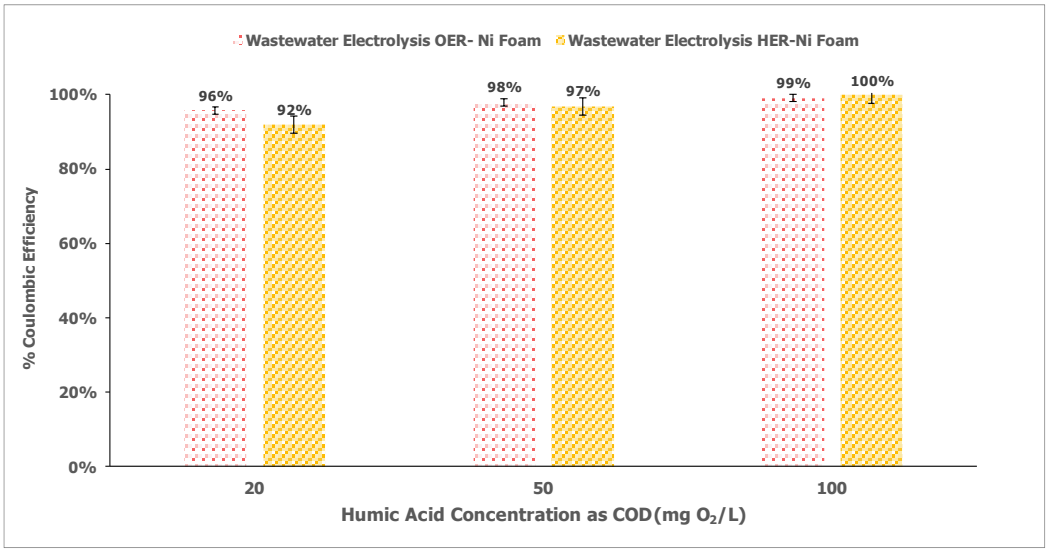

Electrolysis of Municipal Effluent

Effect of KOH- Carbon Fibre

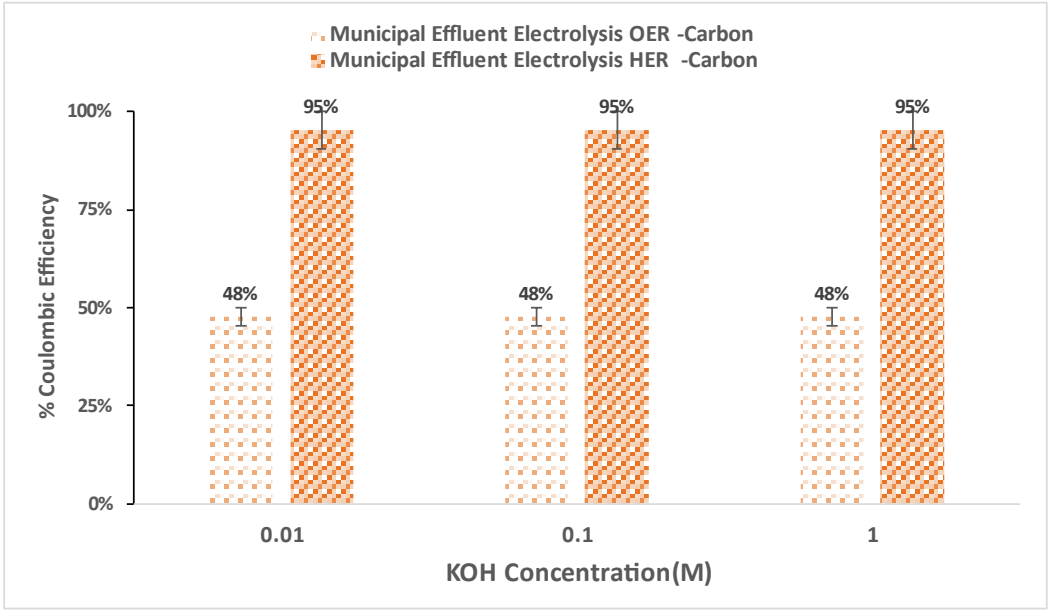

Effect of KOH – Ni-Foam

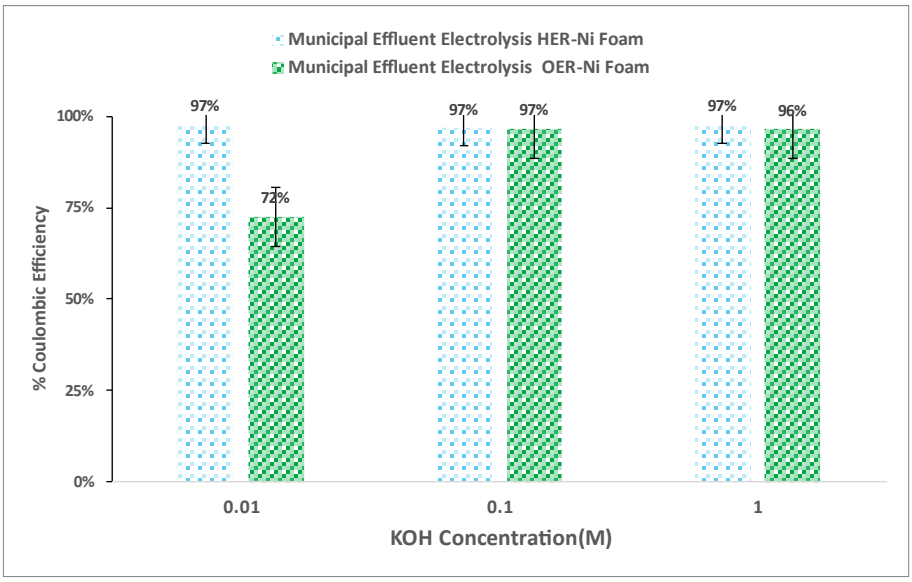

Effect of Current Density – Carbon Fibre

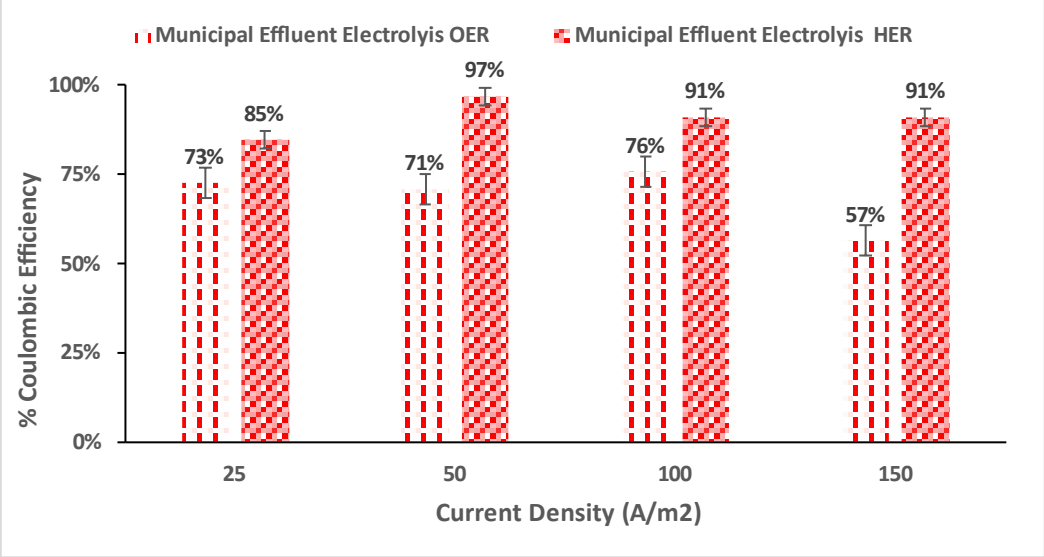

Effect of Current Density – Ni-Foam